Copy No. _____

Defence Research and Development Canada
Recherche et développement pour la défense Canada

DEFENCE R&D DÉFENSE

Development and Verification of a Weld Simulation Capability for VAST

Lei Jiang
Tom MacAdam
Martec Limited

Prepared by:
Martec Limited
1888 Brunswick Street, Suite 400
Halifax, Nova Scotia B3J 3J8

Contractor's Document Number: TR-12-22
Contract Project Manager: Lei Jiang, 902-425-5101 x228
PWGSC Contract Number: W7707-115119
CSA: John R. MacKay, Defence Scientist, Warship Performance, 902-426-3100 ext 382

Defence R&D Canada – Atlantic

Contract Report
DRDC Atlantic CR 2011-164
June 2012

Canada

This page intentionally left blank.

Development and Verification of a Weld Simulation Capability for VAST

Lei Jiang
Tom MacAdam
Martec Limited

Prepared By:
Martec Limited
1888 Brunswick Street, Suite 400
Halifax, Nova Scotia, B3J 3J8

Contractor's Document Number: TR-12-22
Contract Project Manager: Lei Jiang, 902-425-5101 ext 228
PWGSC Contract Number: W7707-115119
CSA: John R. MacKay, Defence Scientist, Warship Performance, 902-426-3100 ext 382

Defence R&D Canada – Atlantic

Contract Report
DRDC Atlantic CR 2011-164
June 2012

Principal Author

Original signed by Lei Jiang

Lei Jiang

Senior Research Engineer

Approved by

Original signed by Neil G. Pegg

Neil G. Pegg

Head, Warship Performance

Approved for release by

Original signed by Calvin V. Hyatt

Calvin V. Hyatt

Chair, Document Review Panel

This work was performed under project 11ga08 with funding provided by DMEPM(SM) 4.

Abstract

This report presents work aimed at developing a weld simulation capability for the VAST suite of finite element codes and the SubSAS submarine structural modelling software. In this study, a number of features required for weld simulations were implemented and verified. For heat transfer analyses, these included an element birth algorithm for tracking the states of weld elements with moving heat sources, a capability for generating thermal load vectors based on Goldak's model, and a capability for treating temperature-dependent thermal properties. For structural analysis, thermal induced strains were first implemented in the elastic-plastic material model to facilitate coupled thermal-mechanical analyses and the resulting thermal-elastic-plastic constitutive model was adjusted to treat melting and solidification of materials during the welding process. Temperature-dependent structural material properties were implemented and multi-pass welding was supported. For heat transfer analysis, weld simulations with different weld sequences were performed successfully. For structural analyses, the VAST capabilities were tested by using various test cases designed to reflect certain features of weld simulations. The VAST element and material model behaved favourably and no convergence difficulties were observed. However, when VAST was applied to a full weld simulation, divergence occurred after the first few solution steps. Further investigations are required to identify the cause of the numerical problem. The new weld simulation tools were not implemented in SubSAS, but a methodology was developed for implementing SubSAS support to define welding simulation models. Modifications to SubSAS's underlying RMGScript schema to support capturing the welding model parameters are detailed. Advanced algorithms for enhancing SubSAS's meshing capability to create brick elements from surface geometry, including a representation of the weld deposit material, are also described.

Résumé

Le présent rapport contient la description de travaux visant à élaborer des capacités de simulation de soudures pour la suite de codes d'éléments finis appelée VAST et le logiciel de modélisation de structures de sous marins appelée SubSAS. Dans le cadre de la présente étude, un certain nombre de caractéristiques nécessaires aux simulations de soudures ont été mises en oeuvre et vérifiées. Dans le cas des analyses relatives au transfert de chaleur, les caractéristiques comprenaient un algorithme de production d'éléments finis permettant de déterminer l'état des composants de la soudure en fonction de sources de chaleur mobiles, ainsi que la capacité de générer des vecteurs de charge thermique basés sur le modèle de Goldak et celle de traiter adéquatement les propriétés thermiques qui dépendent de la température. Dans le cas des travaux d'analyse structurale, les valeurs de déformations causées par la chaleur ont d'abord été intégrées au modèle de matériaux élastiques-plastiques, afin de faciliter l'exécution d'analyses couplées thermiques et mécaniques; le modèle constitutif thermique-élastique-plastique obtenu a été modifié afin de tenir compte des processus de fusion et de solidification des matériaux lors du procédé de soudage. Des propriétés liées à la structure des matériaux qui dépendent de la température ont été intégrées au modèles, notamment pour le cas du procédé de soudage à passes multiples. Dans le cas des analyses relatives au transfert de chaleur, on a réalisé avec succès des simulations de soudures exécutées avec différentes séquences de soudage. En ce qui a trait aux

analyses structurales, les capacités de l'outil VAST ont été mises à l'essai en utilisant divers cas types pouvant témoigner fidèlement de certaines caractéristiques des simulations de soudures. Le modèle de matériaux et d'éléments VAST a présenté un rendement adéquat et aucun problème de convergence n'a été observé. Toutefois, lorsque la suite VAST a été utilisée pour simuler une soudure complète, un problème de divergence a surgi dès les premières étapes de résolution. Des études plus poussées devront être réalisées afin d'identifier la cause du problème numérique. Les nouveaux outils de simulation de soudures n'ont pas été intégrés au logiciel SubSAS, mais une méthode a été élaborée afin de faciliter la mise en oeuvre d'applications de SubSAS qui permettent de définir des modèles de simulation de procédés de soudage. Des détails sont fournis sur les modifications apportées au schéma sous-jacent RMGScript de SubSAS, lesquelles visaient à faciliter l'enregistrement des paramètres du modèles de procédés de soudage. Le présent rapport contient aussi la description d'algorithmes perfectionnés mis au point pour accroître la capacité de maillage de SubSAS et produire ainsi des éléments parallélépipédiques à partir de concepts de géométrie de surface, y compris une représentation du matériau d'apport de la soudure.

Executive summary

Development and Verification of a Weld Simulation Capability for VAST

Lei Jiang; Tom MacAdam; DRDC Atlantic CR 2011-164; Defence R&D Canada – Atlantic; June 2012.

Introduction: Welding of naval ships and submarines during fabrication and repair can introduce residual stresses and distortions that significantly affect the ultimate strength of the hull. For some typical cases, such as welding frames to the hull, analytical or empirical models are available to predict the magnitude of welding induced stresses and/or distortions for subsequent use in structural strength analyses. On the other hand, the effects of welding processes whereby the amount and location of weld deposition varies greatly, such as weld buttering repair of corroded hull plating, are more difficult to predict analytically or empirically. In those cases, a numerical simulation of the welding procedure is the only practical option. The current contract report describes software development that was carried out by Martec Limited to allow the VAST and VASTF finite element (FE) programs to be used in welding simulations. A proposal for the incorporation of the new capability in the SubSAS submarine structural modelling and analysis software is also presented.

Results: Improvements were made to VASTF in order to allow that program to predict the thermal loads introduced into the structure during welding. The developments include support for temperature-dependent thermal material properties, a moving heat source for simulating the energy introduced by the welding torch, and an element birth/death feature used to simulate the deposition of weld material. The thermal load history predicted by VASTF is used by VAST to predict the structural response to the welding process, i.e., stresses and distortions. Improvements made to VAST include the development of temperature-dependent mechanical material models and an element birth/death feature. Weld simulations were performed for simple three-dimensional solid FE models in order to verify the functionality of the coupled thermal-structural analysis. Results of the thermal analysis compared well with benchmark numerical results generated using the ANSYS software. Structural analyses were confounded by convergence difficulties before the entire weld simulation was completed. Those problems could not be practically resolved due to the long computation times required for the VAST analyses. A detailed proposal was developed that describes how the weld simulation tools could be incorporated in SubSAS to allow various types of welding processes to be simulated.

Significance: An in-house capability to efficiently carry out weld simulations would allow the CF to make well-informed decisions regarding the construction and repair of ship and submarine hulls. Of particular importance would be the ability to determine the effectiveness of weld overlay repair for a given case of corrosion damage. The VASTF and VAST programs are not yet ready to be used in that capacity, so in the mean time alternative commercial codes must be used on a case-by-case basis, as required.

Future plans: Martec Limited is currently performing an internally funded project to improve the computational efficiency of the VAST finite element solver. Improved analysis times would facilitate the resolution of the convergence difficulties encountered in this study, and make

welding simulations more practical. Incorporation of the weld simulation tools in SubSAS may be pursued once the computation times for the FE programs have been improved.

Sommaire

Development and Verification of a Weld Simulation Capability for VAST

Lei Jiang; Tom MacAdam; DRDC Atlantic CR 2011-164; R & D pour la défense Canada – Atlantique; juin 2012.

Introduction : Les travaux de soudage réalisés durant la construction et la réparation des sous-marins et navires militaires peuvent provoquer des contraintes résiduelles et des déformations qui influent grandement sur la résistance à la rupture de la coque. Dans certains cas types comme ceux des travaux de soudage de membrures à la coque, il est possible d'utiliser des modèles analytiques ou empiriques pour prévoir l'importance des contraintes causées par le soudage ou celle des déformations, ou les deux; de tels résultats peuvent par la suite servir à réaliser des analyses de résistance structurale. D'autre part, les effets des procédés de soudage pour lesquels la quantité et l'emplacement des dépôts de soudure varie grandement, par exemple les réparations par beurrage d'un bordé extérieur corrodé, sont plus difficiles à prévoir, que ce soit au moyen d'une méthode analytique ou empirique. Dans ces cas particuliers, la simulation numérique du procédé de soudage constitue la seule solution pratique au problème. Le présent rapport de contrat de recherche contient la description des travaux de développement de logiciel, exécutés par la société Martec Limited, dont l'objectif était de permettre l'intégration aux simulations de soudage des programmes d'analyse par éléments finis (EF) nommés VAST et VASTF. Il comporte aussi une proposition de travaux visant à intégrer les nouvelles capacités des programmes à l'outil SubSAS, un logiciel de modélisation et d'analyse de structures de sous-marins.

Résultats : Les améliorations apportées au programme VASTF avaient pour but de permettre à ce logiciel de prévoir les charges thermiques subies par une structure durant l'exécution de travaux de soudage. Les améliorations en question comprennent la capacité de traiter adéquatement les propriétés thermiques des matériaux qui dépendent de la température, l'intégration d'une source de chaleur mobile permettant de simuler l'énergie produite par le chalumeau, ainsi qu'une caractéristique liée à la production et l'élimination d'éléments finis servant à simuler le dépôt du matériau d'apport. Les diverses charges thermiques prévues au moyen de VASTF sont utilisées dans le programme VAST afin de prévoir la réaction de la structure au procédé de soudage, c'est-à-dire les contraintes et les déformations subies par celle ci. Quant aux améliorations apportées au programme VAST, elles comprennent l'élaboration de modèles de propriétés mécaniques des matériaux qui dépendent de la température et d'un module de production et d'élimination d'éléments finis. Des simulations de soudures ont été effectuées pour de simples modèles à EF tridimensionnels afin de vérifier la fonctionnalité de l'analyse couplée thermique et structurale. La comparaison des résultats de l'analyse thermique et de résultats numériques de référence produits par le logiciel ANSYS indique qu'il existe une bonne concordance entre les deux ensembles. Les résultats des analyses structurales ont été caractérisés par un facteur de confusion, car des problèmes de convergence ont surgi avant que le processus de simulation de soudures ne soit complété. Il a été impossible de résoudre ces problèmes en raison des temps de calcul très élevés qu'exige l'exécution des analyses VAST. On a élaboré une proposition de travaux détaillée qui comporte la description des moyens permettant d'intégrer les

outils de simulation de soudures au programme SubSAS et, conséquemment, de simuler divers procédés de soudage.

Importance : La capacité de réaliser, à l'interne, des simulations de soudures adéquates, permettrait aux FC de prendre des décisions éclairées en matière de construction et de réparations de coques de navires et de sous marins. Une capacité particulière serait, entre autres, d'une importance cruciale, soit celle qui permet de déterminer l'efficacité d'une réparation effectuée en réalisant une soudure de rechargement, pour un cas donné de dommage causé par la corrosion. Les programmes VASTF et VAST n'ont pas encore la capacité d'être employés à cette fin; entre-temps, il faudra donc, au besoin, utiliser des codes de substitution commerciaux, selon les exigences de chaque cas.

Perspectives : La société Martec Limited exécute présentement, dans le cadre d'un projet financé à l'interne, des travaux visant à accroître l'efficacité de calcul du solutionneur par éléments finis VAST. La réduction des temps d'analyse faciliterait la résolution des problèmes de convergence rencontrés dans le cadre de la présente étude et elle rendrait plus pratique l'exécution des simulations de procédés de soudage. Les travaux d'intégration des outils de simulation de soudures au programme SubSAS pourraient se poursuivre, une fois que les temps de calcul auront été améliorés.

Table of contents

List of figures

This page intentionally left blank.

List of tables

This page intentionally left blank.

1 Introduction

The gas metal arc welding (GMAW) process has been widely used for joining components of steel structures and is the most common joining method used in the shipbuilding industry, including naval surface ships and submarines. Arc welding relies on intense local heating at a joint where a certain amount of the base metal is melted and fused with additional metal from the welding electrode. The intense local heating causes severe thermal gradients in the welded component and the uneven cooling that follows produces residual stresses and distortion. The welding-induced residual stresses lead to early yielding in some regions of stiffened plates in ship structures, reducing the effective cross-sectional area. Weld-induced distortions contribute to geometric imperfections in the structure, resulting in a reduction of their ultimate load-carrying capacity. Both factors have large influences on the nonlinear collapse behaviour of ship and submarine structures and need to be considered in plastic collapse analyses.

The objective of the current task is to develop thermal and structural analysis capabilities in the VAST suite of finite element programs to facilitate numerical simulation of welding processes used in fabrication and repair of submarine pressure hulls, including prediction of weld-induced residual stresses and distortions for various weld procedures. It should be noted that, while the target application of the current work is submarine structures, the weld simulations capabilities that have been developed are equally applicable to surface ships or any steel structure.

An overview of the computational strategies for welding simulations is presented in the next chapter, where the various coupling effects between the thermal and mechanical fields, as well as the micro-structures, are discussed. Through a series assumptions and simplifications, the commonly used one-way coupling approach is justified.

The modifications and verifications of the VASTF program for the heat transfer analysis component of weld simulations are presented in Chapter 3. That work includes implementation of algorithms dealing with the moving heat source based on the Goldak model [6], temperature-dependent material thermal properties and temperature-dependent heat transfer coefficient. To verify these newly developed heat transfer capabilities, numerical simulation of weld experiments involving multi-pass weld are performed and the VASTF solutions are compared against predictions of another finite element program.

The structural analysis in weld simulations is dealt with in Chapter 4, where modifications to the VAST finite element program are discussed. These modifications include the implementation of temperature-dependent mechanical properties, inclusion of thermal strains in the elastic-plastic material model and development of an element birth-death algorithm to activate/deactivate elements based on the location of the moving heat sources and the solid-liquid phase of the element. These new capabilities are then verified using a group of carefully designed test cases which reflect certain features of the weld simulation before they are applied to the full weld simulation.

Chapter 5 details proposed changes to the Submarine Structural Analysis Suite (SubSAS) to support configuring and performing a welding simulation using the aforementioned capability introduced into VAST/VASTF. Details regarding the model definition in SubSAS's modelling language (RMGScript) are given as well as algorithms for converting the default SubSAS shell

mesh into a brick-based mesh containing elements to model the weld deposit material. Seamlessly running the analysis and postprocessing the results are also considered.

Conclusions and recommendation for future work are presented in Chapter 6.

2 Computational Strategy for Weld Simulation as a Coupled Problem

The welding process involves many different physical phenomena [1-3]. In order to simulate the welding process using numerical methods, different couplings between these physical phenomena must first be considered. In most cases, the ultimate objective of the weld simulations is to predict the mechanical effects of welding, which requires computation of both the thermal and mechanical fields. The material behaviour, due to the changing microstructure, may also depend on the temperature and deformation histories; as a result the microstructure evolution also needs to be considered when modelling the material behaviour. A summary of the possible couplings between the various fields involving in welding was provided by Lindgren [1] and is reproduced below.

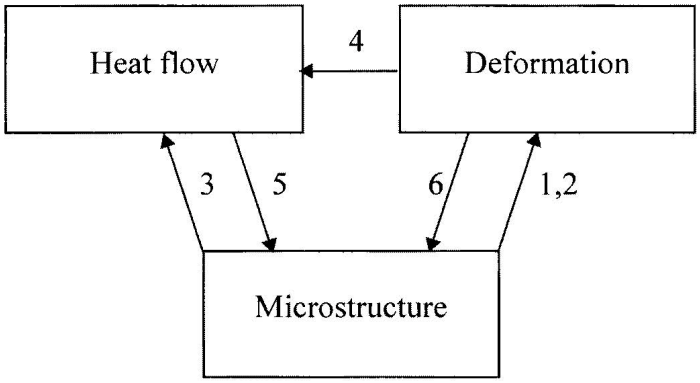

Figure 1: Phenomena occurring during welding. (Reference [1])

Table 1: Couplings in Figure 1

Coupling #	**Explanation**
1a	Thermal expansion depends on microstructure of material.
1b	Volume changes due to phase changes.
2a	Plastic material behaviour depends on microstructure of material.
2b	Elastic material behaviour depends on microstructure of material.
3a	Heat conductivity and heat capacity depend on microstructure of material.
3b	Latent heat due to phase changes.
4a	Deformation changes thermal boundary conditions.
4b	Heat due to plastic dissipation (plastic strain rate).
4c	Heat due to thermal strain rate.
4d	Heat due to elastic strain rate.
5	Microstructure evolution depends on temperature.
6	Microstructure evolution depends on deformation.

Most welding simulations published in the literature were performed in two steps, in which a thermal analysis is followed by a mechanical analysis. The thermal dilatation (coupling#1), which is the sum of the thermal expansion and the volume changes due to phase transformations, drives the deformation. Some analyses only took the thermal expansion into account. Different approaches have been used for including the effects of the microstructure, which depends on the history of the thermo-mechanical process. That dependency can be approximated or ignored in the analysis, thereby making it possible to decouple the heat transfer analysis from the mechanical analysis, so that the weld simulation can be performed in a two-step approach as described in Figure 2.

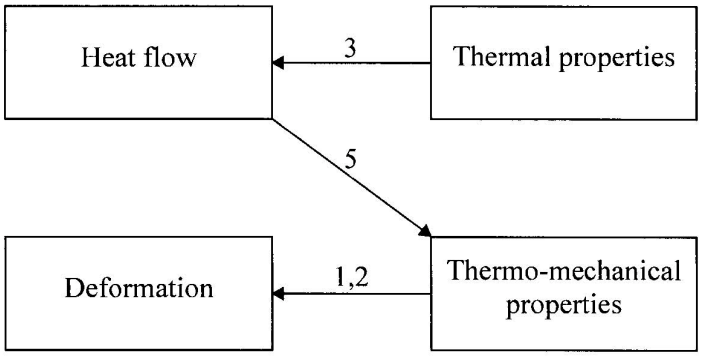

Figure 2: Performing a thermal analysis followed by a mechanical analysis is made possible by ignoring and simplifying some couplings given in Figure 1. (Reference [1])

It may be necessary to update the deformation during the thermal analysis, for example, when fixtures change the thermal boundary conditions due to the deformation (coupling #4a). The thermal and mechanical analyses can then be performed in a so-called staggered approach or simultaneously. Because the thermal dilatation is the driving force, one usually starts each time step by solving for the temperatures, T^{n+1}, for time t^{n+1} using the geometry $\boldsymbol{x}^n$ where the super-script n denotes the time step. The geometry is updated in the subsequent mechanical analysis for this time step. Thus, the updating of the geometry in the thermal analysis lags one time step behind. It is possible to start with the mechanical analysis and perform the thermal analysis afterward during each time step. In that case, the thermal load in the mechanical analysis is one time step behind. It is also possible to iterate between the thermal and mechanical analyses in order to reduce the out-of-phase effect in either thermal or mechanical analysis. Another approach is to solve for temperatures and displacements simultaneously. However, this leads to an unsymmetrical system of coupled nonlinear equations. It is generally considered unnecessary to solve that complicated system of equations since the coupling is normally quite weak for welding processes.

The heat generated by the deformation can be ignored in the case of welding. In addition, it has been demonstrated that it is possible to neglect the heat caused by the strain rate for a wide class of thermo-elastic problems (couplings #4c and #4d) and that it is consistent to ignore the inertia forces at the same time. Thus, the mechanical analysis can be assumed to be quasi-static, meaning

that the inertia forces can be ignored although the deformation is changing with time. The thermal strain rate (coupling #4c) coupling can be accounted for directly in the heat transfer analysis by modifying the heat capacity. It was also shown that the heat generated by the plastic dissipation (coupling#4b) can be safely ignored. This conclusion is confirmed when the heat input is compared to the plastic dissipated energy. However, it is not computationally expensive to include the heat caused by plastic dissipation if the thermal and mechanical analyses are performed using the same software and a staggered approach.

In order to account for the effects of micro-structural changes in welding processes, some researchers performed thermal analysis followed by metallurgical analyses and then, mechanical simulations. Numerical simulations involving fully coupled thermo-metallurgical analyses followed by subsequent mechanical analyses were also performed. However, the effects of the deformation on the microstructure evolution and on the heat conduction (couplings #4 and #6 in Figure 1) were ignored in all these analyses. Fully coupled thermo-metallurgical and mechanical (TMM) analyses of multi-pass welding have been performed using a staggered approach. Some preliminary studies on the influence of stress on the microstructure evolution (coupling #6) have been published, but this has not yet been accounted for in welding simulation.

Based on the previous studies published in the literature, welding often leads to significant distortions, and thus large deformation analyses are often required. Although small strain approximations were normally sufficient for weld simulations, appropriate co-rotational stress measures must be used as even moderate rotations can generate spurious stresses. The uncoupled, quasi-static method for computing the thermal stresses is accurate, but it is often convenient to use the staggered approach. If the whole analysis is performed using the same software, the data communication of the temperatures from the thermal analysis to the mechanical analysis via disk file might be avoided. This approach is necessary if one needs to account for thermal boundary conditions that depend on the deformation (coupling#4a) as well as the microstructure evolutions.

The general considerations for finite element modelling are, of course, also relevant in this field. Two notes in this respect need to be emphasized here. The first concerns the consistency between the thermal and mechanical analysis and the choice of element. The degree of the finite element shape functions for the displacements should be one order higher than for the thermal analysis due to the fact that the temperature field directly becomes the thermal strain in the mechanical analysis, whereas strains related to displacements are evaluated from the derivatives of the nodal displacement. However, in finite element weld simulations, the same elements are usually used in both the thermal and mechanical analyses, and the lower-order elements are often employed as they are preferred for nonlinear problems. In this case, the average temperature should be used to generate a constant thermal strain in the mechanical analysis. The second note is concerned with plastic incompressibility. It is important to under-integrate the volumetric strain when using linear elements in order to avoid locking. Then the volumetric strain is constant in the element.

3 Modification of VASTF for Predicting Welding-Induced Transient Temperature Fields

3.1 Nonlinear transient heat transfer analysis

In order to predict the three-dimensional transient temperature field induced by welding during fabrication and repair of submarine pressure hulls, a nonlinear transient heat transfer capability was required. In the present work, such a capability was achieved by using the VASTF finite element heat transfer program [4]. This thermal analysis program was already able to deal with user-defined temperature dependent thermal material properties, such as thermal conductivity, specific heat and density, and various thermal boundary conditions including both convection and radiation. The algorithm utilized in VASTF for nonlinear heat transfer analyses are outlined below.

Finite element spatial discretization of the transient heat conduction equation results in a system of first-order differential equation with temperature-dependent coefficient matrix:

$$\bar{\boldsymbol{C}}^{*}(\boldsymbol{\theta})\,\dot{\boldsymbol{\theta}}(t)+\boldsymbol{K}\boldsymbol{\theta}(t)=\boldsymbol{f}(t) \tag{1}$$

where $\boldsymbol{\theta}$ denotes the nodal temperature vector, $\boldsymbol{C}$ denotes the heat capacity matrix and $\boldsymbol{K}$ the thermal conductivity matrix. The right hand side vector $\boldsymbol{f}$ indicates the time-dependent thermal load which describes the input of thermal power to the finite element system. In order to integrate this system of differential equations in time, a time integration algorithm must be employed. Enforcing the governing equations at time τ between two adjacent time points, t^n and t^{n+1}, and use the following approximations:

$$\begin{aligned}
\boldsymbol{f}(\tau) &= \beta\,\boldsymbol{f}_{n+1}+(1-\beta)\boldsymbol{f}_n \\
\dot{\boldsymbol{\theta}}(\tau) &= (\boldsymbol{\theta}_{n+1}-\boldsymbol{\theta}_n)/\Delta t \\
\boldsymbol{\theta}(\tau) &= \beta\boldsymbol{\theta}_{n+1}+(1-\beta)\boldsymbol{\theta}_n
\end{aligned} \tag{2}$$

where β is an input parameter between zero and one. When the value of β is taken as 0.5 and 1, the time integration method is referred as the Crank-Nicholson scheme and the backward difference scheme, respectively. The integration scheme becomes unconditionally stable when β>0.5. For nonlinear problems, the backward difference scheme (β=1) is normally used to ensure numerical stability.

In nonlinear transient analyses, Newton-Raphson iterations are required within each time step to find converged temperature solutions. Consider the (k)-th iteration in the (n+1)-th time step, the time derivative of temperature can be approximated by:

$$\dot{\boldsymbol{\theta}}_{n+1}^{k} = \left(\boldsymbol{\theta}_{n+1}^{k} - \boldsymbol{\theta}_{n}\right)/\Delta t \tag{3}$$

Substituting this into the governing equations and after some mathematical manipulations, we obtain a system of linear algebraic equations about the temperature increment as:

$$\left(\frac{1}{\Delta t}\overline{\boldsymbol{C}}^{*}\left(\boldsymbol{\theta}_{n+1}^{k-1}\right) + \boldsymbol{K}\right)\Delta\boldsymbol{\theta}_{n+1}^{k} = \boldsymbol{f}_{n+1} - \frac{1}{\Delta t}\overline{\boldsymbol{C}}^{*}\left(\boldsymbol{\theta}_{n+1}^{k-1}\right)\left(\boldsymbol{\theta}_{n+1}^{k-1} - \boldsymbol{\theta}_{n}\right) - \boldsymbol{K}\,\boldsymbol{\theta}_{n+1}^{k-1} \tag{4}$$

Once the vector of temperature increment is obtained, the nodal temperatures are updated as:

$$\boldsymbol{\theta}_{n+1}^{k} = \boldsymbol{\theta}_{n+1}^{k-1} + \Delta\boldsymbol{\theta}_{n+1}^{k} \tag{5}$$

This iteration process is repeated until

$$\left(\frac{\left(\Delta\boldsymbol{\theta}_{n+1}^{k}\right)^{T}\left(\Delta\boldsymbol{\theta}_{n+1}^{k}\right)}{\left(\boldsymbol{\theta}_{n+1}^{k}\right)^{T}\left(\boldsymbol{\theta}_{n+1}^{k}\right)}\right)^{1/2} < \varepsilon \tag{6}$$

is satisfied, where ε is a pre-set small positive number.

3.2 Improvement of thermal boundary conditions

Heat loss from the free surface of the thermal analysis model due to convection and radiation has a significant effect on the predicted temperature field. These heat fluxes across the free surface can be accounted for using a temperature-dependent heat transfer coefficient, *h(θ)*, that considers the combined effects of convection and radiation given as

$$f_C = h(\theta)(\theta_E - \theta) \tag{7}$$

where f_c denotes the heat flux going into the element through the free surface; θ is the surface temperature and θ_E is the temperature of the environment. For weld simulations, a temperature dependent heat transfer coefficient has been suggested to combine the convection and radiation effects as [5]:

$$h(\theta) = 24.1\times10^{-4}\,\varepsilon\,\theta^{1.61}\ \ (W/m^2K) \tag{8}$$

where ε is the emissivity of the material and θ is the element surface temperature in Kelvin. In the finite element method, the combined convection and radiation heat flux through the element surface, f_c, is converted to the nodal variables so that we have

$$\boldsymbol{f}_c(\boldsymbol{\theta}) = \left[\int_V \boldsymbol{N}^T h(\boldsymbol{\theta})\boldsymbol{N}\,dV\right](\boldsymbol{\theta}_E - \boldsymbol{\theta}) = \boldsymbol{K}_C(\boldsymbol{\theta})(\boldsymbol{\theta}_E - \boldsymbol{\theta}) \tag{9}$$

Substituting Equation (9) into (4) leads to

$$\left(\frac{1}{\Delta t}\boldsymbol{C}\left(\boldsymbol{\theta}_{n+1}^{k-1}\right)+\boldsymbol{K}\left(\boldsymbol{\theta}_{n+1}^{k-1}\right)+\boldsymbol{K}_C\left(\boldsymbol{\theta}_{n+1}^{k-1}\right)\right)\Delta\boldsymbol{\theta}_{n+1}^{k}= \\ \boldsymbol{f}_{n+1}-\frac{1}{\Delta t}\boldsymbol{C}\left(\boldsymbol{\theta}_{n+1}^{k-1}\right)\left(\boldsymbol{\theta}_{n+1}^{k-1}-\boldsymbol{\theta}_n\right)-\boldsymbol{K}\left(\boldsymbol{\theta}_{n+1}^{k-1}\right)\boldsymbol{\theta}_{n+1}^{k-1}-\boldsymbol{K}_C\left(\boldsymbol{\theta}_{n+1}^{k-1}\right)\left(\boldsymbol{\theta}_{n+1}^{k-1}-\boldsymbol{\theta}_E\right) \tag{10}$$

Heat loss due to radiation from the molten weld metal is accounted for in the efficiency of the welding process; therefore heat loss due to radiation from weld elements under the current position of the heat source is not considered.

3.3 Modelling of moving heat source

The heat source, generating heat at rate Q, is modeled using a volumetric heat generation rate within the weld elements being deposited at time t. This heat input is defined by user input values of the welding process efficiency η, arc current I, and voltage V such that:

$$Q = \eta\, I\, V \tag{11}$$

Many models have been proposed for describing the spatial distribution of the volumetric heat generation rate around the weld heat source. These models were developed based on the Gaussian distribution function and the commonly used ones included the hemispherical power distribution model, the ellipsoidal power distribution model and the double ellipsoidal power distribution model. Among these models, the double ellipsoidal heat source model, originally developed by Goldak and co-workers [6], provided the highest flexibility in numerical modelling, and so has been widely accepted for computation weld mechanics. In this model, the volumetric heat generate rate around the weld beam location is expressed as two semi-ellipsoids as:

$$q = f_f\, Q\frac{6\sqrt{3}}{\pi\sqrt{\pi}abc_f}e^{-3(x/a)^2}e^{-3(y/b)^2}e^{-3\left(z/c_f\right)^2} \quad for\ z \geq 0 \tag{12}$$

$$q = f_r\, Q\frac{6\sqrt{3}}{\pi\sqrt{\pi}abc_r}e^{-3(x/a)^2}e^{-3(y/b)^2}e^{-3(z/c_r)^2} \quad for\ z < 0$$

where Q indicates the heat input in Equation (11) and the various geometric dimensions in the above expression are defined in Figure 3. Parameters f_f and f_r indicate fractions of heat deposited in the front and rear quadrants, where $f_f + f_r = 2$.

In the present work, the double ellipsoidal power density model was implemented in VASTF. In this implementation, numerical integration over the volume of the solid element was used to compute the equivalent nodal heat fluxes. In finite element solutions of the heat transfer problems for weld simulations, it is extremely important to ensure that the total energy input in the structure be represented accurately. As a result, a numerical study was been carried out to investigate the effects of the finite element mesh and the order of numerical integrations on the accuracy of the computed nodal fluxes. In this study, the following heat source parameters were considered:

a=5.0 mm, b=5.0 mm, c_f=5.0 mm, c_r =10.0 mm, f_f=0.6, f_r=1.4, Q=1.0

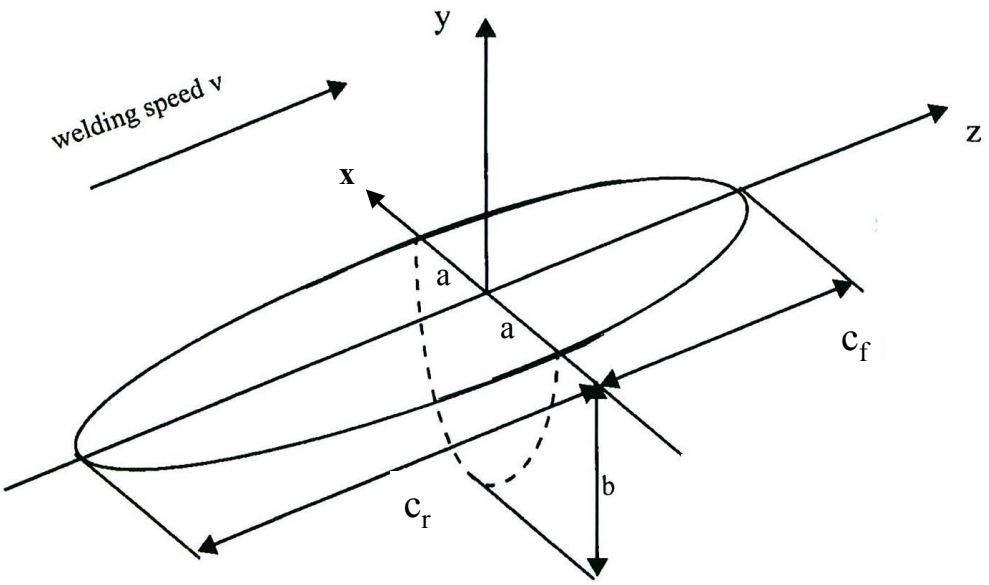

Figure 3: Geometry of a double ellipsoid heat source for welding simulations.

The numerical study was carried out using a three dimensional block with dimensions shown in Figure 4, which was discretized into 8-noded solid finite elements with different levels of mesh refinement as displayed in Figure 5. To describe the power distribution, a local coordinate system must be defined and updated continuously when the weld heat source is moving across the element surface, so at a given time, the heat source may or may not coincide with a node in the model and the axes of the local system may not be parallel to the element edges. In order to cover different situations in the actual weld simulation, four local coordinates were considered. In the first three cases, the axes of the local coordinate system were parallel to the axes of the global coordinate system, but the origin of the local system was placed at different locations as marked in Figure 4. In the fourth case, the origin of the local system was at the center of upper surface of the block (point 1), but the local system was rotated about the local y-axis, so that the weld direction was at an angle to the global X-axis as indicated by the line on the upper surface in Figure 4.

Because the total heat generation rate was set to one in the test case, the sum of all the computed nodal heat fluxes must also be one to preserve the correct heat input. This was used as a criterion to measure the accuracy of the calculation. The results that VASTF generated by using different meshes and various orders of Gaussian integration are summarized in Tables 1-4 for the four local coordinate systems. These results suggest that in order to ensure accuracy of the results, higher order numerical integration should be utilized. Numerical results were also obtained by including only the integration points inside the double ellipsoidal surface. These results indicate that if only these integration points were included, the sum of the nodal heat fluxes is about 88% of the total heat input. In this case, the computed nodal heat fluxes must be scaled up to ensure that the proper amount of thermal energy was applied in the heat transfer analysis.

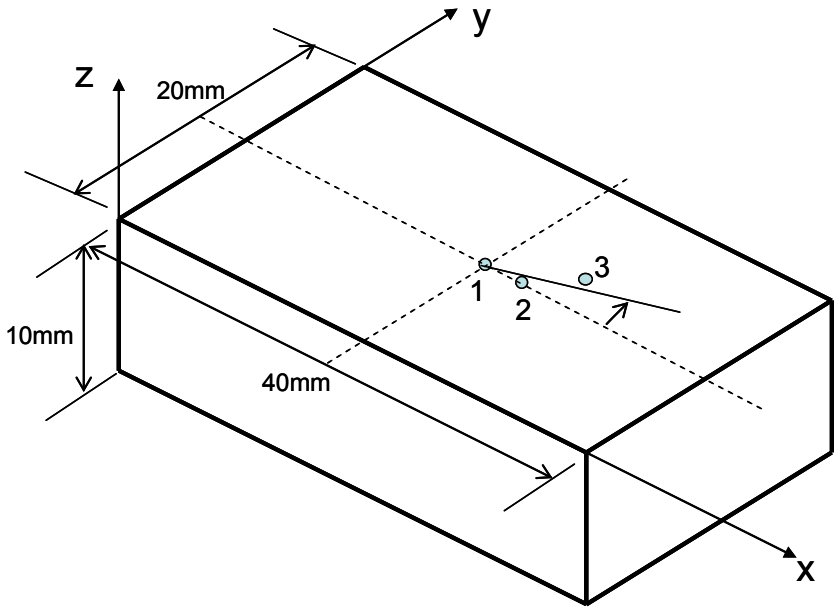

Figure 4: Test case for evaluating accuracy of heat source calculations.

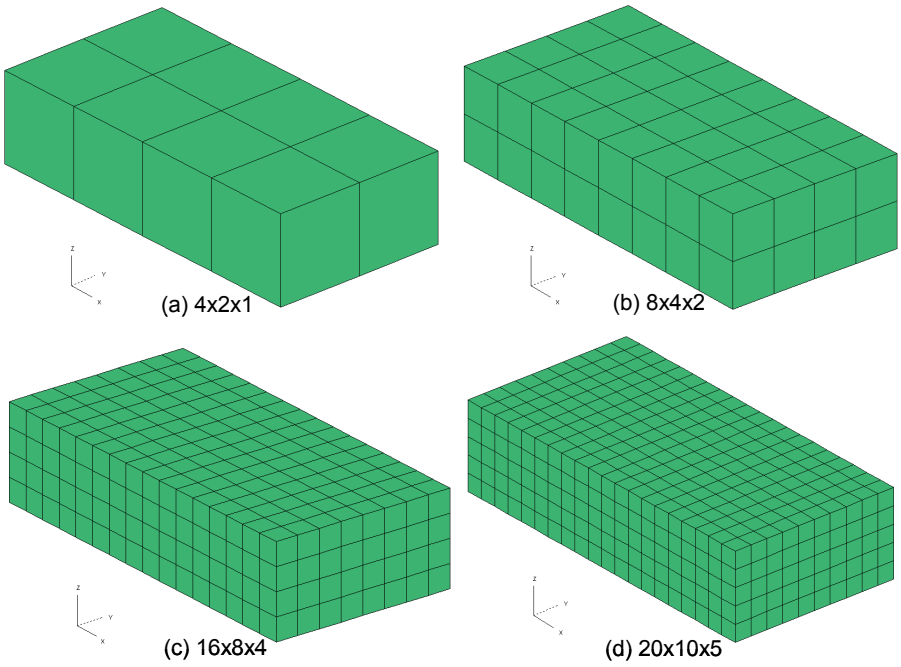

Figure 5: Finite element meshes utilized for investigating accuracy of computed equivalent nodal heat input using the double ellipsoidal power distribution model.

Table 2: Sum of equivalent nodal heat input computed when the origin of weld source coordinate system is at point 1 (20, 10, 0).

Mesh	Order of Numerical Integration			
	2×2×2	**3×3×3**	**5×5×5**	**10×10×10**
4×2×1	1.3054	1.0135	1.0010	0.9999
8×4×2	1.0222	0.9979	0.9999	0.9999
16×8×4	0.9999	0.9999	0.9999	0.9999
20×10×5	0.9999	0.9999	0.9999	0.9999

Table 3: Sum of equivalent nodal heat input computed when the origin of weld source coordinate system is at Point 2 (22.5, 10, 0).

Mesh	Order of Numerical Integration		
	3×3×3	**5×5×5**	**10×10×10**
4×2×1	0.9936	0.9215	1.0235
8×4×2	1.0789	1.0490	0.9997
16×8×4	0.9997	0.9997	0.9997
20×10×5	0.9956	0.9839	1.0044

Table 4: Sum of equivalent nodal heat input computed when the origin of weld source coordinate system is at Point 3 (25, 15, 0).

Mesh	Order of Numerical Integration		
	3×3×3	**5×5×5**	**10×10×10**
4×2×1	1.2193	1.0926	0.9912
8×4×2	0.9891	0.9912	0.9912
16×8×4	0.9912	0.9912	0.9912
20×10×5	0.9867	0.9964	0.9912

Table 5: Sum of equivalent nodal heat input computed when the origin of weld source coordinate system is at point 1 and the weld beam moves in a direction in angles with global X-axis. (Order of numerical integration=3×3×3)

Mesh	Angle Between Weld Beam and X-Axis		
	5°	**10°**	**15°**
4×2×1	1.0102	1.0023	0.9942
8×4×2	0.9980	0.9984	0.9988
16×8×4	0.9999	0.9999	0.9999
20×10×5	0.9999	0.9999	0.9999

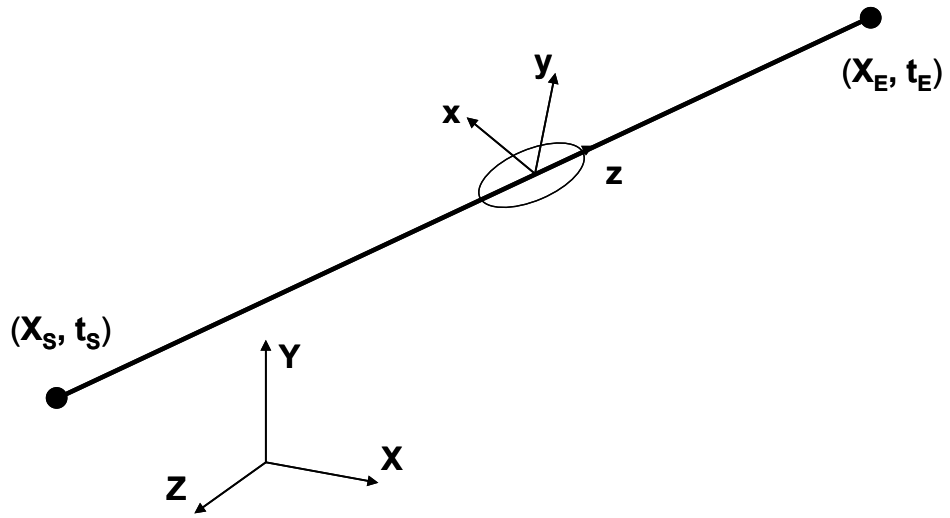

Figure 6: Definition of a weld pass.

During the implementation of the weld simulation capability in VASTF, special care was taken when designing the user input for describing the moving heat source to permit multi-pass weld, while maintaining simplicity of the input data. In order to achieve these requirements, multiple weld pass functions are defined in the solution control file, Prefx.HUS. Each function contains three parts of data. The first part is the geometric parameters of the Goldak double ellipsoidal power distribution model, such as a, b, c_f, c_r, f_f and f_r, and the power input parameters including weld efficiency η, current I and voltage V. The second part of data contains the starting and ending locations and times for the current weld pass, as illustrated in Figure 6 above. That data permits determination of the weld direction and speed. The third part of the data contains direction cosines of the outwards normal of the surface, i.e., the local y-direction, on which the weld heat input is applied. Using these user supplied description of a weld pass, the origin of the double ellipsoidal power distribution function $\boldsymbol{X}_C$ and the associated local coordinate system can be constructed for any given time point t during the welding process as

$$\boldsymbol{X}_C = \boldsymbol{X}_S + \left(\boldsymbol{X}_E - \boldsymbol{X}_s\right)\frac{t - t_S}{t_E - t_S} \tag{13}$$

and

$$\boldsymbol{e}_y = \frac{\boldsymbol{V}}{\|\boldsymbol{V}\|},\ \boldsymbol{e}_z = \frac{\boldsymbol{X}_E - \boldsymbol{X}_S}{\|\boldsymbol{X}_E - \boldsymbol{X}_S\|},\ \boldsymbol{e}_x = \boldsymbol{e}_y \times \boldsymbol{e}_z \tag{14}$$

It should be noted that in this implementation, the weld surface was assumed to be flat and heat source was assumed to move in a straight line. However, this limitation can be eliminated in the future by adopting a general curve description in 3D as long as it is able to return the origin and local axes of the double ellipsoidal heat source function for any given time t.

In VASTF, multiple element groups can be used to represent the weld materials, but each of the element groups must be associated with a certain weld pass function. We believe that this was a reasonable assumption because in weld simulations, a given finite element representing the weld material was normally associated with a specific weld pass. During the computation of element heat capacity and thermal conductivity matrices, an algorithm was used to determine whether the current weld element has been passed by the weld heat source. Three cases were considered. If the current time, i.e., the end time of the current time step, t_{n+1}, was less than the starting time of the weld pass function assigned to this finite element, t_S, this element was not yet passed by the heat source. If the current time was greater than the ending time of the weld pass function, t_E, the element must have been passed by the heat source. If the current time was in the time range of the active weld heat source, the local coordinates of all the nodes and numerical integration points were first computed as

$$x = \boldsymbol{e}_x^{\,T}\left(\boldsymbol{X} - \boldsymbol{X}_C\right),\ \ y = \boldsymbol{e}_y^{\,T}\left(\boldsymbol{X} - \boldsymbol{X}_C\right),\ \ z = \boldsymbol{e}_z^{\,T}\left(\boldsymbol{X} - \boldsymbol{X}_C\right) \tag{15}$$

and then checked against the double ellipsoid by evaluating

$$R = \begin{cases} \left(\dfrac{x}{a}\right)^2 + \left(\dfrac{y}{b}\right)^2 + \left(\dfrac{z}{c_f}\right)^2 & for\ z \geq 0 \\ \left(\dfrac{x}{a}\right)^2 + \left(\dfrac{y}{b}\right)^2 + \left(\dfrac{z}{c_r}\right)^2 & for\ z < 0 \end{cases} \tag{16}$$

where R=1 indicates that the point is on the surface of the double ellipsoid, while R>1 (R<1) denotes that the point is outside (inside) the double ellipsoid. If any of these points were inside or behind the ellipsoid, the element was considered to have been passed by the heat source. In this case, the element will be activated and the real material properties were assigned to this element. For elements that were not yet passed by the heat source, the thermal conductivity was reduced by a factor of 1000 to prevent heat leak through these elements. However, all elements were maintained in the finite element model during the transient solution. This element birth and death algorithm is summarized in Table 6, where IPASS=1 means that the element has been passed by the heat source, so the element needs to be activated.

Table 6: Summary of element birth/death algorithm for weld simulation

t	***R***	***z***	**IPASS**
$t>t_E$	-	-	1
$t_S \leq t \leq t_E$	$R\leq 1$	-	1
	$R>1$	$z<0$	1
		$z>0$	0
$t<t_S$	-	-	0

3.4 Verification of VASTF for weld simulation

In order to verify the weld simulation capability in VASTF, the flat-bar welding example initially considered by Deng et al [7] and later by Gannon [8] was utilized. The thermal properties of the base metal and the weld materials were assumed to be identical and temperature-dependent as shown in Figure 7. These material property data were taken from the ANSYS model prepared by Gannon [8]. The finite element mesh used in the present verifications was also identical to the one used by Gannon [8] which is reproduced in Figure 8.

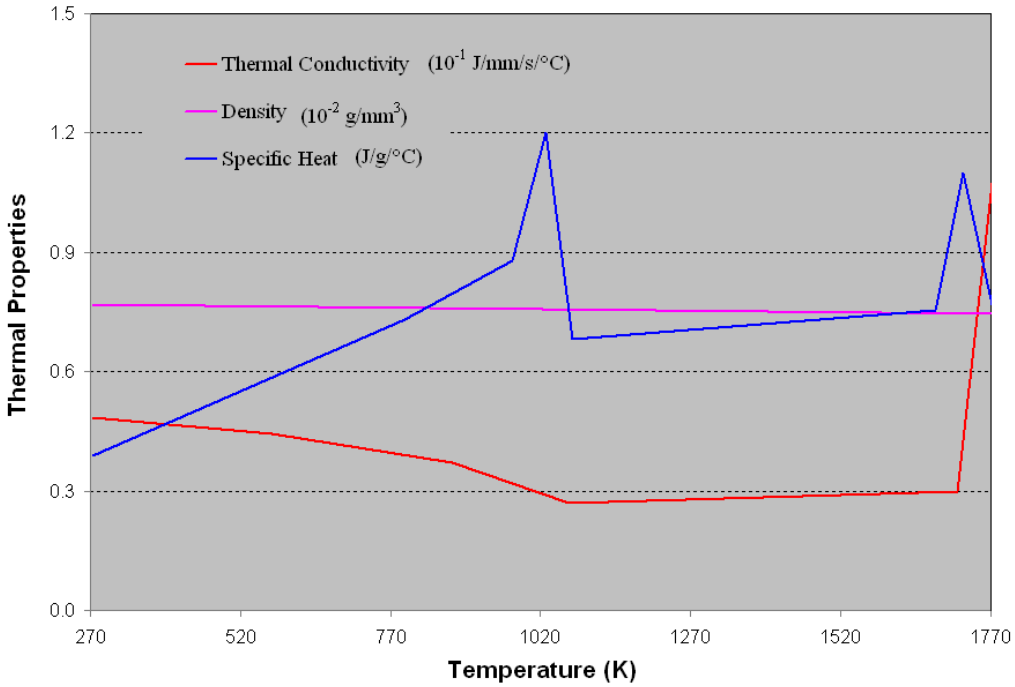

Figure 7: Temperature-dependent thermal properties used in verification of VASTF for weld simulation.

Four different weld sequences were considered as shown in Figure 9. In the VASTF model, each of the four weld passes involved in these weld sequences were represented by a weld pass function, where the parameters of the double ellipsoidal heat source model were defined as

$$a=b=c_f=c_r=4\ mm, f_f=f_r=1.0, I=270\ A, v=29\ V, \eta=0.8.$$

The weld speed was 400 mm/min or 6.666 mm/s. The weld elements, as shown at the bottom of Figure 8, were divided into four element groups, and each group was associated with a weld pass function. The time-dependent nodal heat flux vectors were generated using a time interval of 0.75 second.

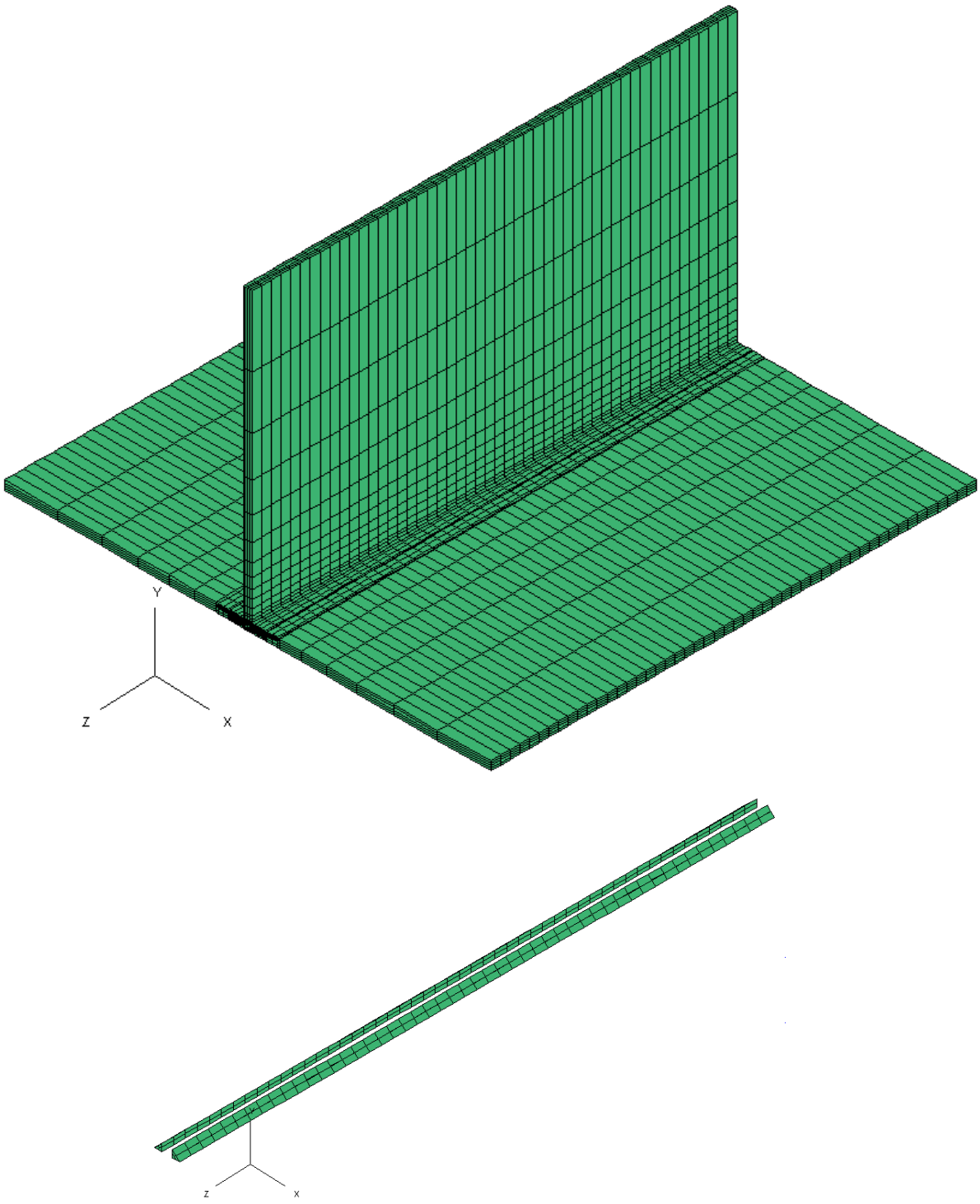

Figure 8: Structural (upper) and weld (lower) elements in heat transfer finite element model for welding simulations.

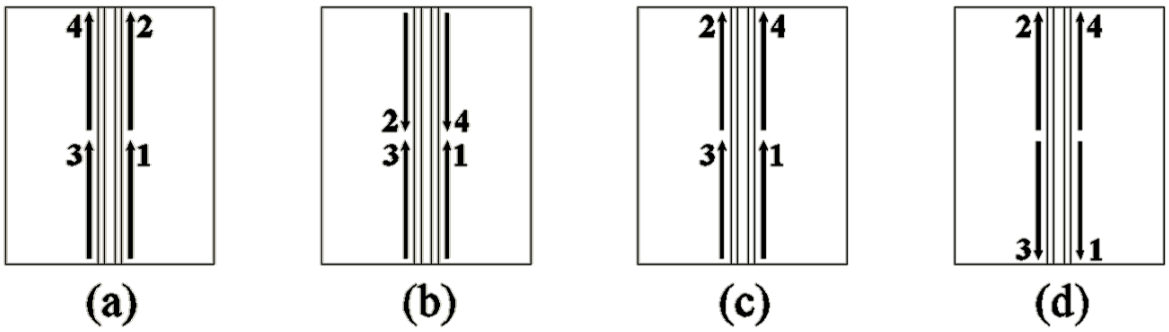

Figure 9: The four weld sequences considered in the present weld simulations.

The VASTF predicted temperature time histories at selected points on both sides of the flat-bar and temperature contours at different time points are shown in Figures 8-15, where points A and C were at the toe of the weld and points B and D were on the bottom of the plate on the left and right sides of the stiffener, respectively, at the mid-span of the model. Numerical experiments demonstrated that to achieve convergence, at least five steps (Δt=0.3 s) were required to let the heat source pass a weld element. In order to benchmark the accuracy of numerical results obtained using different time step sizes, two heat transfer analyses were performed using time step sizes of 0.3 s and 0.15 s, for which 500 and 100 time steps were required to cover the whole weld sequences of around 150 s. Using the sparse solver in VASTF with the default options, these heat transfer analyses took 5 and 10 hours, respectively, on a reasonably fast computer. The VASTF results for weld sequence #1 obtained using different time steps are compared with Gannon's ANSYS solutions in Figure 14. A good agreement is obtained between VASTF and ANSYS solutions.

Spurious oscillations with negative temperature increment (spurious cooling) appeared in front of the weld heat source in VASTF solutions. Similar temperature profiles were also observed in the ANSYS solutions [9]. Numerical investigations showed that these spurious oscillations were related neither to the element birth algorithm (reduction of thermal conductivity) nor to an excessively large time step size. It was suspected that this numerical error was due to the coarseness of the finite element model. Because the finite element mesh was too coarse to properly represent the extremely high temperature gradient behind the heat source, the enforcement of the governing equations resulted in negative temperature increment. This hypothesis is still to be confirmed by using a locally refined model.

In order to generate a smoothed temperature field for stress analysis and also to reduce spurious oscillations in temperature solutions, a smoothing algorithm was developed for the temperatures by averaging nodal temperatures over each element. The smoothed temperatures are also shown in the Figures and will be used in the thermal stress calculations to be addressed in the next chapter.

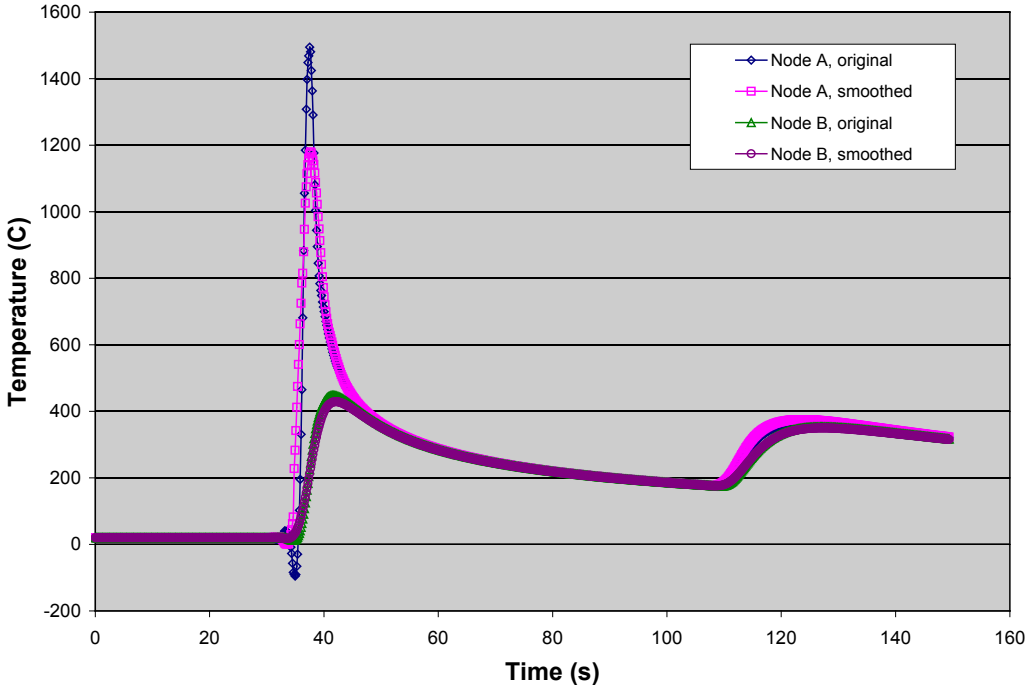

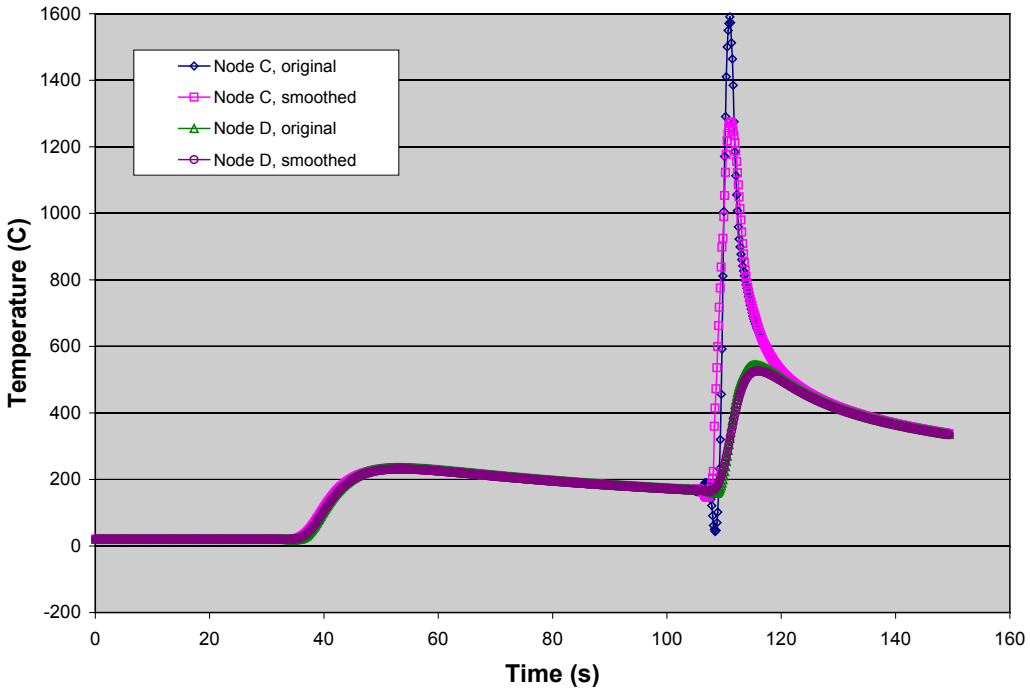

Figure 10: VASTF predicted temperature time histories at points A-D for weld sequence 1 (Δt=0.15 s).

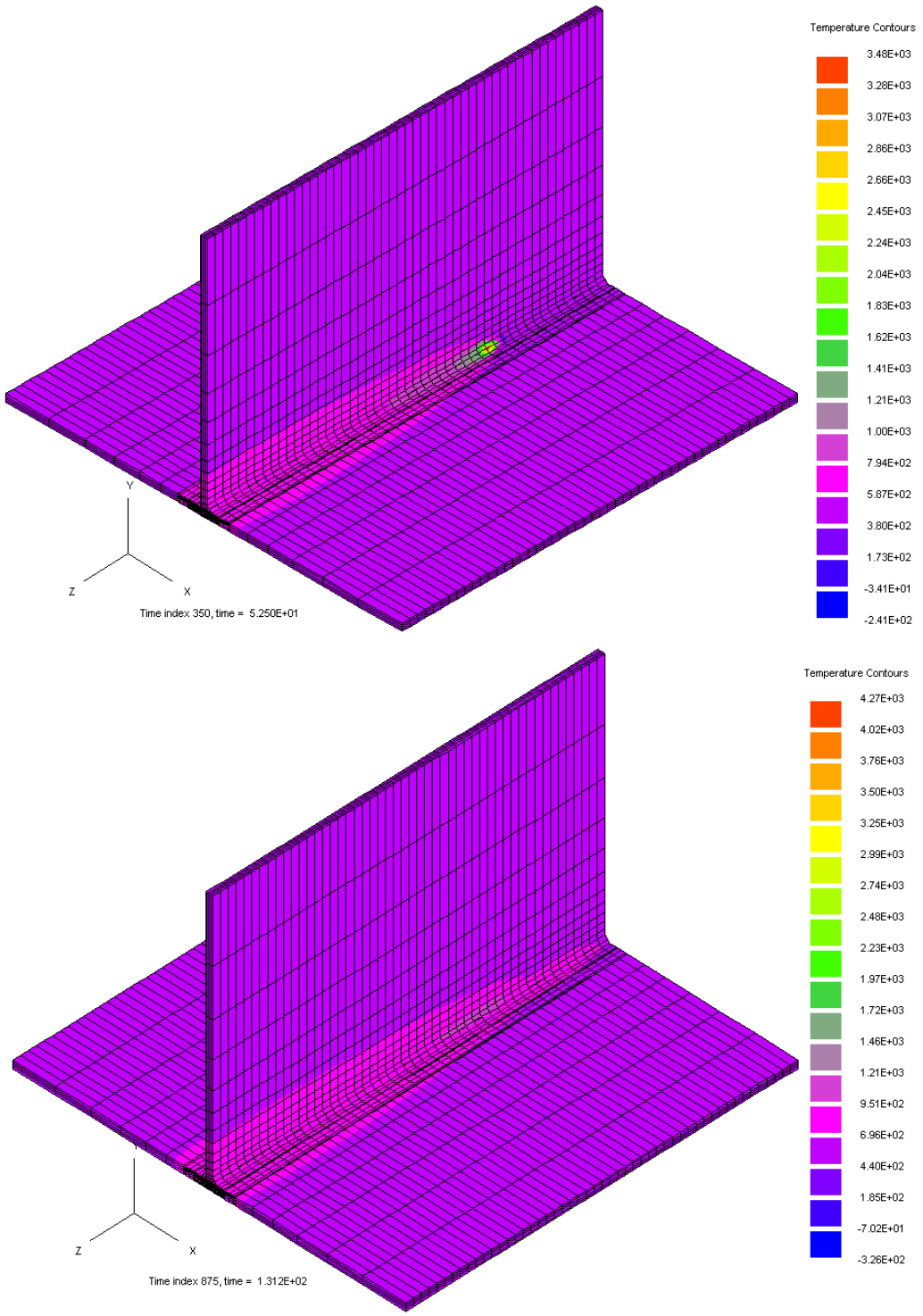

Figure 11: VASTF predicted temperature fields at different time points for weld sequence 1 (Δt=0.15 s).

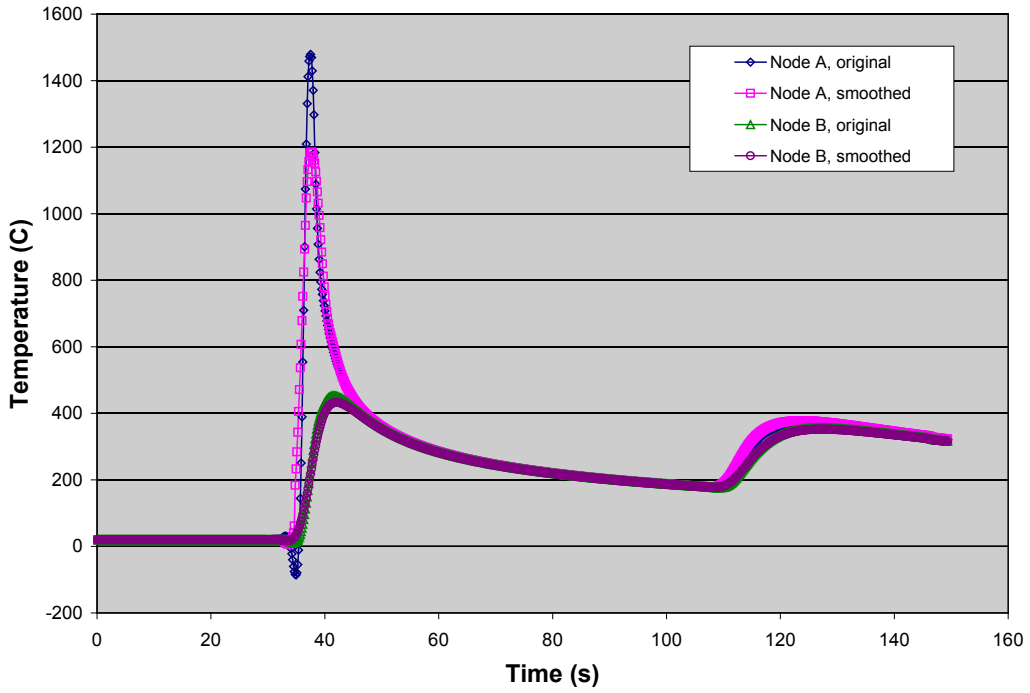

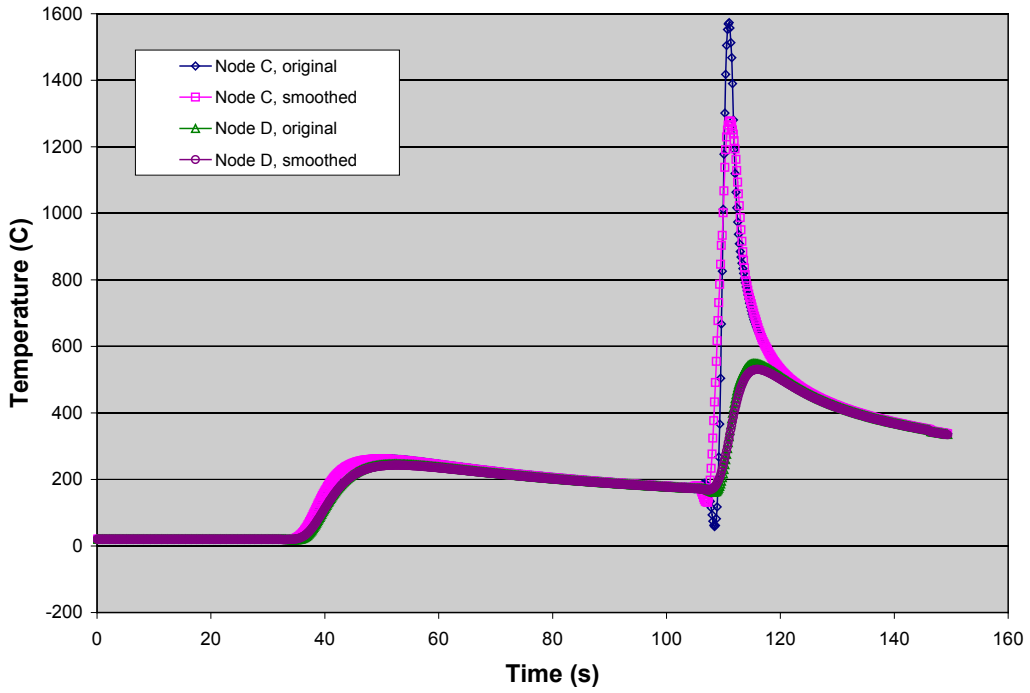

Figure 12: VASTF predicted temperature time histories at points A-D for weld sequence 1 (Δt=0.15 s) in which full thermal conductivity was used in weld elements in front of the weld heat source.

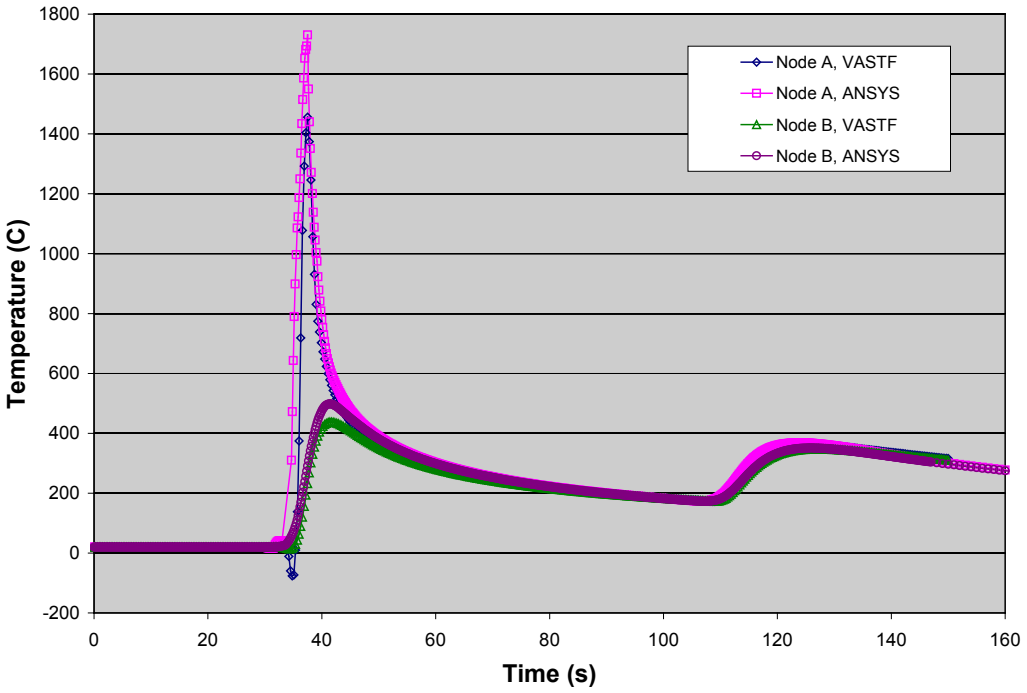

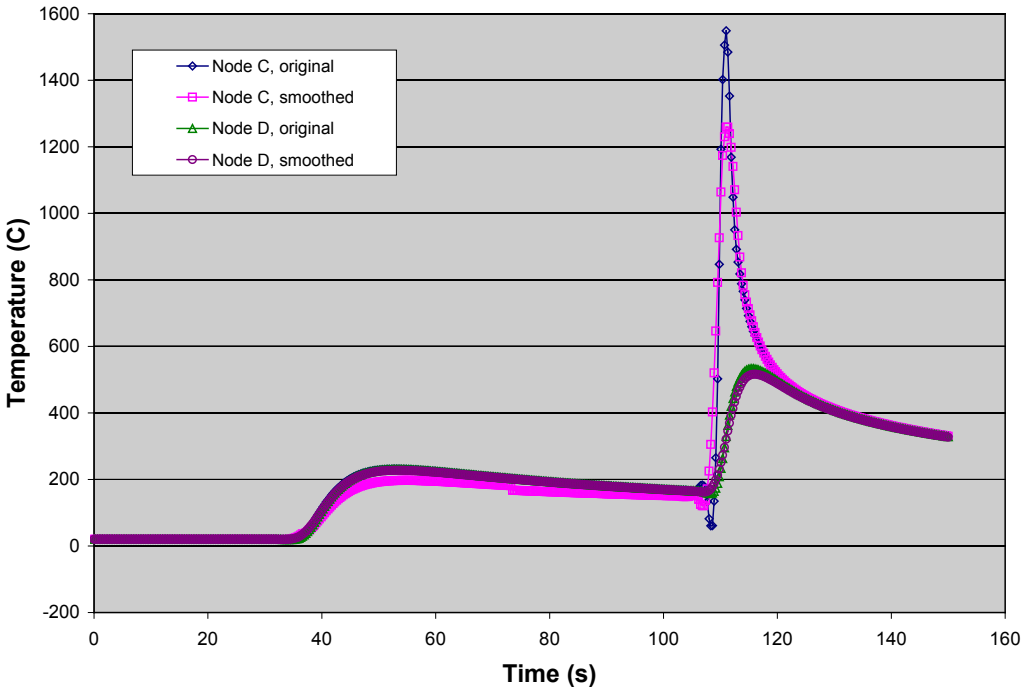

Figure 13: VASTF predicted temperature time histories at points A-D for weld sequence 1 (Δt=0.3 s).

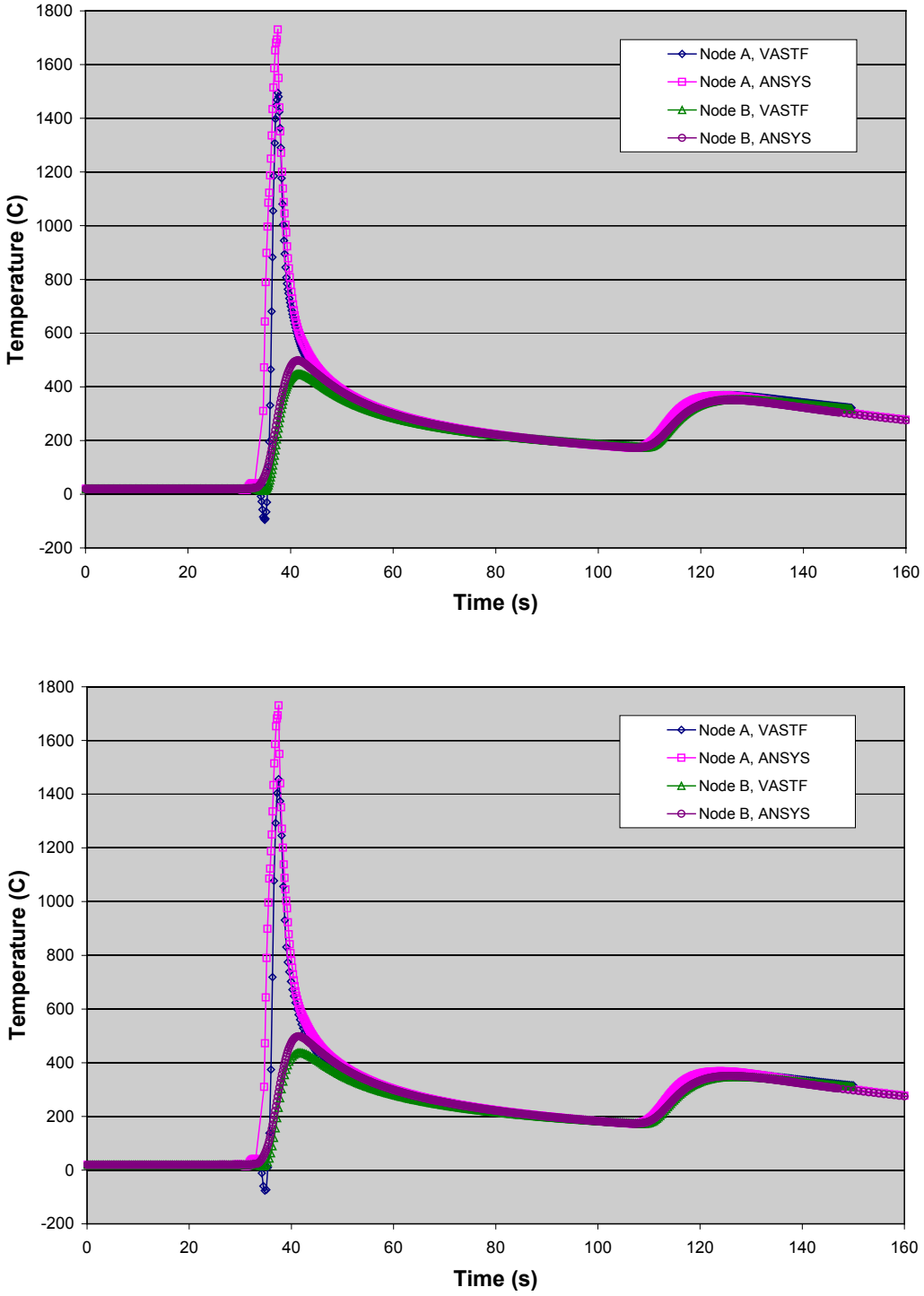

Figure 14: Comparison of VASTF and ANSYS predicted temperature time histories at points A-D for weld sequence 1. The VASTF results were obtained using Δt=0.15 s (upper) and 0.3 s (lower), respectively.

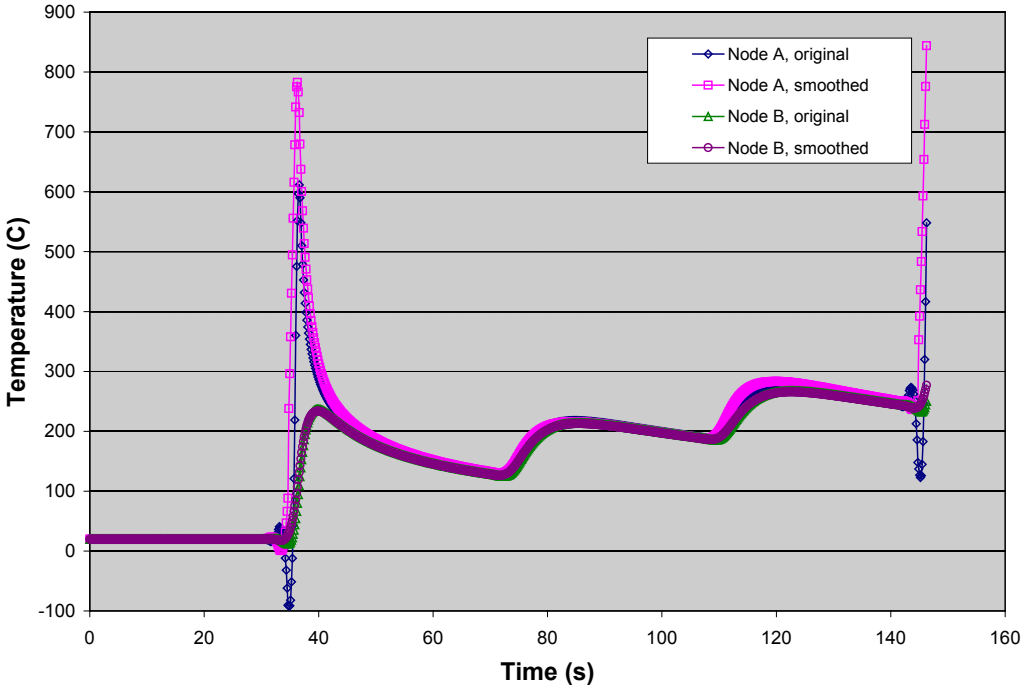

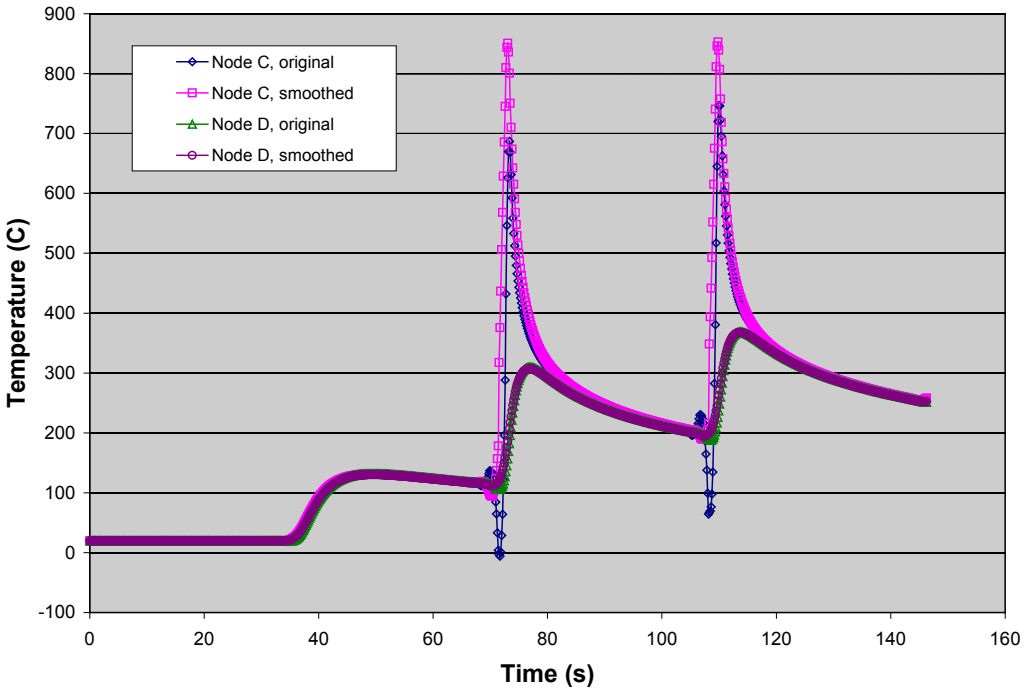

Figure 15: VASTF predicted temperature time histories at points A-D for weld sequence 2 (Δt=0.15 s).

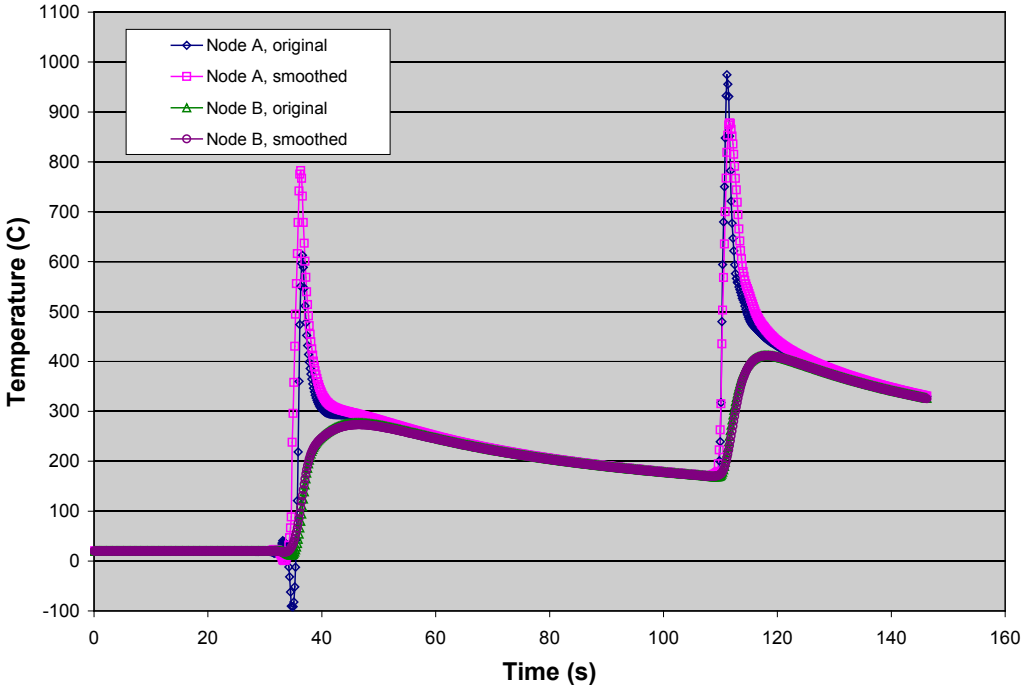

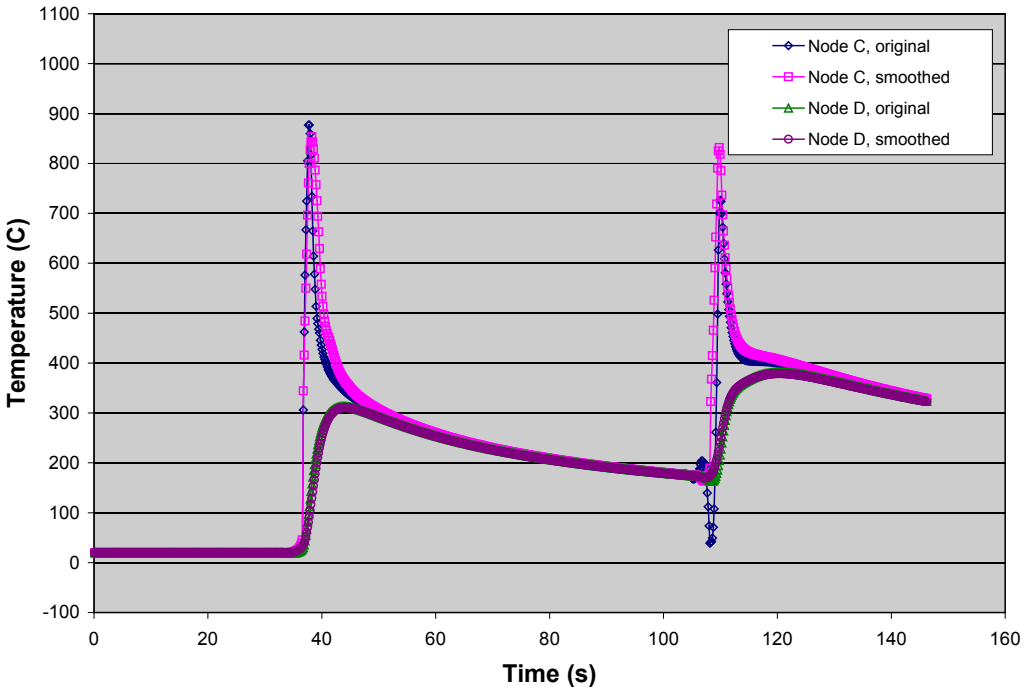

Figure 16: VASTF predicted temperature time histories at points A-D for weld sequence 3 (Δt=0.15 s).

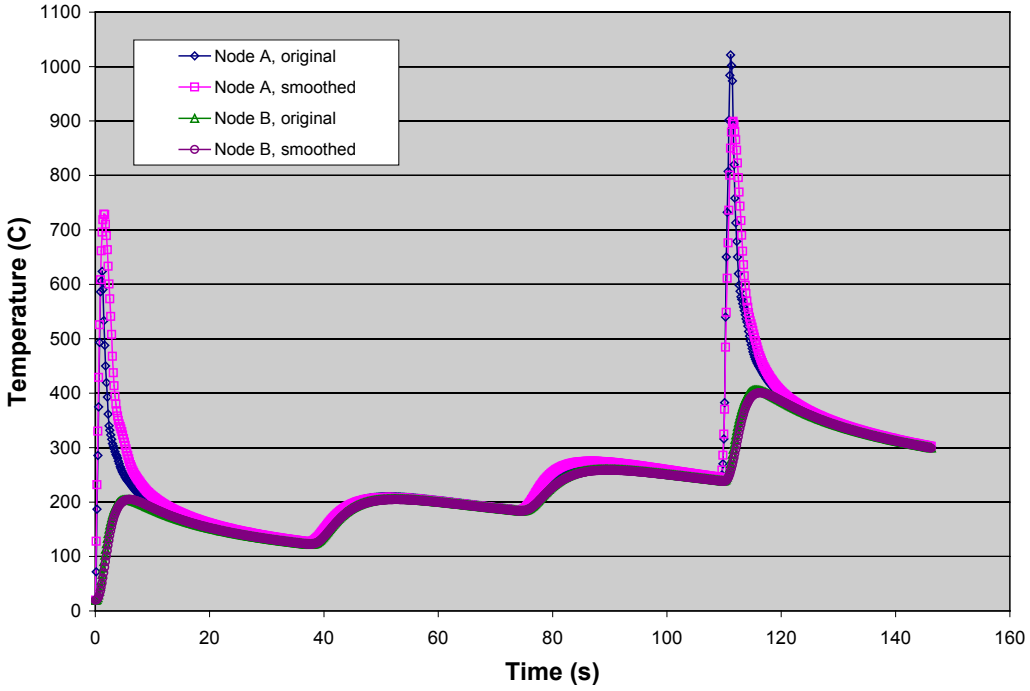

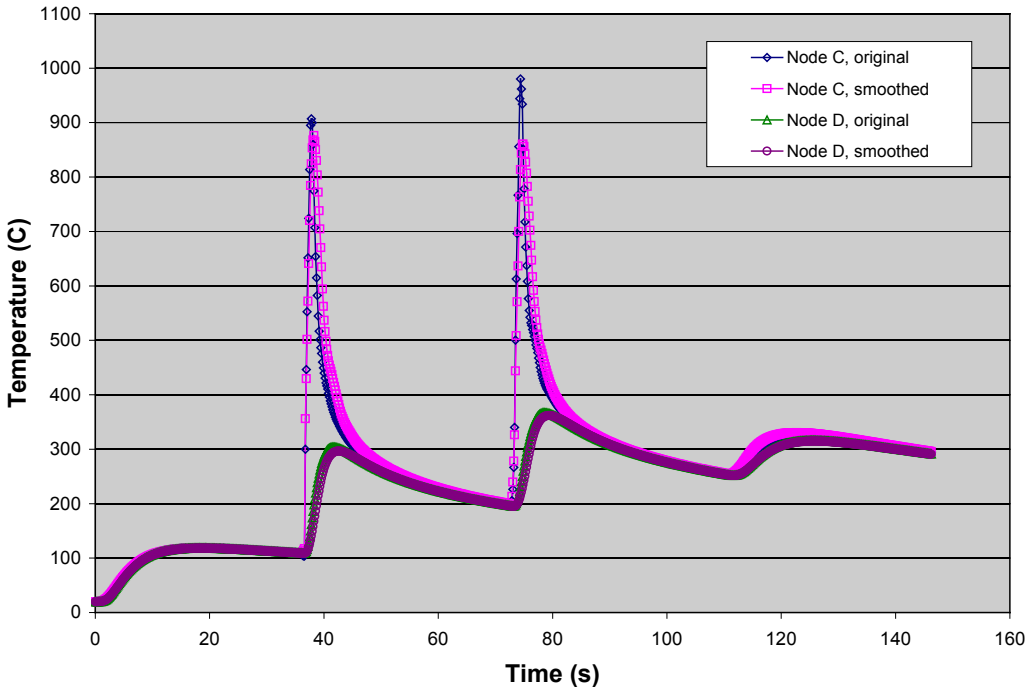

Figure 17: VASTF predicted temperature time histories at points A-D for weld sequence 4 (Δt=0.15 s).

4 Modification of VAST for Predicting Welding-Induced Residual Stress and Distortion

4.1 Temperature-dependent material properties

In order to perform nonlinear thermal-elastic-plastic analysis required in weld simulations, the structural analysis capabilities of the VAST finite element program was first enhanced to permit temperature-dependent nonlinear material properties. These properties include:

- Young's modulus, E
- Poisson's ratio, ν
- Yield stress, σ_Y
- Hardening modulus, H
- Coefficient of thermal expansion, α

The melting and solidification temperatures T_m were included as user-defined variables.

In VAST implementation, these temperature-dependent material properties were defined in the form of data tables. During nonlinear dynamic analyses, the values at the desired time points were computed by VAST automatically through interpolation. In addition, an element birth algorithm similar to that described in section 3.3 was also implemented in VAST to keep track of the current location of the moving source. For weld elements that are not yet passed by the heat source, the Young's modulus and coefficient of thermal expansion were reduced by a factor 1000 to avoid excessive stiffness contributions from and stress accumulations in these elements.

4.2 Integration of constitutive relations

The second modification in the VAST program to make it capable for weld simulation was to add thermal strain in the elastic-plastic constitutive model. For a given time step from t^n to t^{n+1}, the thermal strain increment in each direction can be expressed as

$$\Delta\varepsilon_{th}^{n+1} = \alpha\left(T^{n+1}\right)\left(T^{n+1} - T^{n}\right) \tag{17}$$

where the superscript denotes the time and T indicates the temperature. The thermal-elastic-plastic constitutive relation can then be expressed as

$$\boldsymbol{\sigma}^{n+1} = \boldsymbol{\sigma}^{n} + \boldsymbol{D}\left(T^{n+1}\right)\left(\Delta\boldsymbol{\varepsilon}^{n+1} - \Delta\boldsymbol{\varepsilon}_{th}^{n+1} - \Delta\boldsymbol{\varepsilon}_{p}^{n+1}\right) \tag{18}$$

where the thermal strain vector contains thermal strain in all three directions as

$$\Delta\boldsymbol{\varepsilon}_{th}^{n+1} = \left[\Delta\varepsilon_{th}^{n+1} \quad \Delta\varepsilon_{th}^{n+1} \quad \Delta\varepsilon_{th}^{n+1} \quad 0 \quad 0 \quad 0\right]^{T} \tag{19}$$

We noticed that the thermal-elastic-plastic constitutive relation can be decomposed into deviatoric and volumetric components as

$$\begin{aligned} \boldsymbol{S}^{n+1} &= \boldsymbol{S}^{n} + 2G\left(T^{n+1}\right)\left(\Delta\mathbf{e}'^{\,n+1} - \Delta\boldsymbol{\varepsilon}_{p}^{n+1}\right) \\ \sigma_{m}^{n+1} &= \sigma_{m}^{n} + \kappa\left(T^{n+1}\right)\left(\Delta e_{m}^{n+1} - \Delta\varepsilon_{th}^{n+1}\right) \end{aligned} \tag{20}$$

where the mean stress, mean strain, deviatoric stress and deviatoric strain components are defined as

$$\begin{aligned} &\sigma_{m} = \left(\sigma_{11} + \sigma_{22} + \sigma_{33}\right)/3, \quad \Delta\mathrm{e}_{m} = \left(\Delta\varepsilon_{11} + \Delta\varepsilon_{22} + \Delta\varepsilon_{33}\right)/3 \\ &S_{ij} = \sigma_{ij} - \sigma_{m}\,\delta_{ij}\ , \quad \Delta\mathrm{e}'_{ij} = \Delta\varepsilon_{ij} - \Delta\mathrm{e}_{m}\,\delta_{ij} \end{aligned} \tag{21}$$

Equation (20) contains shear and bulk moduli which are related to Young's modulus and Poisson's ration as

$$G\left(T^{n+1}\right) = \frac{E\left(T^{n+1}\right)}{2\left(1+\nu\left(T^{n+1}\right)\right)}, \quad \kappa\left(T^{n+1}\right) = \frac{E\left(T^{n+1}\right)}{1-2\nu\left(T^{n+1}\right)} \tag{22}$$

This decomposition of the thermal-elastic-plastic constitutive relation suggested that the thermal strain components are only related to the mean stress and mean strain, and the plastic strains are fully determined by the deviatoric stress and strain components. This observation indicated that the inclusion of thermal strain could be accomplished by including the thermal strains into the total strain increments as

$$\boldsymbol{\sigma}^{n+1} = \boldsymbol{\sigma}^{n} + \boldsymbol{D}\left(T^{n+1}\right)\left(\Delta\boldsymbol{\varepsilon}'^{\,n+1} - \Delta\boldsymbol{\varepsilon}_{p}^{n+1}\right) \tag{23}$$

where

$$\Delta\boldsymbol{\varepsilon}'^{\,n+1} = \Delta\boldsymbol{\varepsilon}^{n+1} - \Delta\boldsymbol{\varepsilon}_{th}^{n+1} \tag{24}$$

In addition to the element birth algorithm that activated weld elements based on the current location of the moving heat source in a weld simulation, element activation and deactivation in structural analyses also depend upon the average temperature of the element. When the average temperature is above the melting temperature, the element is deactivated so it neither contributes to the global stiffness nor accumulates stress and plastic strains. When the average temperature falls below the material solidification temperature, these elements are reactivated with zero initial plastic strain. The average temperatures in all elements in the finite element model (including both structural and weld elements) were checked at each time step to ensure that any elements whose temperature exceeded the melting temperature were deactivated again during subsequent weld passes.

4.3 Verification of VAST for weld simulations

4.3.1 Single Element Model

In order to verify the thermal stress capability implemented in VAST for weld simulations, we first utilized a single element model with linear elastic material properties subjected to a uniform temperature increment. Three sets of boundary conditions were considered as shown in Figure 18. The first set contained minimum boundary conditions that just suppressed the six rigid body modes of the element, but did not provide any constraints on the deformation of the element. In the second set, the displacements of all eight nodes of the element were fully constrained. In the third set, motions in the X- and Y-directions were constrained, but the Z-direction was left unconstrained to permit thermal expansion.

In order to provide references for verifying the finite element solutions, analytical results for all three boundary conditions were obtained. As mentioned in the previous section, when thermal strains exist, the stress-producing strain components are

$$\varepsilon'_{11} = \varepsilon_{11} - \alpha \Delta T, \quad \varepsilon'_{22} = \varepsilon_{22} - \alpha \Delta T, \quad \varepsilon'_{33} = \varepsilon_{33} - \alpha \Delta T \tag{25}$$

Because the first set of boundary conditions did not produce any stress in the element, we have

$$\varepsilon_{11} = \varepsilon_{22} = \varepsilon_{33} = \alpha \Delta T \tag{26}$$

From these strain values, the nodal displacements in all three directions can be obtained. In the second boundary conditions, the element was fully constrained against any deformation, so

$$\varepsilon_{11} = \varepsilon_{22} = \varepsilon_{33} = 0 \tag{27}$$

From Hooke's law, we obtained the stresses in the element as

$$\sigma_{11} = \sigma_{22} = \sigma_{33} = -\left(\frac{E}{1-2\nu}\right)\alpha \Delta T = -\kappa \alpha \Delta T \tag{28}$$

The treatment of the third set of boundary conditions was more interesting. Because the motions of the element in X and Y directions were fully constrained, we have

$$\varepsilon_{11} = \varepsilon_{22} = 0 \tag{29}$$

so the stress-producing strains were expressed as

$$\varepsilon'_{11} = -\alpha \Delta T, \quad \varepsilon'_{22} = -\alpha \Delta T, \quad \varepsilon'_{33} = \varepsilon_{33} - \alpha \Delta T \tag{30}$$

Substituting this strain expressions into the Hooke's law

$$\sigma_{ii} = \frac{\nu E}{(1+\nu)(1-2\nu)}\left(\varepsilon'_{11}+\varepsilon'_{22}+\varepsilon'_{33}\right)+\frac{E}{1+\nu}\varepsilon'_{ii} \tag{31}$$

and noting that the stress in the Z-direction was zero, we obtained

$$\sigma_{33} = \frac{\nu E}{(1+\nu)(1-2\nu)}\left(-3\alpha\Delta T+\varepsilon_{33}\right)+\frac{E}{1+\nu}\left(-\alpha\Delta T+\varepsilon_{33}\right)=0 \tag{32}$$

Rearranging the terms in this equation resulted in

$$-\frac{E}{1-2\nu}\alpha\,\Delta T+\frac{(1-\nu)E}{(1+\nu)(1-2\nu)}\varepsilon_{33}=0 \tag{33}$$

From this equation, we obtained the strain in the Z-direction as

$$\varepsilon_{33} = \frac{1+\nu}{1-\nu}\alpha\,\Delta T \tag{34}$$

Substituting this strain expression back the Hooke's law, the stresses in the X and Y directions can be obtained as

$$\sigma_{11}=\sigma_{22}=-\frac{E}{1-2\nu}\alpha\,\Delta T+\frac{\nu E}{(1+\nu)(1-2\nu)}\varepsilon_{33}=-\frac{E}{1-\nu}\alpha\,\Delta T \tag{35}$$

For all three sets of boundary conditions, stresses and strains produced by VAST were in exact agreement with these analytical solutions.

Following the success with the linear elastic test cases, we moved on to consider thermal-elastic-plastic deformation of the element under various temperature cycles. The third set of boundary conditions described above was utilized in these nonlinear test cases, where the element was fully constrained in the X and Y directions, but could deform freely along the Z-direction, producing a bi-axial stress state. The temperature-dependent material properties were taken from Gannon's ANSYS model for weld simulations [8] and are shown in Figure 19.

The temperature cycles considered are shown in Figure 20, where the temperature of the element was increased to a maximum temperature T_m from the room temperature 293K and then reduced to the room temperature. This temperature cycle was to simulate the heating and cooling cycles in a weld simulation. Five maximum temperatures, i.e., 600K, 800K, 1000K, 1200K and 1400K, were considered to represent temperatures in elements at different distances from the heat source. In these quasi-static nonlinear thermal stress analyses, the deformation process was induced by the temperature variation in the element which was in turn governed by time. So from the nonlinear finite element solution point of view, time is represented by the load parameter and a load control solution method must be utilized. The arc-length methods and all its variations, including the displacement control method, are not applicable to this problem.

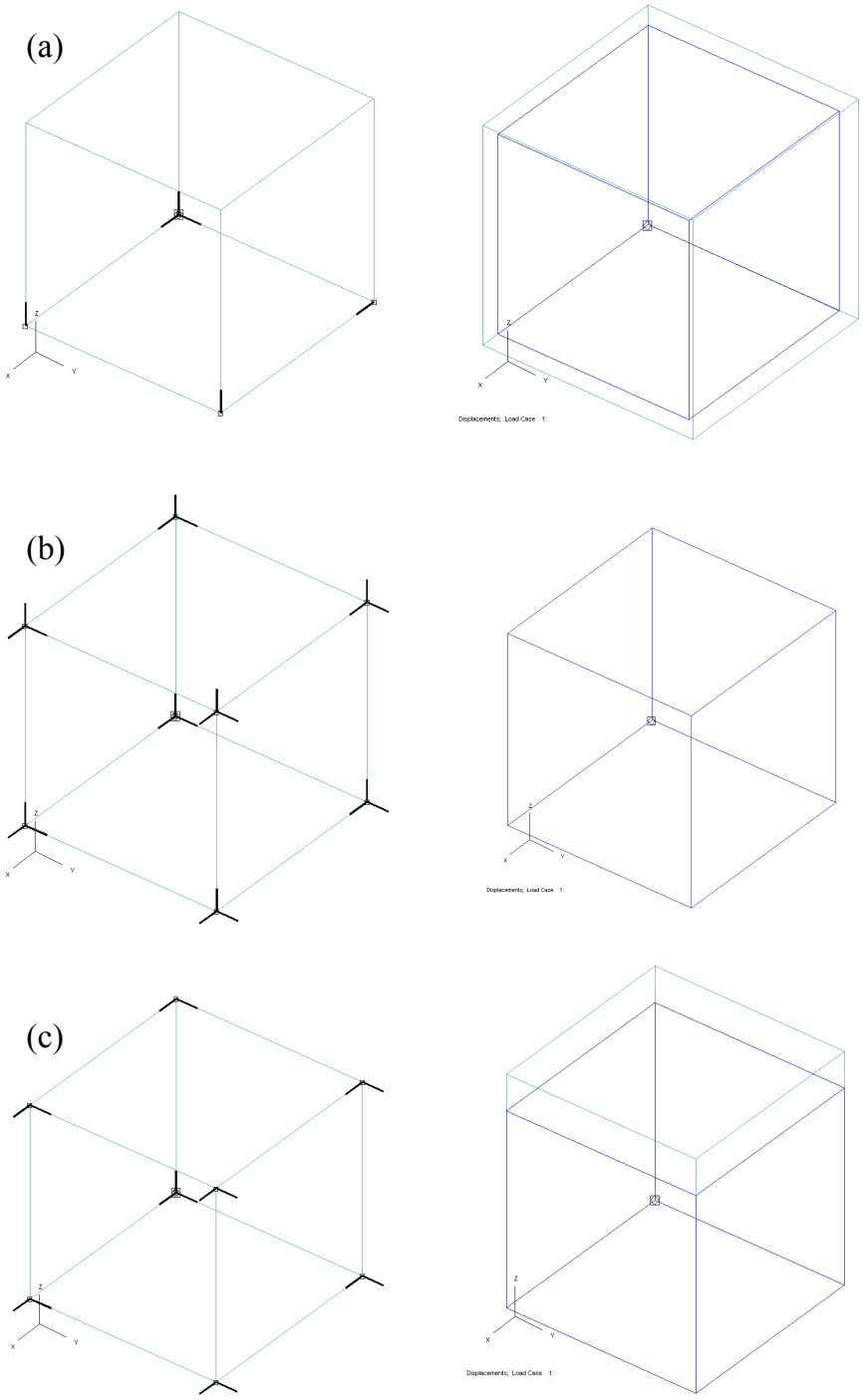

Figure 18: Single element models with different boundary conditions. (a) totally free, (b) fully constrained, (c) constrained in x and y, but free in z-direction.

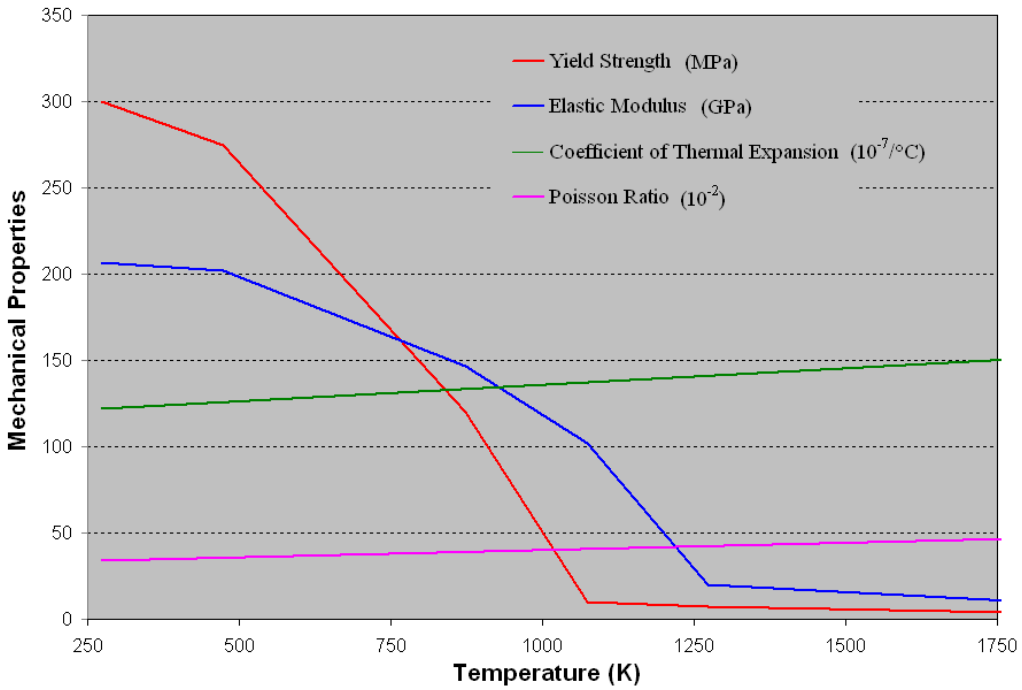

Figure 19: Temperature-dependent mechanical properties used in verification of VAST for weld simulation.

The predicted displacement time histories in the Z-direction subjected to the five different temperature cycles are presented in Figure 21 and the predicted normal stress in the X-direction are given in Figure 22 as a function of temperature. These results indicate that the thermal-elastic-plastic loading, unloading and reloading processes were modelled correctly. It was noted that for equi-biaxial stress states, the yield stress equalled the magnitudes of both stress components. To verify the correctness of the VAST stress solutions, the temperature-dependent yield stress curves in both tension and compression are plotted in Figure 22. The computed stresses are in almost exact agreement with these input material properties.

In all these nonlinear solutions, 40 time steps were employed. In order to test the convergence property of VAST for nonlinear thermal-stress analyses, the case with T_m=800K was reanalyzed using 20 and 10 time steps and the computed stress-temperature relations are compared in Figure 23. These results confirmed that the convergence rate of the VAST element for coupled thermal-elastic-plastic analyses was very satisfactory.

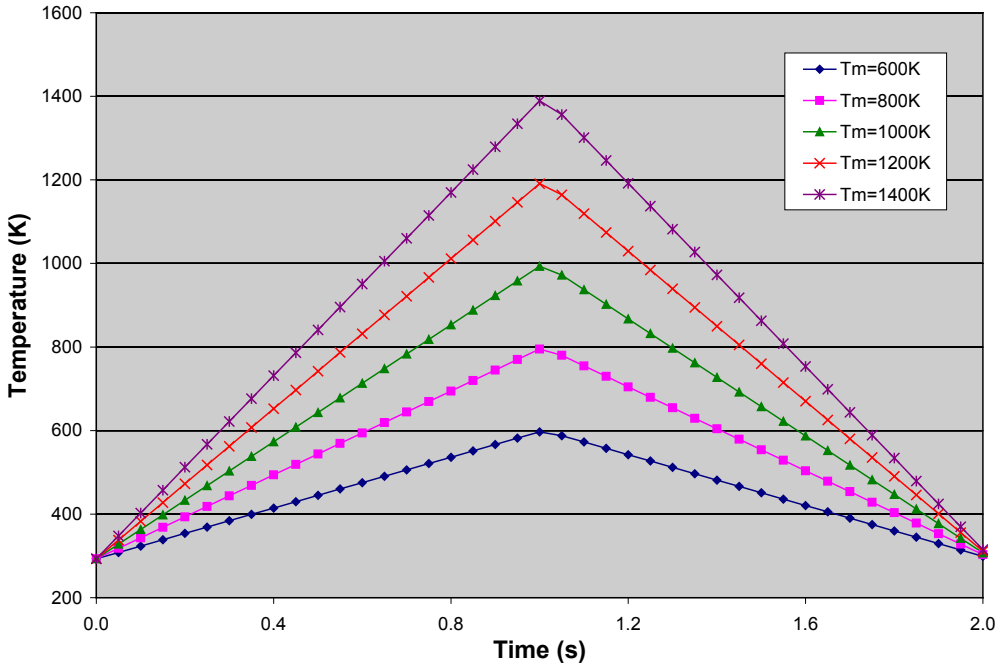

Figure 20: Prescribed temperature time histories for single element test.

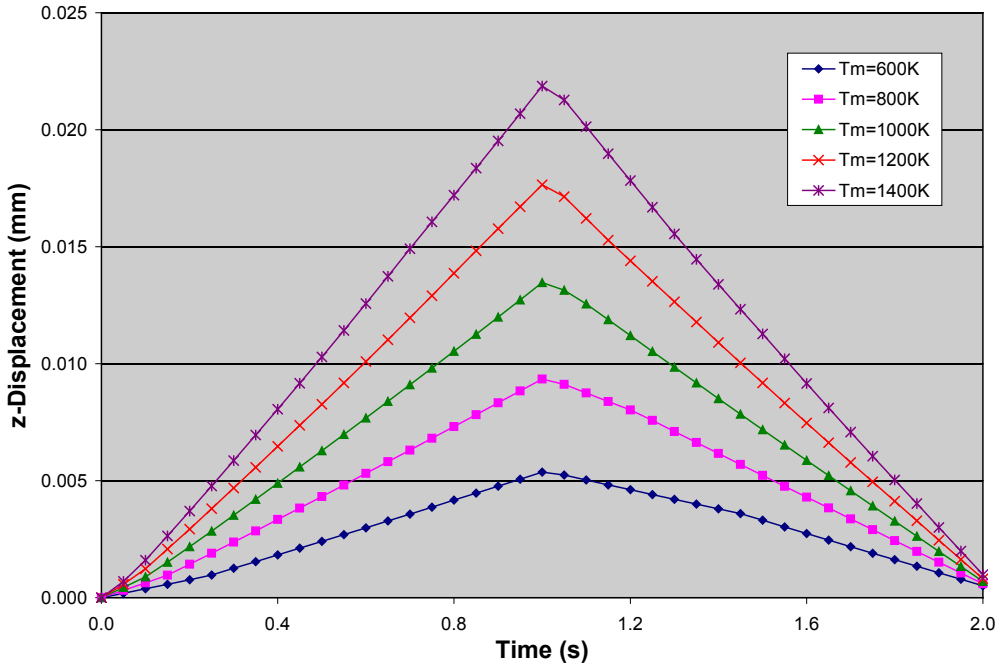

Figure 21: Computed displacement time histories in the z-direction.

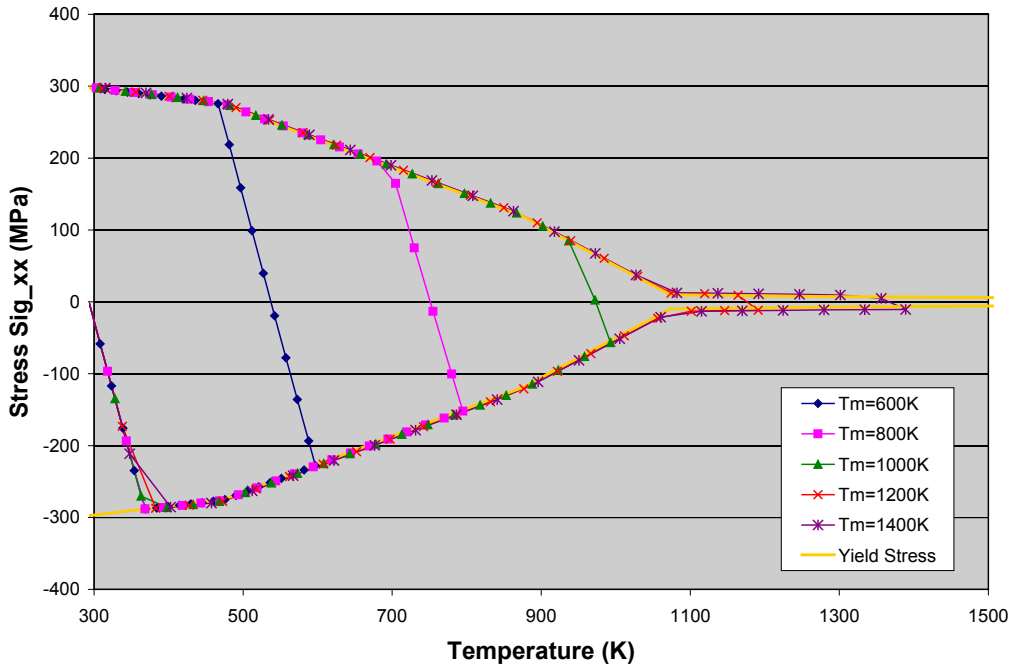

Figure 22: Computed normal stress σ_X as functions of temperature for various temperature time histories. The temperature-dependent yield stress is shown.

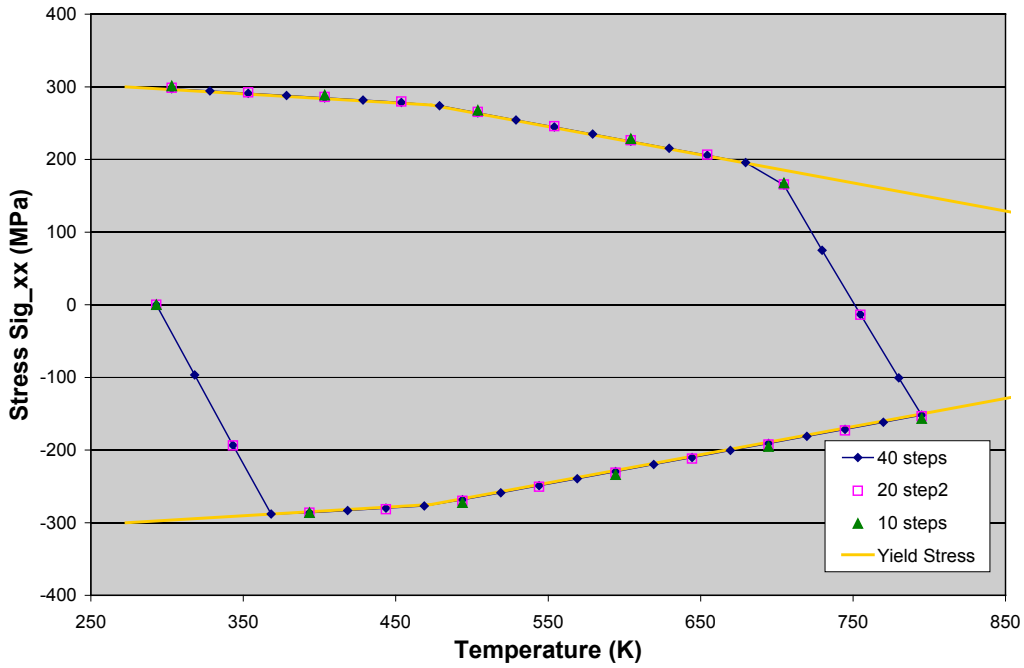

Figure 23: Normal stress σ_X vs temperature obtained using different time step sizes for temperature cycle with Tm=800K.

4.3.2 Cantilever Beam Model

The previous test cases confirmed that the thermal-elastic-plastic constitutive model as well as the various treatments related to temperatures, such as input of nodal temperatures, computation of thermal stresses and evaluation of temperature-dependent material properties, were implemented correctly and behaved reasonably well. However, these test cases only involved a single element and did not contain any geometric nonlinearity. In order to further verify this element for situations closer to the weld simulations, we considered a second test case that involved large displacements and rotations of a cantilever beam. The finite element model and a typical deformed configuration are depicted in Figure 24, where a single layer of ten 8-noded solid elements were utilized. Because of the inclusion of the incompatible displacement modes or so-called "bubble" functions, a single layer of the lower element was able to represent bending stiffness correctly.

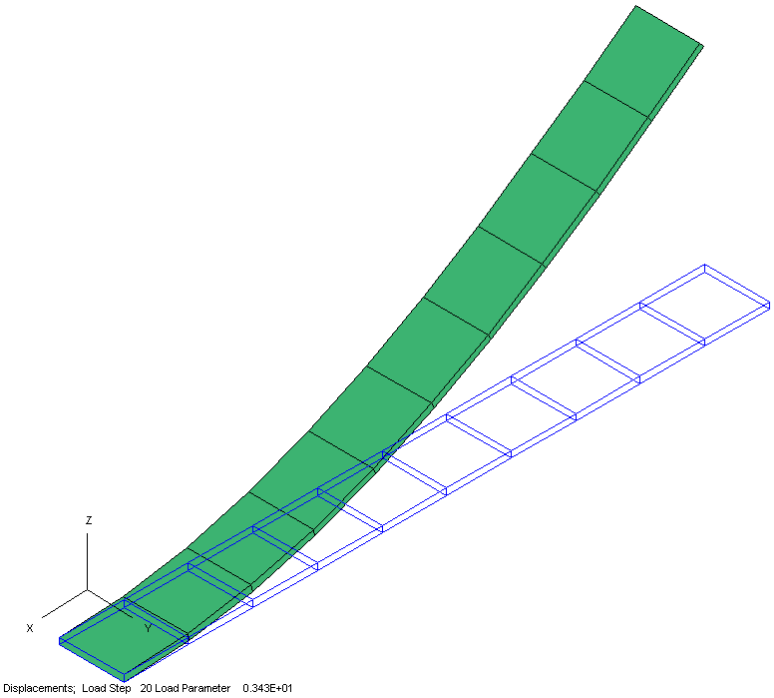

Figure 24: Cantilever beam model.

In the current test, we first verified the temperature-dependent material properties. For doing this, two geometric nonlinear analyses were performed. In the first analysis, the option of temperature-dependent material properties was turned off and constant Young's modulus and Poisson's ratio at 293K were employed. In the second analysis, the capability for temperature-dependent material properties was utilized, but constant temperature functions were specified in the VAST input data. The load-vertical deflection curves obtained from both analyses were identical as shown in Figure 25. In the second nonlinear run mentioned above, the use of the option for temperature-dependent material properties made load-control the only choice for solving the nonlinear problem.

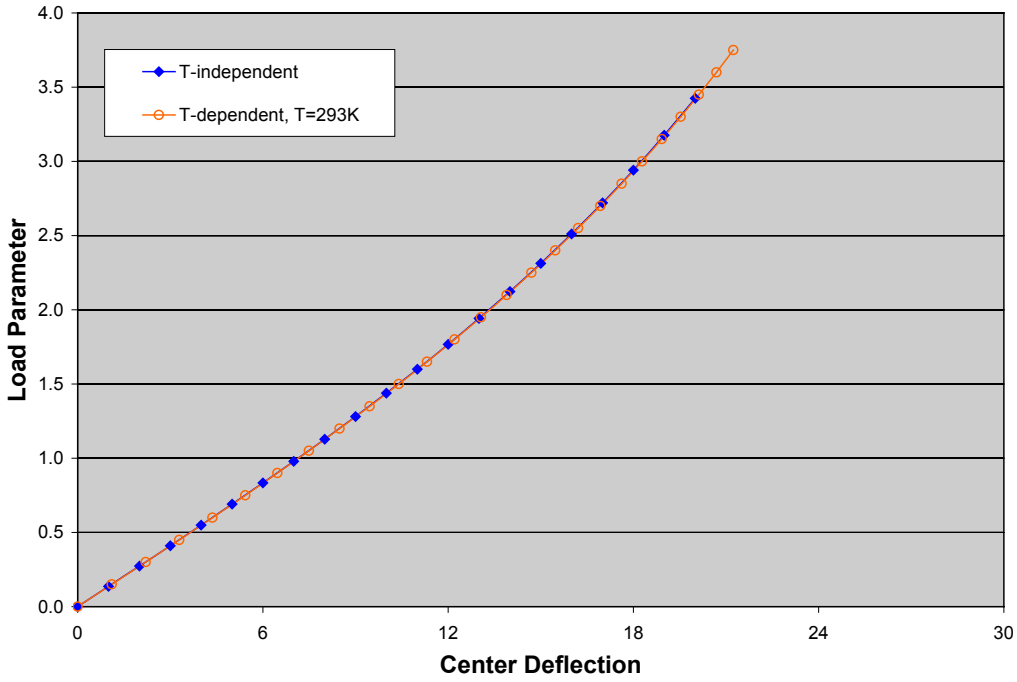

Figure 25: Geometric nonlinear load-deflection curves of the cantilever beam obtained using options for constant and temperature-dependent material properties.

The effects of temperature on geometrical nonlinear response of the cantilever beam were then investigated. This included conducting analyses for a higher constant temperature of 1000K and a temperature cycle shown in Figure 26. The load-deflection curves obtained for different constant and variable temperatures are shown in Figure 27. These results are quite reasonable and no convergence difficulties were encountered.

In the third set of test cases, plastic deformations were taken into account. Load-deflection curves were obtained for different constant temperatures, ranging from the room temperature to 800K. The results are presented in Figure 28. With the increase of temperature, we observed a decrease in the initial slope of the load-deflection curve and also an earlier onset of plastic deformation. This is because an increase in temperature results in decreases in both elastic modulus and yield strength of the material.

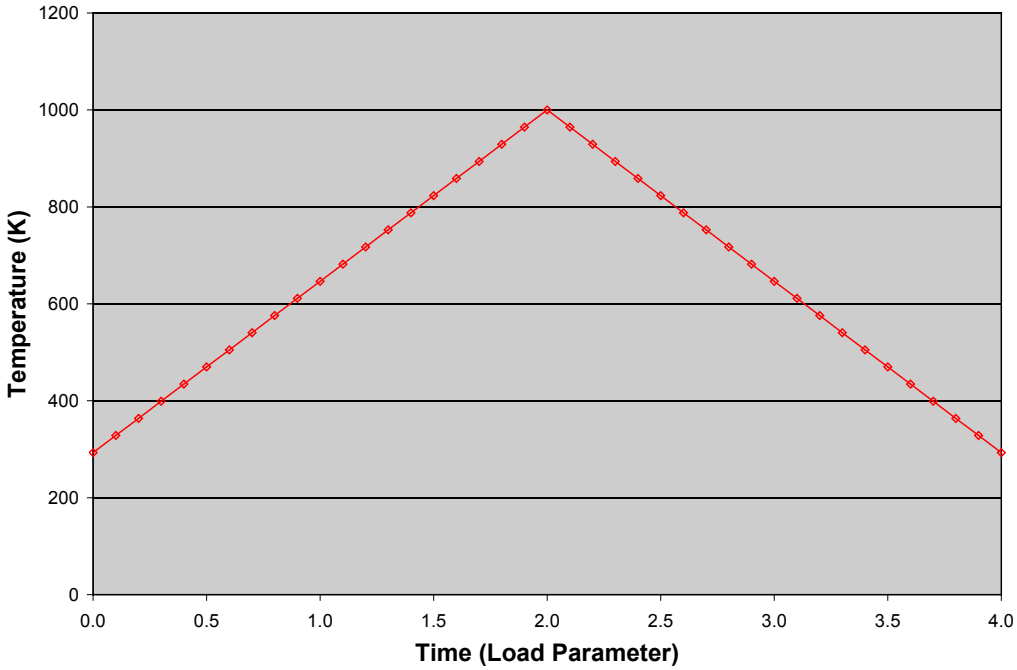

Figure 26: A temperature time history utilized in nonlinear analysis of cantilever beam.

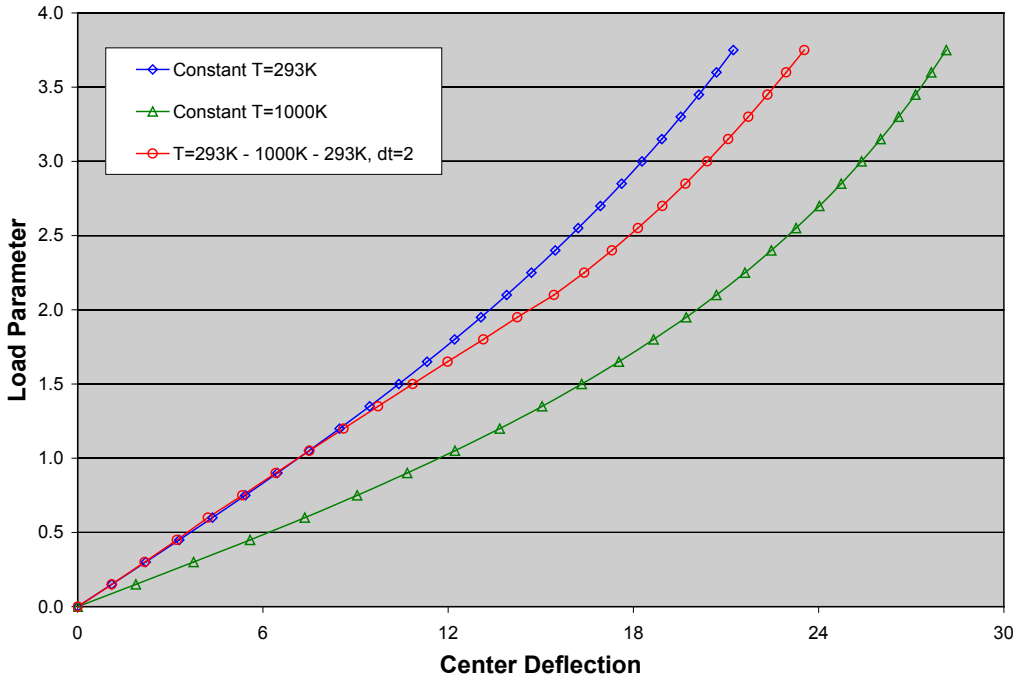

Figure 27: Geometric nonlinear load-deflection curves of the cantilever beam obtained for constant and variable temperatures for temperature dependent material properties.

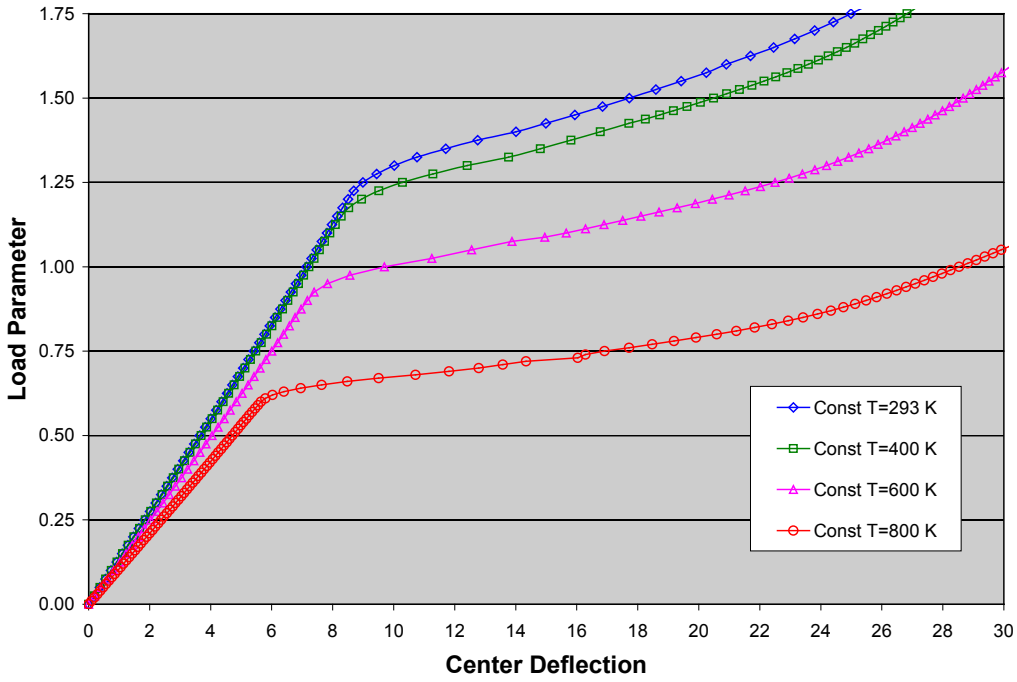

Figure 28: Combined nonlinear load-deflection curves obtained for the cantilever beam at different constant temperatures.

The next set of test cases involved three temperature cycles shown in Figure 29, which all started from the room temperature 293K had a peak temperature of 800K. The differences between them were the time periods of the temperature cycles, in which each of the heating or cooling phases took 0.75, 1.0 and 2.0 s, respectively. The predicted load-deflection curves are shown in Figure 30, where the solutions obtained for the three temperature cycles are all between the solutions for constant temperatures 293K and 800K, respectively. For simplicity, the effect of thermal strains was temporarily excluded in these solutions. Examining these results, we realized that the load-deflection curves obtained for the temperature cycles coincided with the solution for 293K and gradually approached the curve for 800K as the temperature increased with time (assumed to equal to the load parameter). When the temperature reached 800K, the solution curves for the temperature cycles intersected with the curve for 800K. In the cooling phase, the response was virtually linear elastic because for this particular test case, the yield surface grew faster than the stress magnitude, so no additional plastic deformations were predicted.

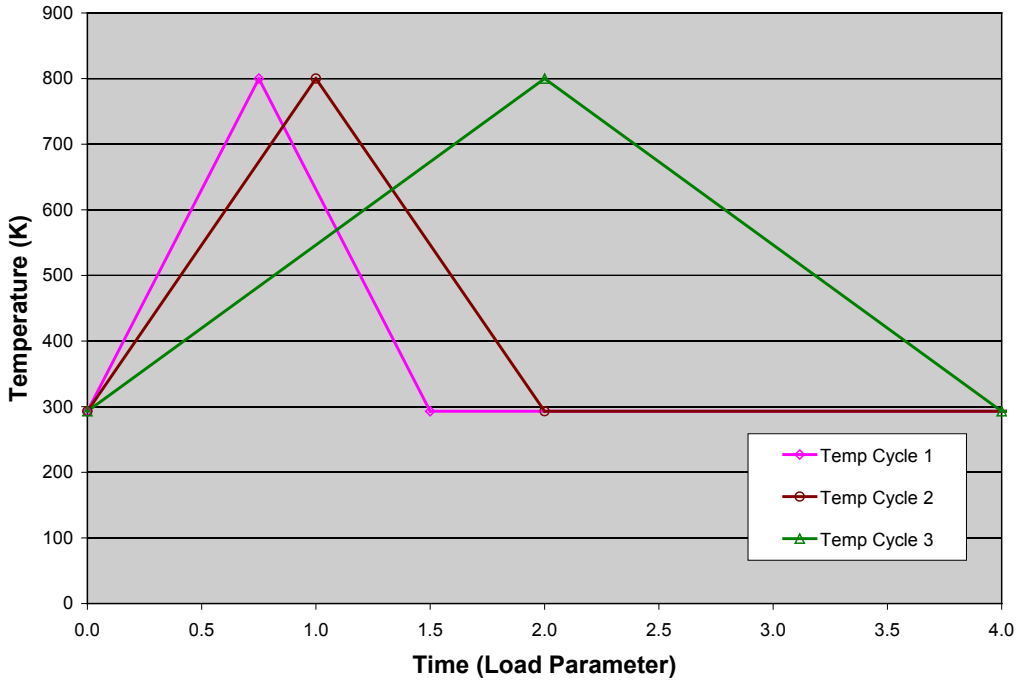

Figure 29: Temperature time histories used in combined nonlinear analyses of the cantilever beam with temperature-dependent material properties.

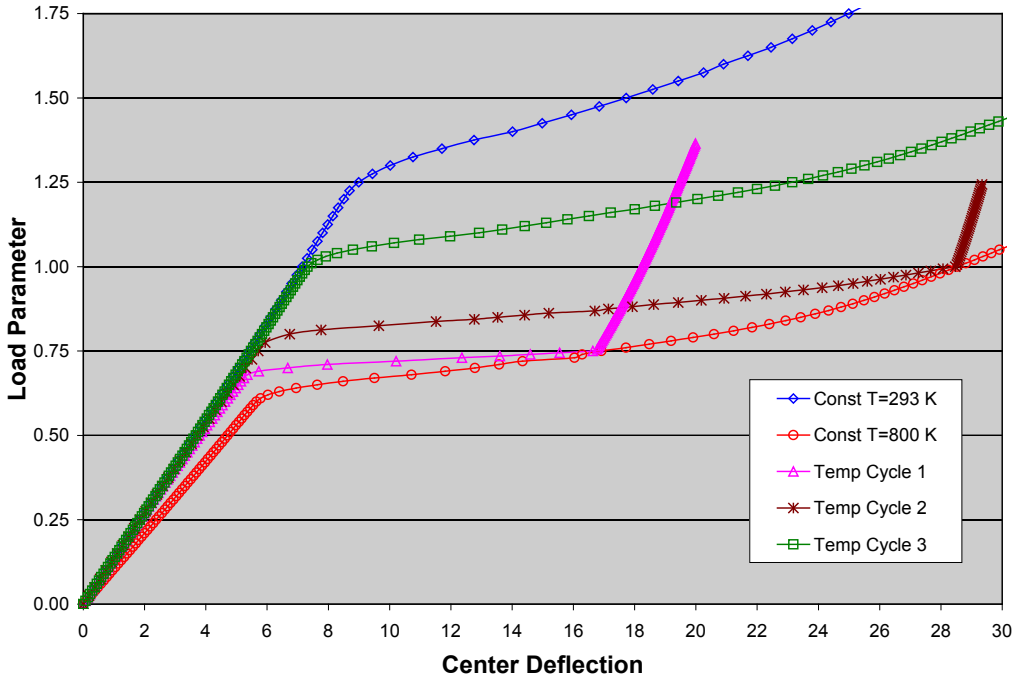

Figure 30: Combined nonlinear load-deflection curves obtained for the cantilever beam under constant and variable temperatures.

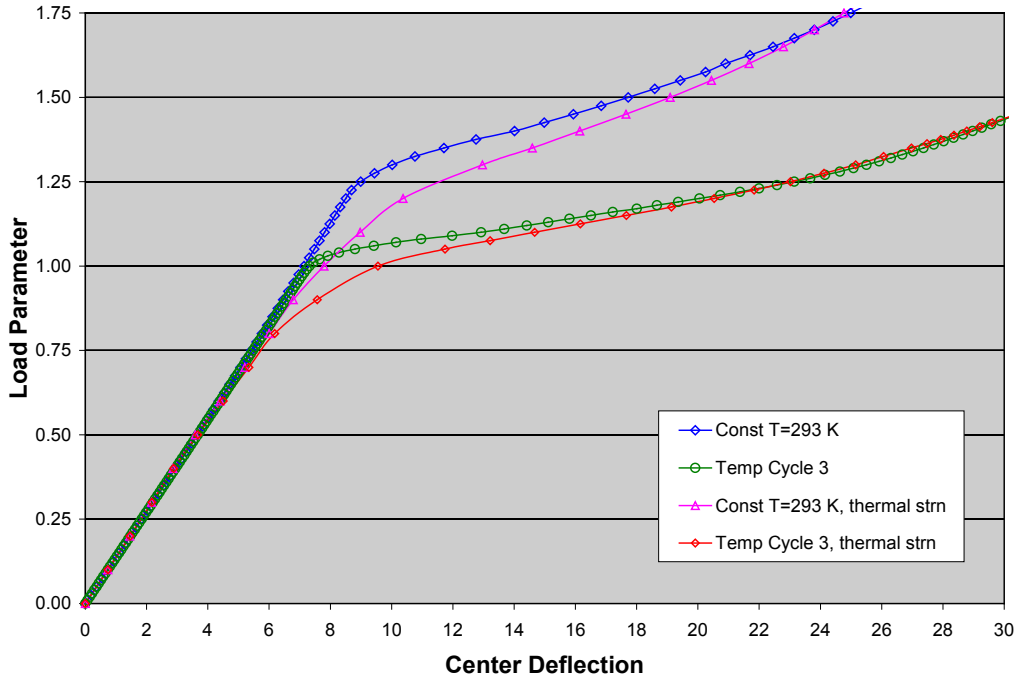

Figure 31: Combined nonlinear load-deflection curves obtained for the cantilever beam under constant and variable temperatures with thermal strain.

In the final set of test cases, the effect of thermal strains on the thermal-elastic-plastic responses of the cantilever beam was investigated. Four test cases were considered and the load-deflection curves are displayed in Figure 31. The temperature cycle #3 displayed in Figure 29 was used in all these test cases and the differences between these test cases were the temperature dependency of material properties and whether the thermal strains were included. In particular, the first and third test cases assumed temperature-independent materials and the material properties at 293K were employed. However, in test cases 2 and 4, the temperature-dependent properties shown in Figure 19 were utilized. These results indicated that the inclusion of thermal strain resulted in early onset of plastic deformation. However, the thermal strain effect became less significant with the progress of deformation. It was also observed that the inclusion of thermal strains enhanced the convergence rate and numerical stability of VAST for nonlinear coupled thermal-structural analyses because convergence could be achieved with much larger solution steps.

4.3.3 Weld Simulation

Following the verifications presented in the preceding sections, attempts were made to perform the full weld simulations. The weld experiments performed by Deng et al [7] and later simulated numerically by Gannon [8] were adopted as a test case and the ANSYS finite element model generated by Gannon was utilized as a starting point for creating the VAST model. A special-purpose program was developed to convert the ANSYS model to VAST format and introduce all the input data required for weld simulations.

A number of test runs were performed using the transient nodal temperature files generated from the VASTF heat transfer analyses discussed in the previous chapter. Unfortunately, the thermal-structural analyses for full weld simulations always crashed after the first few time steps. The VAST solutions were examined closely, but no obvious cause of the divergence was identified. Compared to the heat transfer analysis, the structural analysis was considerably more time-consuming because of the increased number of degrees of freedom per node from 1 to 3. The slowness of the numerical computation made it extremely difficult to investigate the cause of the convergence difficulties.

A careful comparison has been conducted [9] between the nonlinear finite element algorithms utilized in the ANSYS analysis of Gannon [8] and the present work. This comparison concluded that the algorithms and assumptions used in both programs were almost identical and that the most significant difference was on the finite element formulations. ANSYS used a reduced integrated solid element with hourglass control, but VAST utilized a fully integrated element with bubble functions. In addition, the ANSYS element was formulated using a finite strain theory, but VAST adopted a small strain elastic-plastic constitutive model measured in co-rotational framework. It is difficult to verify whether the finite element formulation and constitutive model in VAST is the cause of its convergence problem in weld simulation because implementation of new nonlinear element formulation and material models are clearly outside the scope of the present contract.

5 Modifications to SubSAS to Support Welding Simulation

This section details a proposed set of changes to the Submarine Structural Analysis Suite (SubSAS) to support performing a welding analysis as described in the previous sections of this report. The objective of the proposal is to design an integrated set of tools in SubSAS to easily generate a finite element model for weld simulation based on the SubSAS geometric model. Futhermore, SubSAS should be able to automatically prepare input files for VASTF and VAST, seamlessly run the FE analyses, and post-process the results.

SubSAS stores data concerning the submarine's geometry and material that are used in quasi-static structural analyses. The welding simulation model requires the following additional data and parameters:

1. temperature dependent mechanical material properties,

2. temperature dependent material conductivity and heat capacity properties,

3. heat source definition,

4. weld pass curve(s) definition,

5. initial temperatures, and

6. convection loads.

Additionally, the welding simulation:

a. must be conducted using 8-node brick elements,

b. requires appropriate element refinement in the vicinity of the weld path,

c. must include elements representing the weld deposit material, and

d. requires the definition of element groups to aid in specification of simulation data and parameters.

SubSAS will require modification to support managing the data required to set up and run a welding simulation. Each of these points is discussed in detail below.

5.1 Welding Data Requirements

5.1.1 Temperature dependent mechanical material properties

In the case that temperature dependent mechanical material properties are going to be used, each of the following properties must be specified as a function of temperature: Young's Modulus, Poisson's Ratio, density, yield stress, tangent modulus for isotropic hardening and tangent modulus for kinematic hardening. It is recommended that these functions be supplied in a manner consistent with how a nonlinear stress-strain curve is supplied in RMGScript: as a sorted series of child entities of the Material_Iso record, each representing points on the function curve. New function point entities will have to be devised to supply this data (e.g. YoungsModulusCurvePoint, YieldStressCurvePoint, PoissonsRatioCurvePoint, etc.).

It is recommended that the following convention be followed with respect to applying temperature-dependent mechanical material properties: if any temperature functions are present, then the material will be considered temperature dependent when setting up the VAST weld simulation (i.e., the element's ITM flag (see ref. [10]) will be 1); additionally if any temperature functions are present, then all must be present (e.g. cannot have a temperature dependent Young's Modulus with any other properties specified as constant). Temperature-dependent properties can be stored in the SubSAS material database, but will only be applied to a model if performing a welding simulation analysis.

VAST has also been modified to support three models for specifying thermal expansion. In the first case, thermal expansion is considered to be linear, requiring a new coefficient of thermal expansion attribute be added to the RMGScript Material_Iso entity. In the second and third case, nonlinear functions are required to define temperature-dependent thermal expansion and thermal strain, respectively. It is recommended that these functions be supplied in the same manner as the mechanical properties described above. Two new entities, ThermalExpansionCurvePoint and ThermalStrainCurvePoint should be created to distinguish between the two functions.

It is recommended that the following convention be followed with respect to applying the thermal expansion model: either the constant value or one of the functions is required; a function overrides the constant if both are supplied; and at most one function can be supplied. According to this convention, if only the constant of thermal expansion is supplied, then the element's ITP flag will be set to 1; if a series of ThermalExpansionCurvePoints are found, the ITP flag (see ref. [10]) will be 2; or if a series of ThermalStrainCurvePoints are found, the ITP flag will be 3. Using this convention, if the user desires to supply all 3 models for a given material, then 3 separate, aptly named, Material_Iso entities need to be created, and the desired one assigned to model geometry on a per-analysis basis.

5.1.2 Temperature-dependent material conductivity and heat capacity properties

VASTF supports the following models for element thermal properties:

- Constant thermal properties.

- Thermal conductivity and heat capacity are both temperature dependent.
- Thermal conductivity is temperature dependent but heat capacity is time dependent.
- Thermal conductivity is time dependent but heat capacity is temperature dependent.
- Thermal conductivity and heat capacity are both time dependent.

For the first phase of development, only two will be made available for welding simulation in SubSAS: the ability to supply constant thermal properties and to define both thermal conductivity and heat capacity as a function of temperature. In the former case, two new properties on the Material_Iso entity will be required: a vector to define thermal conductivity in the three principal directions, and a constant for the specific heat of the material (the density is also required, but that property already exists in the current SubSAS material entity). In the latter case, the function values will be accepted in the same manner as the temperature-dependent mechanical properties – as a sorted series of child entities of the Material_Iso entity defining points on the function curve. Two new entities will be needed to support these functions: ThermalConductivityCurvePoint and HeatCapacityCurvePoint.

The following convention is recommended for selecting the model to apply for analysis: a function overrides a constant for either of the values, and if a function is supplied for one, it must be supplied for both. If the two functions are supplied, the element's IMTYPE flag (see Ref. [10]) will be set to 1, else it will be set to 0.

Convection loading (described below, Section 5.1.6) requires the specification of a heat transfer coefficient for the material. It is proposed to support only a constant coefficient, so a single new attribute should also be added to the Material_Iso entity for this purpose.

5.1.3 Weld pass curve(s) definition

Weld pass curves are used to capture the heat source movement through the model as simulation time increments. This, in turn, dictates the thermal loading and the creation of weld deposit material in the model. The manner used to create weld pass curves differs depending on the type of weld being simulated. It is recommended to support weld pass curves arising from three types of welding: fillet welding, butt welding and overlay welding. Defining the path shape for each of these cases is described below.

5.1.3.1 Fillet Welds

Fillet weld pass curves (Figure 32) should be defined in a way that is consistent with the general methodology used throughout RMGScript – i.e., in a high-level, parametric manner that is easy for the user to specify. To this end, it is proposed the weld pass curve definition be based on the specification of an intersection between two RMGScript plate entities. The intersection defines a curve, which must be bounded by trimming objects at either end in the same way as a PlanarWebStiffener (i.e., the 'e1' and 'e2' attributes). A potential representation of a fillet weld pass curve as an RMGScript entity could, therefore, resemble:

<FilletWeldPassCurve name="" fidelity="" plate1="" plate2="" p="" e1="" e2="" w="" m=""/>

where the attributes are defined as:

- **name**: a descriptive name for the weld pass function
- **fidelity**: if "off", omit from analysis; otherwise include
- **plate1**: an object reference to the first plate contributing to the intersection
- **plate2**: an object reference to the second plate contributing to the intersection
- **p**: an optional point used to resolve possible ambiguity in defining the curve or to assist in defining the curve direction
- **e1**: an object reference or anonymous object which will bound the intersection and define its starting point
- **e2**: an object reference or anonymous object which will bound the intersection and define its ending point
- **w**: the width of the fillet weld to use
- **m**: the welding material

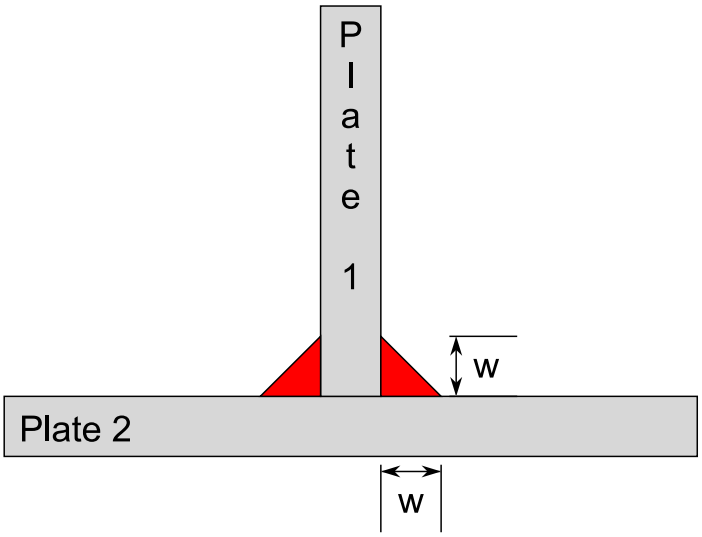

Figure 32: Fillet weld definition.

It is necessary to know the direction the heat source will take over the weld pass curve. This will be achieved by orienting the curve in the desired direction. Two methods are proposed for informing the curve of the desired direction. First, parameters 'e1' and 'e2' can be specified to introduce intersection points on the curve; the intersection point caused by 'e1' will be the begin

point of the curve and the point caused by ‘e2’ will be the end. If used, ‘e1’ and ‘e2’ must each intersect the overall curve exactly once. Otherwise an alternative method of supplying ‘p’ to be a point on the curve, nearest to its beginning, can be used. This latter method would be most useful for closed weld paths or paths which run to the natural boundary of the plates involved.

The width of the fillet is specified as parameter ‘w’. It is assumed that the fillet will extend in equal measure on each of the connecting plates, and that all fillets will be of the same width (i.e., on all sides of all plates joining at the intersection). The fillet width will be used when generating the brick mesh (see sub-section 5.2.3.1 below).

It is worth noting that although the FilletWeldPassCurve entity seemingly defines a single weld pass curve at the intersection of the plates involved, in actuality multiple weld pass curves will be generated, each running through the centroids of the weld deposit elements. If two plates are welded together in a ‘T’ configuration (as in Figure 32); two weld pass curves will be generated. If two plates are welded in an “X” configuration, four weld pass curves will be generated.

5.1.3.2 Butt Welds

Butt welds run along the common edge of two plates that are joined either in plane or in such a way that their surface tangent directions at the weld are near continuous (Figure 33). The edges are typically prepared in some manner (e.g. trimmed off to form a wedge shape), and the weld can be either a fully penetrating weld, or partially penetrating. It is proposed to provide a capacity to only model a fully-penetrating weld made from a single direction – either above or below the plates. The end preparation will consist of a single angle to which the square butts will be trimmed to form a V-shaped wedge when the plates are joined.

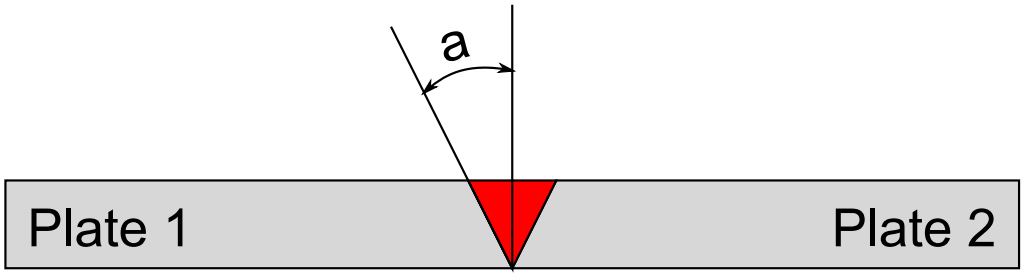

Figure 33: Butt weld definition.

It is proposed to define the butt weld path using the common RMGScript Trim object that would have been used to trim the two plates in the first place (it is assumed both plates will share at least one common Trim definition). A potential representation of a butt weld pass curve as an RMGScript entity could resemble:

<ButtWeldPassCurve name=”” fidelity=”” plate1=”” plate2=”” trim=”” p=”” e1=”” e2=”” normside=”” a=”” m=””/>

where the attributes are defined as:

- **name**: a descriptive name for the weld pass function
- **fidelity**: if "off", omit from analysis; otherwise include
- **plate1**: an object reference to the first plate contributing to the butt join
- **plate2**: an object reference to the second plate contributing to the butt join
- **trim**: an object reference or anonymous object used to trim both plate1 and plate2 along their shared butt connection
- **p**: an optional point used to resolve possible ambiguity in defining the curve or to assist in defining the curve direction
- **e1**: an object reference or anonymous object which will bound the butt intersection and define its starting point
- **e2**: an object reference or anonymous object which will bound the butt intersection and define its ending point
- **normside**: "1" if the plates are welded on the normal side of plate 1, "0" for the anti-normal side (as determined by the orientation of the plate's underlying plane normal)
- **a**: equal to the angle to cut the plate edges in preparation for butt welding
- **m**: the welding material

The interpretation of the attributes of the ButtWeldPassCurve is similar to the FilletWeldPassCurve in all respects except: the attribute 'trim' is used to specify which edge the plates connect along and the 'normside' and 'a' attributes are collectively used to set up the edge preparation cuts (i.e., the V notch). In the case of butt welds, a single weld pass curve will be generated running through the centroids of the weld deposit material inserted into the V notch.

5.1.3.3 Overlay Welds

Weld overlay, also known as "buttering," consists of a series of weld passes depositing material to cover an area on the surface of a plate (Figure 34). Overlay can be used, for example, to restore areas of diminished thickness on a plate. It is proposed to support a very limited capability to simulate weld overlay, namely a rectangular patch consisting of multiple rows of weld deposit, possibly multiple layers deep, on either a planar or cylindrical plate. Each deposit row will consist of a single series of 8-node brick elements, with rows stacked to represent multiple layers. SubSAS will generate a weld pass function for each deposit row.

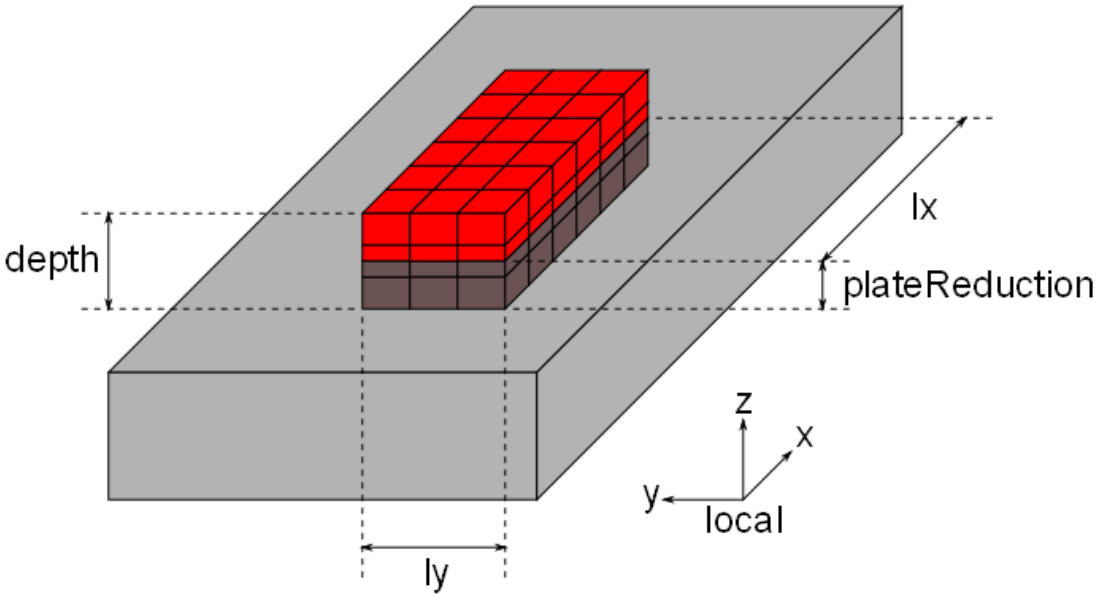

Figure 34: Overlay weld definition.

Weld overlay should be captured in a manner similar to defining a property map on a plate. Namely, a local coordinate system (planar or cylindrical) should be positioned and oriented on the surface on which the weld overlay will be applied. After the local coordinate system is defined, the overlay patch extent can be given as a simple rectangle. It should be specified in which direction the overlay weld rows will be oriented in the local coordinate system (either x or y for planar plates, or axially or circumferentially for cylindrical plates).

After the patch extent and orientation is defined, it remains only to specify the particulars as to the dimensions of the weld overlay rows. The number of rows should be specified as well as a total depth and number of layers. The dimensions of each row of material will therefore be equal to the width of the patch divided by the number of rows wide by the total depth divided by the number of layers deep. For a $n \times m$ (rows × layers) patch, nm individual weld pass functions will be defined, each at the centroid of the elements comprising the row.

If the weld overlay is being applied to a region of diminished thickness on the plate, the thickness reduction must be supplied as part of the weld overlay definition (i.e., weld overlays should not be used atop TZones or advanced thickness maps). Furthermore, it should be a user option as to whether or not the overlay is applied to the normal or anti-normal side of the plate.

Accordingly, a potential representation for a weld overlay definition on a planar plate would be:

<PlanarPlateWeldOverlay name=”” fidelity=”” pl=”” lx=”” ly=”” rowsX=”” numRows=”” depth=”” numLayers=”” plateReduction=”” normside=”” m=””/>

where the attributes are defined as:

- **pl**: a plane definition setting up the local x and y coordinate space of the weld overlay
- **lx**: the dimension of the overlay patch in the local x direction
- **ly**: the dimension of the overlay patch in the local y direction
- **rowsX**: equal to “1” if the overlay rows are running in the local x direction, “0” if they run in the local y direction
- **numRows**: the number of overlay rows
- **depth**: the total depth of the overlay
- **numLayers**: the number of overlay layers
- **plateReduction**: a reduction to apply to the plate before “filling” with overlay
- **normside**: “1” if the overlay will be deposited on the normal side of the plate, “0” for the anti-normal side (as determined by the orientation of the plate’s underlying plane normal)
- **m**: the welding material

Similarly, a potential representation for a weld overlay on a conic plate would be:

<ConicPlateWeldOverlay name=”” fidelity=”” pl=”” h=”” amin=”” amax=”” rowsAxial=”” depth=”” numLayers=”” plateReduction=”” normside=”” m=””/>

where the attributes are the same as for the planar case with the exception of:

- **pl**: a plane defining the base of a cylindrical coordinate system; the axial direction is in the direction of the plane normal, and the cylinder sweeps clockwise from the plane local x axis when looking in the direction of the plane normal
- **h**: the height of the cylindrical patch above the plane defined by ‘pl’
- **amin**: the angle of the begin of the cylindrical patch, measured in degrees from the local x axis of the plane in a clockwise direction when looking in the direction of the plane normal
- **amax**: the angle of the end of the cylindrical patch, measured in degrees from the local x axis of the plane in a clockwise direction when looking in the direction of the plane normal
- **rowsAxial**: equal to “1” if the overlays rows are running in the axial direction, “0” if they are running in the circumferential direction

5.1.3.4 General Comments

The proposed methodology for defining weld curve paths for fillet, butt and overlay welding is based on intersections between RMGScript geometry. These intersections may involve nonplanar surfaces, in which case the resulting intersection curve will be described by NURBS curves in 3D space. The welding simulation capability presently supported in VAST/VASTF only allows for linear weld paths (corresponding to the intersection of planar surfaces). As such, the user will be restricted to such cases for the time being, but SubSAS will be able to provide curved weld paths once they are supported. Note that this precludes support for the ConicPlateWeldOverlay entity if 'rowsAxial' is set to "0" as it would require support for arc-shaped weld paths.

The above weld pass definitions cover defining the path shape, but do not include attributes to define the movement of the heat source with time. VASTF assumes constant velocity of the heat source between a beginning and ending time value. As such, this can be trivially included by augmenting each of the weld pass entities with two new attributes:

- **bt**: beginning time
- **et**: ending time

In the case of fillet weld pass curves, the heat source will move along all paths resulting from the single definition (i.e., two separate paths for a 'T' junction as shown in Figure 32) at a constant velocity between these two time points. In the case of butt welds, only a single path is involved, but the velocity is still constant between the two time points. In the case of overlay welding, the heat source will move at a constant velocity across each of the $m \times n$ paths in succession, beginning at the surface of the plate and building up through the layers. The deposit rows will be oriented in a consistent direction, meaning the heat source will finish with one row and have to travel back to the beginning of the next row. This will be assumed to happen instantaneously – i.e., the overall interval between 'bt' and 'et' will be divided between the number of deposit rows only.

5.1.4 Heat source definition

The weld pass curves must go hand-in-hand with a heat source definition. The geometry of the heat source to be supported in the present work is given in Figure 3. A new RMGScript entity DoubleEllipsoidHeatSource should be created to accept the parameters defining the heat source as per this model. Specifically, this new entity will resemble:

<DoubleEllipsoidHeatSource name="" a="" b="" cf="" cr="" ff="" fr="" current="" voltage="" efficiency=""/>

where each attribute corresponds to one of the parameters described in section 3.3.

Since a heat source is intended to be associated with a weld pass curve definition, it is proposed to make this association by requiring that a weld pass curve RMGScript entity provide an attribute to reference a heat source object using standard RMGScript object reference syntax. This would augment each of the weld pass curve entities described in the previous section with a further attribute, 'hs' as in, for example:

<FilletWeldPassCurve name=”” fidelity=”” plate1=”” plate2=”” p=”” e1=”” e2=”” w=”” m=”” **hs=”[Heat Source 1]”**/>

If a weld pass curve entity fails to reference a heat source, it should be considered incomplete and give an error if an attempt is made to include it in an analysis.

5.1.5 Initial Temperatures

Initial temperatures must be supplied for both the thermal analysis with VASTF as well as the structural analysis with VAST. In both cases initial temperatures are trivially specified by assigning a constant temperature to each and every node in the model. The temperature should be defaulted to room temperature and possibly also requested as an option on the Analysis Type Wizard (i.e., to override the default).

5.1.6 Convection Loads

All non-weld elements in the simulation model that are exposed to the environment must have convection loads applied for the thermal analysis only. Specifically, the environmental temperature and heat transfer coefficient must be applied to each exposed element surface. Although VASTF supports defining convection properties at multiple points in time as well as defining a temperature-dependent heat transfer coefficient, it is proposed for an initial implementation to limit the capability provided in SubSAS to capture constant convection properties at all times using a constant heat transfer coefficient. As such, a single new attribute will be added to the Material_Iso entity to capture the constant heat transfer coefficient for use setting up convection loads (see above section on temperature dependent material conductivity and heat capacity properties).

The convection loads must be specified on a per-surface basis for solid elements. As such, SubSAS will need to analyze the FE model and determine all element faces exposed to the environment. It is felt this can be done easily by building up a map of element faces to connected elements. Once the map is complete, any faces which reference only a single element should be considered exposed to the environment. A trivial refinement of the rule to exclude elements corresponding to weld deposit should also be applied, as such elements are not meant to include convection loads. Also, elements overlaid with weld deposit elements are not to be considered exposed to the environment, and hence, will be left out of the list to be assigned convection loads.

5.2 Welding Model Requirements

5.2.1 8-Node Brick Elements

The welding simulation as described in this report cannot be applied to the default FE model generated from SubSAS non-manifold surface-based geometry. Such a geometric model yields shell and beam elements when meshed, whereas the welding simulation requires 8-node solid, or brick, elements. As such, a process to generate a brick-based model from a SubSAS thin-shell model is required. Ideally, SubSAS would be able to perform this operation in a fully-automatic manner.

This problem could be approached from two directions: either convert the SubSAS geometry to a manifold solid-based geometry and then mesh, or mesh first and then convert the mesh to a solid-based mesh. It is felt the former approach is the more difficult of the two, so the latter was chosen for consideration. Converting a shell mesh to a brick mesh in the general case is still a difficult operation, however. This proposal outlines an automatic algorithm that will perform the operation on limited geometric configurations. The limitations are imposed in order to maximize the chances of the algorithm completing successfully. Any such limitations are clearly stated in the description of the algorithm.

The input to the proposed algorithm is a mesh originating from SubSAS and consisting of quadrangle shell elements only. All shell elements will be midsurface-aligned and not contain any offsets (i.e., thickness is symmetric on either side of the midsurface). Furthermore, for a given element, nodal thicknesses will be uniform, and for a given continuous plating region, thicknesses will be uniform (i.e., no discrete changes in thickness between two adjacent, continuous, shell elements; this precludes applying a weld path over plate regions covered by TZones). The region being supplied to the algorithm can, however, have multiple continuous plating regions intersecting (e.g. a deck and a bulkhead intersecting), and each of the continuous plating regions can themselves have different thicknesses (i.e., the deck one thickness and the bulkhead another). Finally, the shell element edge size should be much larger than the maximum element thickness (at least by a factor of 3 or 4). This affords the algorithm enough room to safely create brick elements in the vicinity of any discontinuous plating region intersections.

The algorithm begins by replacing the shell elements with brick elements created by extruding the shells along their normal axis. The user will specify the desired number of elements, N_T, through the plate thickness as a power of 2 ($N_T=2^4=16$ is recommended; only one value will be entered and will be applied to all plates). Brick elements will be created both above and below the midsurface – i.e., N_T /2 elements representing half the thickness both above and below (Figure 35). This operation is easy for all elements except in the vicinity of discontinuous plating region intersections (e.g. a deck and bulkhead intersection).

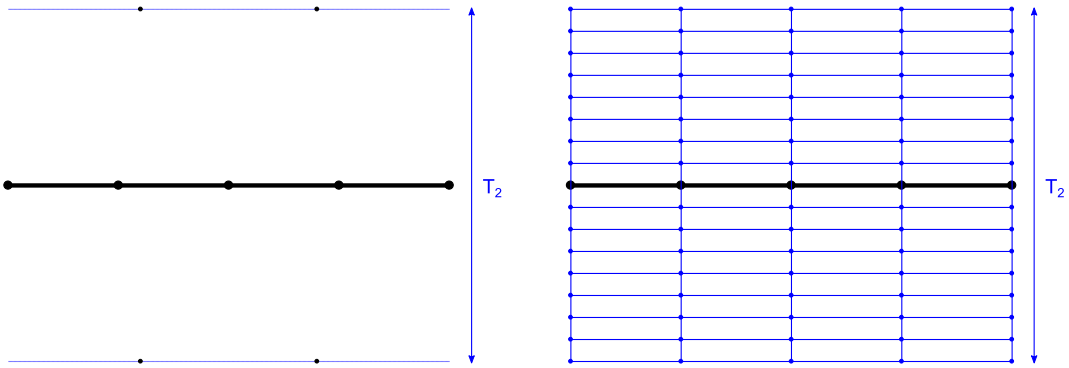

Figure 35: Extruding shell elements on either side of the plate to form bricks.

In such regions, interference between elements belonging to one surface and those belonging to another will occur if each is treated in isolation. To overcome this, the surfaces must be considered together. At the intersection of the two surfaces, a plane will be created (normal to the intersection curve) onto which four points will be located, $p_1,..,p_4$ (Figure 36) based on the

thicknesses of the two plates. The four points will be used to generate a rectangular patch within which a regular grid of nodes can be trivially generated by bilinear interpolation. Figure 36 demonstrates the patch placement in the case that two surfaces are fully intersecting each other; variations where one or more surfaces are joining at an edge rather than intersecting are simplifications of this case (e.g. “L” or “T” intersections).

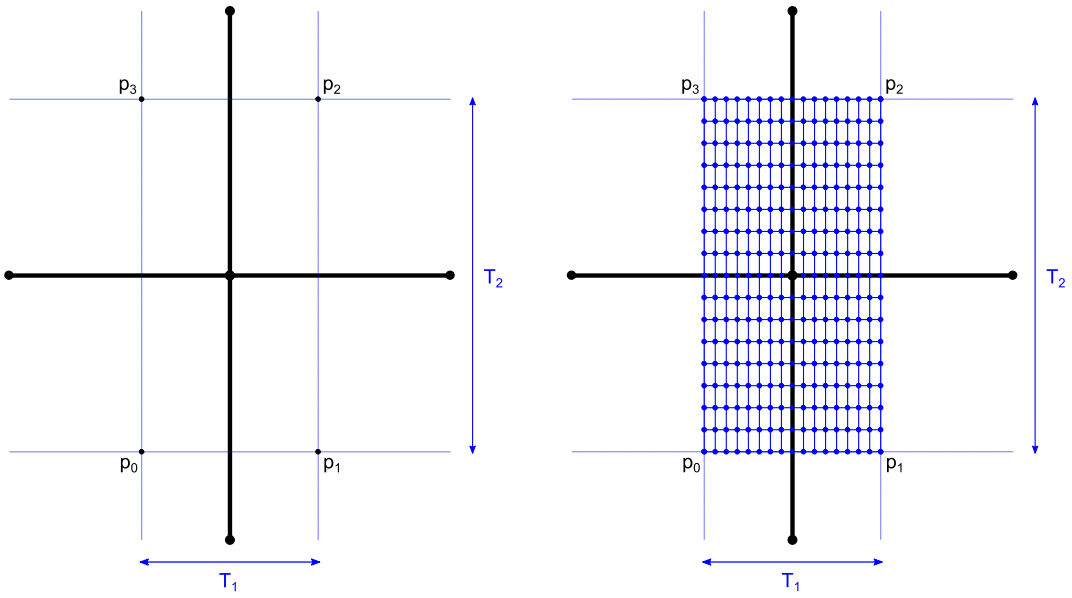

Figure 36: Bilinear interpolation to create brick elements.

This process will be repeatedly applied down the length of the intersection curve at each existing nodal location, and the points within each adjacent patch will be connected up to form bricks (Figure 37).

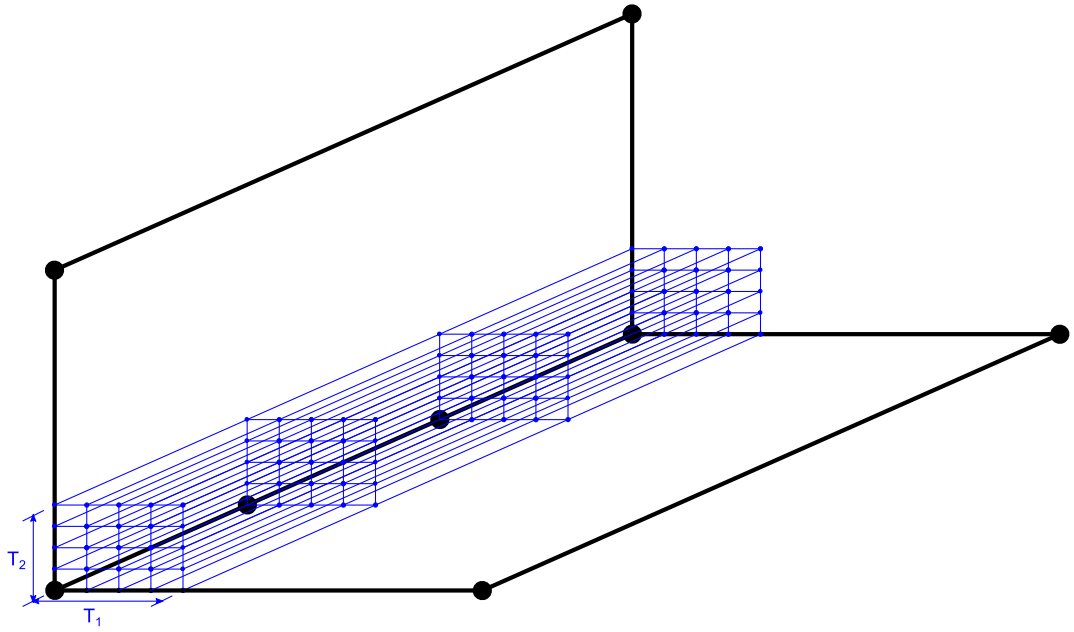

Figure 37: Repeating bilinear interpolation to create brick elements.

In the case that three surfaces are joining at a single point (e.g. deck, transverse bulkhead and longitudinal bulkhead), a generalization of the bilinear patch to 3D can be employed. In this case, a cube will be used and a trilinear interpolation applied to generate nodes within the cube (Figure 38). The algorithm will not support more than three surfaces intersecting at one location.

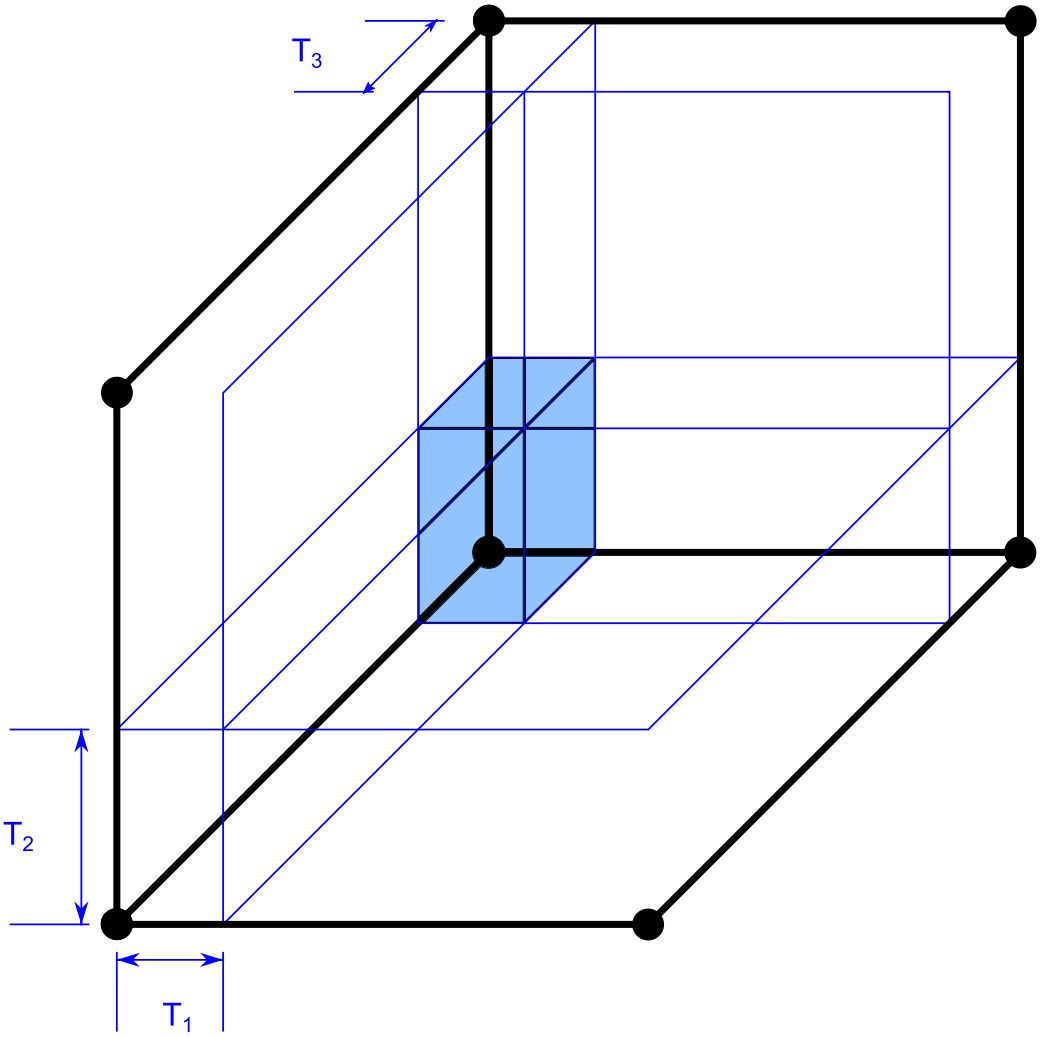

Figure 38: Trilinear interpolation to create brick elements.

Using this algorithm, an existing shell mesh of a thin-walled structure can be converted into brick elements. A slight complication exists if the model is to include a patch of overlay weld. In this case, a reduction of the plate may be desired before the weld overlay can be applied. The thickening algorithm should proceed as normal and apply the plate reduction as a postprocessing step by removing successive layers of bricks and fine-tuning by adjusting the nodes of the last remaining layer of bricks (Figure 39). Note that the original shell mesh will already be aligned to the weld overlay patch boundary, so no moving of nodes in the plane of the plate will be necessary.

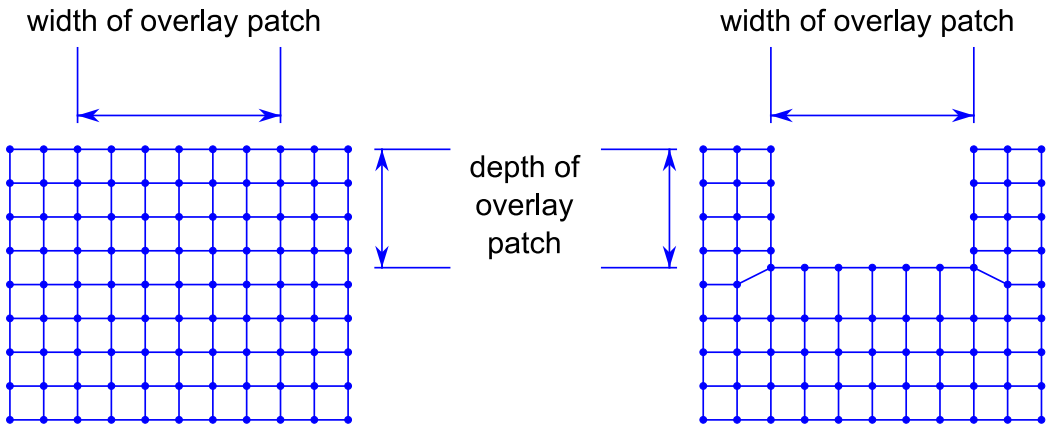

Figure 39: Setting up plate removal for overlay welding.

5.2.2 Element Refinement in the Vicinity of the Weld Path

Up to this point, the thickening algorithm uses the original shell elements as the template for extruding brick elements, except in the vicinity of plate intersections (as described above). As such, over most of the mesh, the aspect ratio of the elements will be quite extreme. Global refinement of the original shell elements can help the aspect ratio, but at the cost of dramatically increasing the model size. Instead, a strategy of local refinement in the vicinity of the weld path and grading to a coarser mesh further away from the path is desirable. This strategy must be applied to the mesh pattern both on the surface of the plates as well as through their thickness.

To this end, the algorithm is modified to define three tiers of mesh refinement. In the first tier, encompassing the weld path, a fine mesh will be used. In the second tier, a given distance from the weld path, the mesh will be coarsened by a factor of two. The third tier will further refine by a factor of two over the intermediate tier. Formally, let

- $\mathbf{d_{T1}}$, $\mathbf{d_{T2}}$ be the distance from the weld path for the boundary between tiers 1 and 2 and 2 and 3 respectively,
- $\mathbf{n_{T1}}$ be the number of elements through the thickness of the plate within tier 1, and
- $\mathbf{s_{T3}}$ be the element size of shell elements in tier 3

SubSAS will be modified to introduce boundaries into the surfaces being meshed to delineate the tiers. For instance, the intersection curve defining a weld path will be offset d_{T1} and d_{T2} along all participating surfaces, as shown in Figure 40. It should be noted that in order for this process to work correctly, there has to be at least $2(d_{T1}+d_{T2})+C$ distance between structure intersecting a given plate, where C represents a buffer to afford the SubSAS mesher the opportunity to create a reasonable mesh between the refinement fronts (i.e., the tier 3 area between the two refined regions). In general, the process will work best if $d_{T1}+d_{T2}$ is quite small relative to measures such as plate dimensions and stiffener spacing.

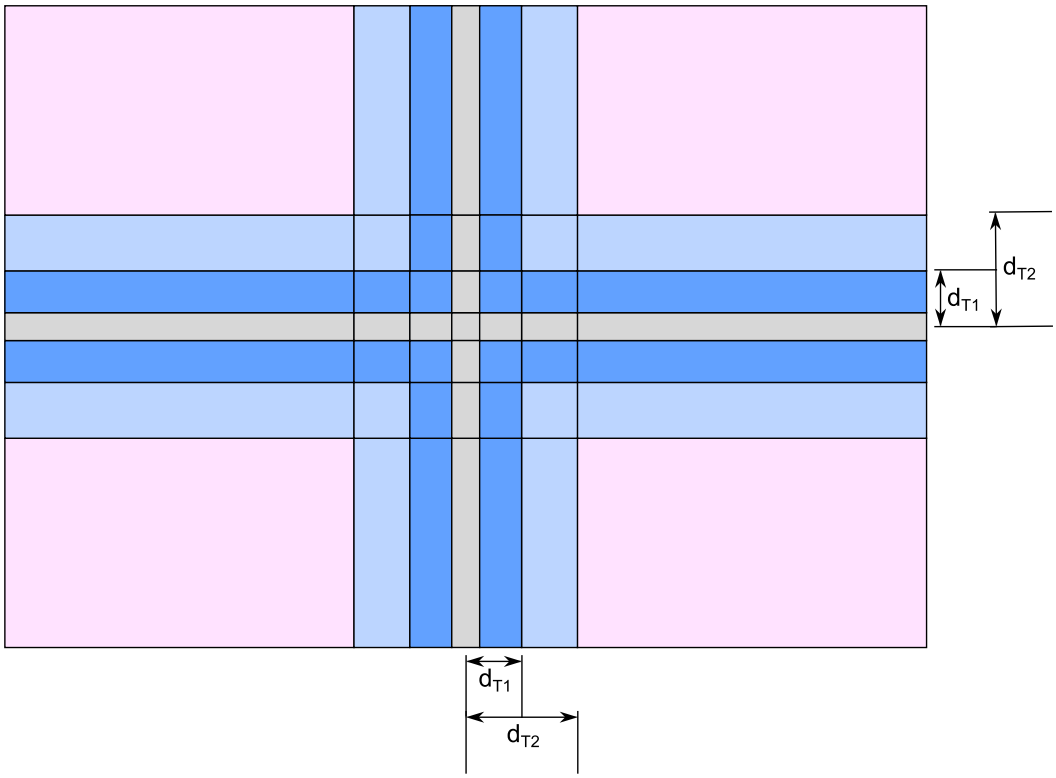

Figure 40: Element refinement tiers shown in the plane of a plate.

Through the thickness of the plate, n_{T1} elements will be used within tier 1 and coarsened away from the weld path. As such, n_{T1} will be halved in tier 2, and halved again in tier 3. A mesh transition pattern will be applied to achieve the coarsening. Figure 41 shows the coarsening strategy through the thickness of the plate.

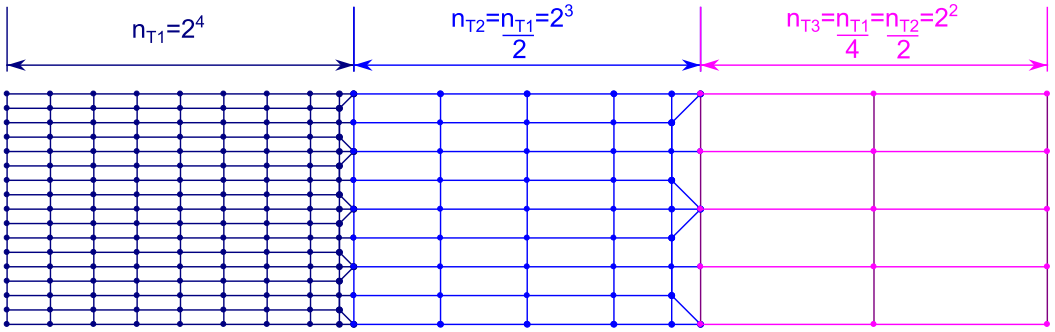

Figure 41: Element refinement tiers shown in the cross section of a plate.

This thickening strategy can be applied simultaneously in the plane of the plates as well. In this case, the overall element size used to mesh the original shell model, s_{T3}, will be refined towards

the weld path. As such, it will be doubled in tier 2 and doubled again in tier 1. The mesh transition pattern employed will be an extension of the pattern shown in Figure 41 to 3D (Figure 42). The pattern consists of five 8-node bricks, two 6-node wedges, and one 5-node pyramid. In the surface of the plates, it will appear as in Figure 43.

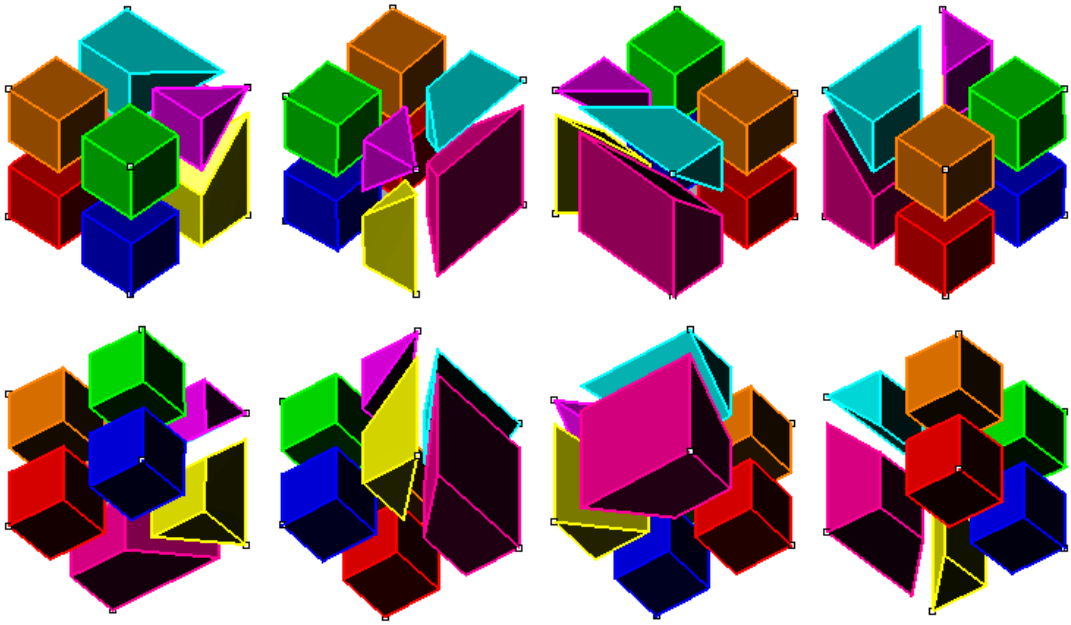

Figure 42: Brick element refinement pattern.

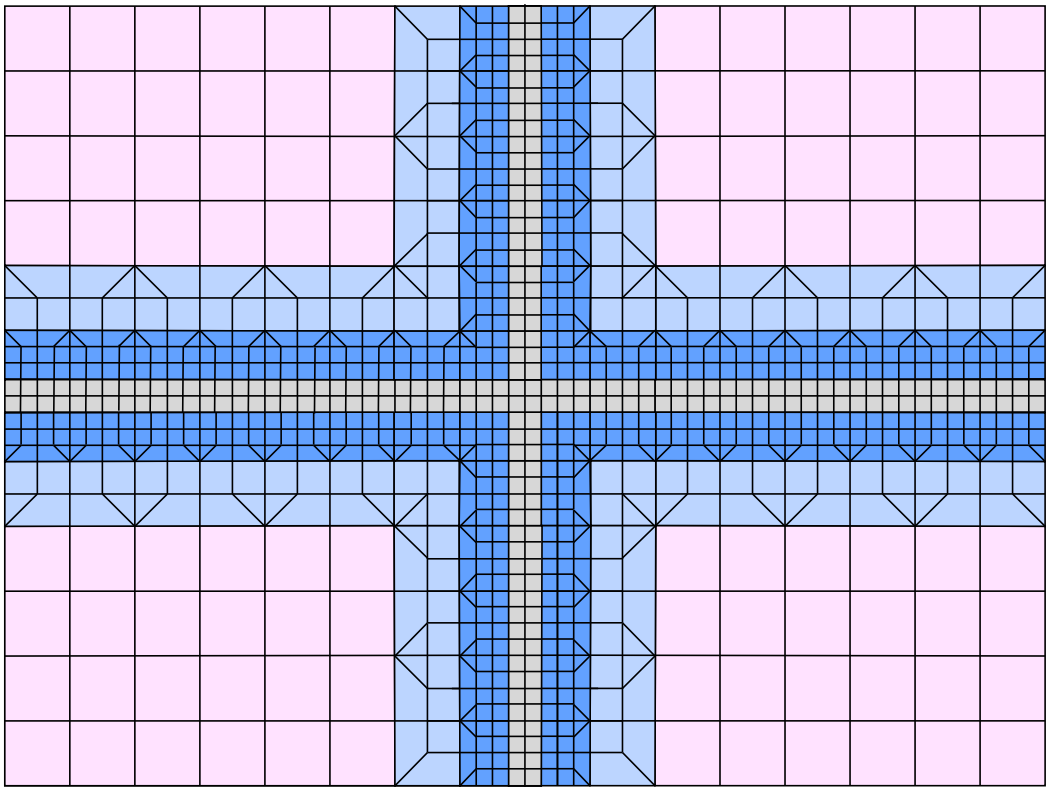

Figure 43: Example element refinement in the plane of a plate about two perpendicular plate intersections.

5.2.3 Elements Representing the Weld Deposit Material

Generating the weld deposit material should go hand-in-hand with creating the brick elements from the shell model, and requires access to the weld pass curve definition entities defined above in sub-section 5.1.3. The arrangement of elements comprising the weld deposit material will be different for each of the three weld types supported.

5.2.3.1 Fillet Welds

For fillet welds, one or more triangular wedges of elements will be placed as shown in Figure 44. The length of the triangle edges along each plate is given by the parameter ‘w’ in the weld pass curve definition, and each edge will be meshed using two elements. In order to support inserting the weld deposit elements to a precise distance of ‘w’ from the join of the surfaces, an offset of the intersection edge should be added to each surface. The exact distance from the actual intersection to place the offset on a given plate surface will be w+t/2 where t is the thickness of the other participating plate. This intersection will have to be added by SubSAS prior to meshing, in the same manner that the refinement region boundaries are added.

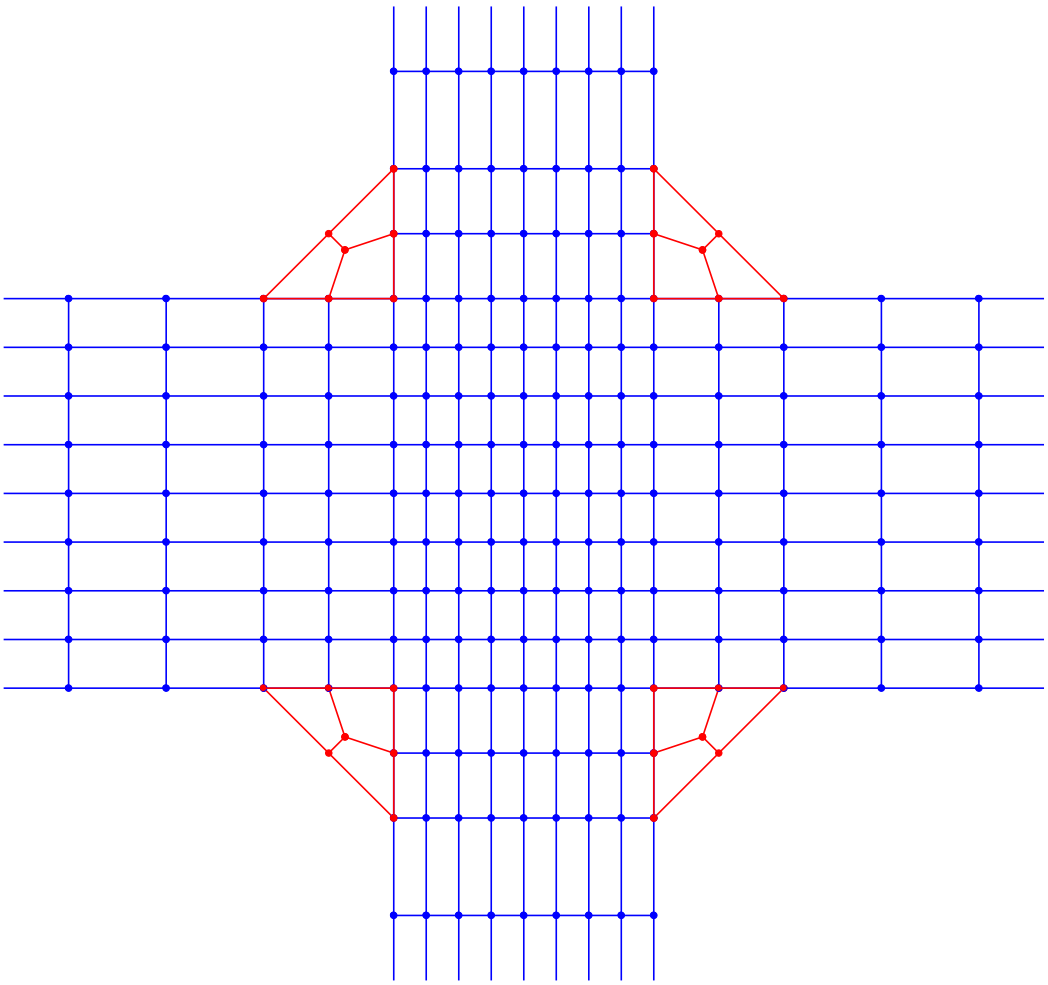

Figure 44: Fillet weld elements.

5.2.3.2 Butt Welds

For butt welds, knowledge of the weld pass curve parameters is required while the through-thickness brick elements are being generated for the two surfaces. The algorithm will make use of the angle specified in the weld pass curve definition to shift nodes belonging to the first few rows of elements on either side of the seam in order to introduce the V wedge. Once the wedge is introduced, the weld deposit elements can be trivially created as shown in Figure 45.

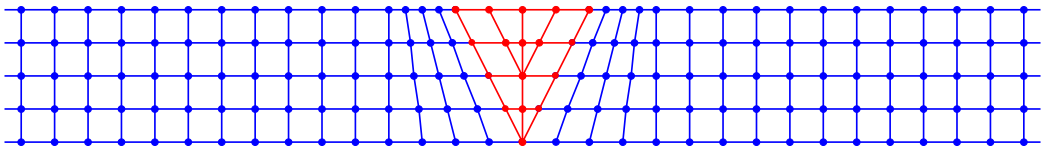

Figure 45: Butt weld elements.

5.2.3.3 Overlay Welds

Overlay weld deposit elements must be added carefully such that they properly connect to the elements belonging to the plate. Since the weld deposit element size is likely quite different from the plate element size, this can be a nontrivial operation. It is proposed to employ a three-step strategy that aims to keep the plate mesh static and refine the weld deposit elements to align to it (Figure 46). The first step will be to add the deposit elements without regard to the plating elements (i.e., using their "ideal" dimensions). Step two will be to adjust the weld deposit nodes such that they connect to their nearest counterpart in the plating mesh. This should leave no deposit element nodes unconnected to the plate mesh (below the surface of the plate, that is; nodes above the surface can stay disconnected). The last step will be, then, to refine the weld deposit elements such that they accommodate any left-over nodes in the plate mesh. This will be a symmetric operation on opposing sides of the overlay patch (meaning the refinement will carry "straight" through layers of overlay elements), but must be performed simultaneously in the local x and y directions of the patch. It is felt that trilinear cubic interpolation can be employed to achieve this.

It is worth noting that although the above process will refine the weld overlay elements, the weld pass functions will still be located at the centroids of the "ideal" elements (i.e., those introduced in the first step).

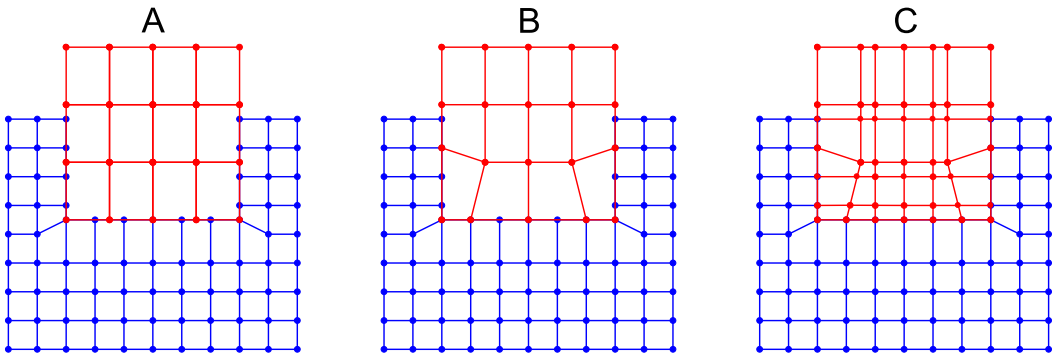

Figure 46: Overlay weld element; three steps in the process shown.

5.2.4 Definition of Element Groups

Element groups are relied upon in the welding simulation analysis to associate weld pass functions to the finite elements representing the weld deposit material. This could be achieved rather trivially in SubSAS by assigning element group IDs to weld deposit elements as they are being created. SubSAS could carry this group ID with each element and pass it on to the Trident Database when it is written. Unfortunately, the Trident Database does not currently accept element group IDs, and as such it too would have to be modified to track and use them when writing the VAST/VASTF input files.

VAST presently requires that if element groups are used at all, they must be used for all elements in the model. As such, all elements comprising the model, not just the weld deposit elements, would require group IDs. While this is not difficult to achieve, it should be noted that it is not enough to simply lump all non-weld-deposit elements into a single group. Rather, since element groups support only a single set of values for material properties, any change whatsoever in material properties between elements necessitates definition of another group. As such, all such elements must be aggregated and divided into groups according to their material properties.

5.3 Preparing Input for VASTF and VAST

The input files for the VASTF and VAST analysis programs were updated as part of this task to include sections for accepting the data pertaining to welding simulation. SubSAS would need to be updated to support populating these input files based on its welding model definition, as described above.

It is proposed, as a general strategy, to continue the use of the Trident Database as an interface between SubSAS and VAST (and now additionally VASTF). As such, the preferred strategy for conveying the data and control parameters for a welding simulation to VAST/VASTF would be for SubSAS to first write them into the Trident Database intermediate representation, and then use API functions to output the properly-formatted input files for these codes.

Trident/FEA, from which Trident Database functionality typically originates, presently supports setting up models for thermal analysis and writing the appropriate input files for VASTF. However, not all the data structures and operations pertaining to this capability are exposed through the Trident Database API. As such, some effort should be directed at moving that functionality into the Database. In addition, Trident/FEA does not yet support the various features that were introduced as part of this task, namely temperature dependent mechanical material properties, modelling the heat source, and modelling the weld pass paths. Further effort will be necessary to introduce support for these data into Trident/FEA and/or the Trident Database.

5.4 Running the Analysis

The overall welding simulation consists of two analyses: first, a thermal analysis using VASTF, and second, a structural analysis using VAST. Assuming the bulk of the input files for each program can be populated as described in the previous section, the only thing that remains is for SubSAS to gather the control parameters for the analyses and launch each in turn.

The analysis control parameters will be queried in a manner consistent with other analysis types in SubSAS, namely using an Analysis Type wizard. This wizard will gather such information as:

- first and last time step, maximum number of iterations and convergence tolerance for the thermal analysis
- number of time points and time interval for definition of the heat flux load
- the maximum time to be used in setting up the convection loads (recall the heat transfer coefficient is constant, so time will run from 0 to a given maximum value)
- the environmental temperature to use to set the initial temperatures for both analyses

Once the control parameters are gathered, SubSAS will write the analysis input files and call the analysis programs. SubSAS has an existing means to call VAST by synchronously launching a new process, and it is expected that the same capability will be sufficient to handle launching VASTF as well. SubSAS will treat both analyses as a "single" analysis from the user's point of view, and automatically handle passing the results from the first analysis to the second (i.e., the location of the .H52 file). SubSAS will block its own GUI until both analyses are complete (a 'busy' dialog is shown to inform the user that it is waiting, and the VAST/VASTF console window will be displayed to inform the user of progress).

The results of the second (structural) analysis will be a set of stresses and displacements that could be considered residual stresses/displacements for a further structural analysis. For example, a nonlinear collapse analysis considering the residual stresses/displacements in addition to a typical hydrostatic load case might be desired. In order to enable this, SubSAS must support passing the welding simulation results to subsequent analyses.

VAST supports including previous analysis results when running a new analysis. This mechanism could be leveraged to provide, for example, residual stresses resulting from a welding analysis to a downstream analysis, provided that the same mesh was used in both analyses. As such, the downstream analysis would either be limited to the same geometry as included in the welding analysis, or would have to embed the welding analysis geometry, unchanged, into a larger model. Since SubSAS supports embedding solid models into shell models using multipoint constraint equations, this would be a viable option for allowing the welding model to be included in a regular SubSAS' shell model.

If, however, the downstream analysis was using a different mesh, or was limited to only using shell elements, a means to map the residual stresses to the new mesh would be required. No work was undertaken to devise such a strategy as part of this task.

5.5 Postprocessing the Results

It is anticipated that postprocessing the results of the welding simulation will be quite straightforward. The second analysis in the simulation, the VAST structural analysis using the temperature field calculated in the first (VASTF) analysis, yields stress and displacement results that are already handled by the SubSAS postprocessing tools. As such, it is only anticipated that new postprocessing functionality will be needed to support visualizing the results of the VASTF

thermal analysis. This will include the requirement to visualize the time progression of the analysis, including the birth of weld deposit elements as the heat source moves along the weld pass curves.

The only pertinent output of the VASTF analysis code is the PREFIX.H52 file. This file is analogous to the PREFIX.V52 file that VAST generates to store nodal displacements for a structural analysis. In the VASTF thermal analysis case, the H52 file stores the temperature time history for each node in the model. The temperature at a given time is a single scalar value.

In order to visualize the H52 temperatures, it is recommended that Trident Visualizer be modified to plot temperatures using its generic color contouring feature. A new menu item, Visualize Temperatures, should be added to the Postprocessing menu, and enabled when the program detects the presence of a PREFIX.H52 file. Clicking the menu will bring forth a postprocessing property grid similar to the one visible when plotting displacement results. The "Load Case/Time Step" group will be changed to simply "Time Step" and will accept entering the step ordinal in order to swap values in the time history. The "Displacement Visualization" group will no longer be required, and the "Contouring" group will be simplified to remove the options relating to alternative coordinate systems and displacement components. There will be one option only – turn the contour plot on or off.

A new postprocessing option should be added to allow visualizing an animation of the temperature-time history. This capability would be analogous to animating displacement-load history for a structural analysis – an oft-requested feature that has not been fully realized to date. The animation capability will have to consider issues such as the number of elements and the number of time steps in order to derive an efficient means to swap values between each animation frame that can handle the potentially large volume of results (i.e., # elements * # time steps).

Finally, the action hyperlinks "Inquire nodal displacement by picking" and "Inquire nodal displacement by index" should be changed to allow querying of temperature. In addition, a new hyperlink should be added to allow plotting a nodal temperature vs. time step plot.

6 Conclusions

This report presents work performed for a recent contract aimed at developing a weld simulation capability in the VAST suite of nonlinear finite element programs. During this contract, a number of features required for weld simulations were implemented and verified. For heat transfer analyses, an element birth algorithm for tracking the states of the weld elements with the propagation of the weld heat sources and a capability for generating thermal nodal load vectors based on the widely accepted Goldak heat source model were incorporated in VASTF. Temperature-dependent thermal properties were also implemented, including thermal conductivity, heat capacity and mass density, and temperature-dependent coefficient of heat transfer. For structural analysis, thermal induced strains were first implemented in the elastic-plastic material model in VAST to facilitate coupled thermal-mechanical analyses. An element birth algorithm, similar to that for heat transfer analysis, was also developed in VAST to properly simulate deposition of the weld material. The thermal-elastic-plastic constitutive model was adjusted to treat melting and solidification of materials during the welding process. Temperature-dependent structural material properties, such as Young's modulus, Poisson's ratio, density, yield stress and hardening modulus, were all permitted for temperature dependent solutions. Multi-pass weld was supported.

All these newly developed capabilities were extensively verified using numerical examples. For heat transfer, weld simulations with different weld sequences were performed successfully. The VASTF solutions were compared to ANSYS predictions, giving very good agreement. For structural analyses, the VAST capabilities were tested by using various test cases designed to reflect certain features in weld simulations. These test cases involved a single element model with different boundary conditions and a cantilever beam with large displacements and rotations. For linear elastic cases, the VAST stress and strain results were compared against analytical solutions and exact agreement between them was found. In nonlinear test cases, thermal loadings involving temperature cycles were utilized to simulate heating and cooling phases of elements with different distances from the heat source. The VAST element and material model behaved favourably in all the test cases and no convergence difficulties were observed. However, when VAST was applied to weld simulation, divergence occurred after the first few solution steps. Attempts were made to investigate the cause of these numerical difficulties. However, the slowness of the computation for this solid element model made the investigation extremely difficult.

A proposed methodology for implementing support in the SubSAS application to configure welding simulations based on the new VAST/VASTF features was also given. The proposal detailed two broad categories of modifications. Firstly, enhancements to the RMGScript language were detailed to capture the new data required by welding analysis. Namely, changes to the RMGScript material entities were covered to include properties defining temperature dependent mechanical response and heat capacity and conductivity. New entities to capture the heat source definition and weld pass curves as well as initial material temperatures and convection properties were also given.

Secondly, various enhancements to SubSAS functionality were proposed to support welding simulation. An approach was detailed to convert an initial shell mesh to a brick mesh including mesh coarsening away from the weld pass curves. Strategies for introducing welding deposit material for fillet, butt and overlay welding configurations were proposed, along with a plan for

dividing elements into groups as required by the VAST solver. Finally, a methodology to pass the analysis data to VAST/VASTF via enhancements to the Trident Database routines was given, along with a list of enhancements to the Trident Visualizer to support postprocessing a welding analysis.

With regard to future work related to the VAST/VASTF simulation capability, it is strongly believed that the most important task is to speed up the VAST program by implementing a highly efficient matrix equation solver for solid element models and minimizing I/O operations by using an improved data structure. That would not only ease the investigation of the convergence problem experienced in the present contract, but also make the weld simulations more practical. Furthermore, additional numerical experiments are required to better understand the behaviour of the finite element formulations in weld simulations which involve extremely high temperatures and stress gradients. For this purpose, some highly refined local models will be very useful.

Finally, although the present work proposed enhancements to allow SubSAS to be used to configure, run and postprocess a welding simulation, no prototyping or implementation of the ideas was undertaken. It is recommended that future work be done to implement the design set forth in this report to enable welding simulations of, in particular, submarine pressure hull structures. In order to fully realize such a capability, however, the VAST/VASTF definition of weld pass curves will require support for curved paths.

References

[1] Lindgren, L.E., “Finite element modeling and simulation, part 1: increased complexity”, *Journal of Thermal Stresses*, Vol. 24, pp.141-192, 2001.

[2] Lindgren, L.E., “Finite element modeling and simulation, part 2: improved material modeling”, *Journal of Thermal Stresses*, Vol. 24, pp.195-231, 2001.

[3] Lindgren, L.E., “Finite element modeling and simulation, part 3: efficiency and integration”, *Journal of Thermal Stresses*, Vol. 24, pp.305-334, 2001.

[4] VASTF User’s Manual, Version 90, Martec Limited, Halifax, March 2010.

[5] Tiku S, Pussegoda N, Begg D., Monitoring of welding induced strains during cladding. DRDC Atlantic CR 2008-183, April 2008

[6] Goldak, J.A. and Akhlaghi, M., *Computational Welding Mechanics*, Springer, New York, 2005.

[7] Deng D, Liang W, Murakawa H., “Determination of welding deformation in fillet-welded joint by means of numerical simulation and comparison with experimental results”. *Journal of Materials Processing Technology*, Vol. 183, pp.219-25, 2007.

[8] Gannon, L., Liu, Y., Pegg, N. and Smith M., “Effects of welding sequence on residual stress and distortion in flat-bar stiffened plates”, *Marine Structures*, 2011.

[9] Gannon, L., Private communication, April, 2011.

[10] VAST User's Manual, Version 91, Martec Limited, Halifax, Canada, 2012.

This page intentionally left blank.

Distribution list

Document No.: DRDC Atlantic CR 2011-164

LIST PART 1: Internal Distribution by Centre

1 Project Authority
3 DRDC Atlantic Library (1 paper copy, 2 CDs)
1 Dr. Christopher Bayley, DLP
1 Dr. Liam Gannon, WP

6 TOTAL LIST PART 1

LIST PART 2: External Distribution by DRDKIM

1 NDHQ/DRDKIM 3 (1 CD)
2 NDHQ/DNPS 4-2 (1 paper copy, 1 CD)
1 Library & Archives Canada, Attn: Military Archivist, Government Records Branch

4 TOTAL LIST PART 2

10 TOTAL COPIES REQUIRED

This page intentionally left blank.

DOCUMENT CONTROL DATA

(Security classification of title, body of abstract and indexing annotation must be entered when the overall document is classified)

1. ORIGINATOR (The name and address of the organization preparing the document. Organizations for whom the document was prepared, e.g. Centre sponsoring a contractor's report, or tasking agency, are entered in section 8.)

Martec Limited
1888 Brunswick Street, Suite 400
Halifax, Nova Scotia, B3J 3J8

2. SECURITY CLASSIFICATION (Overall security classification of the document including special warning terms if applicable.)

UNCLASSIFIED
(NON-CONTROLLED GOODS)
DMC A
REVIEW: GCEC JUNE 2010

3. TITLE (The complete document title as indicated on the title page. Its classification should be indicated by the appropriate abbreviation (S, C or U) in parentheses after the title.)

Development and Verification of a Weld Simulation Capability for VAST

4. AUTHORS (last name, followed by initials – ranks, titles, etc. not to be used)

Jiang, L.; MacAdam, T.

5. DATE OF PUBLICATION (Month and year of publication of document.)	6a. NO. OF PAGES (Total containing information, including Annexes, Appendices, etc.)	6b. NO. OF REFS (Total cited in document.)
June 2012	86	10

7. DESCRIPTIVE NOTES (The category of the document, e.g. technical report, technical note or memorandum. If appropriate, enter the type of report, e.g. interim, progress, summary, annual or final. Give the inclusive dates when a specific reporting period is covered.)

Contract Report

8. SPONSORING ACTIVITY (The name of the department project office or laboratory sponsoring the research and development – include address.)

Defence R&D Canada – Atlantic
9 Grove Street
P.O. Box 1012
Dartmouth, Nova Scotia B2Y 3Z7

9a. PROJECT OR GRANT NO. (If appropriate, the applicable research and development project or grant number under which the document was written. Please specify whether project or grant.)	9b. CONTRACT NO. (If appropriate, the applicable number under which the document was written.)
11ga08	W7707-115119

10a. ORIGINATOR'S DOCUMENT NUMBER (The official document number by which the document is identified by the originating activity. This number must be unique to this document.)	10b. OTHER DOCUMENT NO(s). (Any other numbers which may be assigned this document either by the originator or by the sponsor.)
Contractor's Document Number: TR-12-22	DRDC Atlantic CR 2011-164

11. DOCUMENT AVAILABILITY (Any limitations on further dissemination of the document, other than those imposed by security classification.)

Unlimited

12. DOCUMENT ANNOUNCEMENT (Any limitation to the bibliographic announcement of this document. This will normally correspond to the Document Availability (11). However, where further distribution (beyond the audience specified in (11) is possible, a wider announcement audience may be selected.))

Unlimited

13. ABSTRACT (A brief and factual summary of the document. It may also appear elsewhere in the body of the document itself. It is highly desirable that the abstract of classified documents be unclassified. Each paragraph of the abstract shall begin with an indication of the security classification of the information in the paragraph (unless the document itself is unclassified) represented as (S), (C), (R), or (U). It is not necessary to include here abstracts in both official languages unless the text is bilingual.)

This report presents work aimed at developing a weld simulation capability for the VAST suite of finite element codes and the SubSAS submarine structural modelling software. In this study, a number of features required for weld simulations were implemented and verified. For heat transfer analyses, these included an element birth algorithm for tracking the states of weld elements with moving heat sources, a capability for generating thermal load vectors based on Goldak's model, and a capability for treating temperature-dependent thermal properties. For structural analysis, thermal induced strains were first implemented in the elastic-plastic material model to facilitate coupled thermal-mechanical analyses and the resulting thermal-elastic-plastic constitutive model was adjusted to treat melting and solidification of materials during the welding process. Temperature-dependent structural material properties were implemented and multi-pass welding was supported. For heat transfer analysis, weld simulations with different weld sequences were performed successfully. For structural analyses, the VAST capabilities were tested by using various test cases designed to reflect certain features of weld simulations. The VAST element and material model behaved favourably and no convergence difficulties were observed. However, when VAST was applied to a full weld simulation, divergence occurred after the first few solution steps. Further investigations are required to identify the cause of the numerical problem. The new weld simulation tools were not implemented in SubSAS, but a methodology was developed for implementing SubSAS support to define welding simulation models. Modifications to SubSAS's underlying RMGScript schema to support capturing the welding model parameters are detailed. Advanced algorithms for enhancing SubSAS's meshing capability to create brick elements from surface geometry, including a representation of the weld deposit material, are also described.

Le présent rapport contient la description de travaux visant à élaborer des capacités de simulation de soudures pour la suite de codes d'éléments finis appelée VAST et le logiciel de modélisation de structures de sous marins appelée SubSAS. Dans le cadre de la présente étude, un certain nombre de caractéristiques nécessaires aux simulations de soudures ont été mises en oeuvre et vérifiées. Dans le cas des analyses relatives au transfert de chaleur, les caractéristiques comprenaient un algorithme de production d'éléments finis permettant de déterminer l'état des composants de la soudure en fonction de sources de chaleur mobiles, ainsi que la capacité de générer des vecteurs de charge thermique basés sur le modèle de Goldak et celle de traiter adéquatement les propriétés thermiques qui dépendent de la température. Dans le cas des travaux d'analyse structurale, les valeurs de déformations causées par la chaleur ont d'abord été intégrées au modèle de matériaux élastiques-plastiques, afin de faciliter l'exécution d'analyses couplées thermiques et mécaniques; le modèle constitutif thermique-élastique-plastique obtenu a été modifié afin de tenir compte des processus de fusion et de solidification des matériaux lors du procédé de soudage. Des propriétés liées à la structure des matériaux qui dépendent de la température ont été intégrées au modèles, notamment pour le cas du procédé de soudage à passes multiples. Dans le cas des analyses relatives au transfert de chaleur, on a réalisé avec succès des simulations de soudures exécutées avec différentes séquences de soudage. En ce qui a trait aux analyses structurales, les capacités de l'outil VAST ont été mises à l'essai en utilisant divers cas types pouvant témoigner fidèlement de certaines caractéristiques des simulations de soudures. Le modèle de matériaux et d'éléments VAST a présenté un rendement adéquat et aucun problème de convergence n'a été observé. Toutefois, lorsque la suite VAST a été utilisée pour simuler une soudure complète, un problème de divergence a surgi dès les premières étapes de résolution. Des études plus poussées devront être réalisées afin d'identifier la cause du problème numérique. Les nouveaux outils de simulation de soudures n'ont pas été intégrés au logiciel SubSAS, mais une méthode a été élaborée afin de faciliter la mise en oeuvre d'applications de SubSAS qui permettent de définir des modèles de simulation de procédés de soudage. Des détails sont fournis sur les modifications apportées au schéma sous-jacent RMGScript de SubSAS, lesquelles visaient à faciliter l'enregistrement des paramètres du modèles de procédés de soudage. Le présent rapport contient aussi la description d'algorithmes perfectionnés mis au point pour accroître la capacité de maillage de SubSAS et produire ainsi des éléments parallélépipédiques à partir de concepts de géométrie de surface, y compris une représentation du matériau d'apport de la soudure.

14. KEYWORDS, DESCRIPTORS or IDENTIFIERS (Technically meaningful terms or short phrases that characterize a document and could be helpful in cataloguing the document. They should be selected so that no security classification is required. Identifiers, such as equipment model designation, trade name, military project code name, geographic location may also be included. If possible keywords should be selected from a published thesaurus, e.g. Thesaurus of Engineering and Scientific Terms (TEST) and that thesaurus identified. If it is not possible to select indexing terms which are Unclassified, the classification of each should be indicated as with the title.)

Weld Simulation; Finite Element Analysis; VAST; SubSAS

This page intentionally left blank.

Defence R&D Canada

Canada's leader in defence
and National Security
Science and Technology

R & D pour la défense Canada

Chef de file au Canada en matière
de science et de technologie pour
la défense et la sécurité nationale

DEFENCE DÉFENSE

www.drdc-rddc.gc.ca